

2018

Investigating micro-crack and local crack formation and propagation in ultra-high performance concrete (UHPC)

Chris James Levandowski
Iowa State University

Follow this and additional works at: <https://lib.dr.iastate.edu/etd>

 Part of the [Civil Engineering Commons](#)

Recommended Citation

Levandowski, Chris James, "Investigating micro-crack and local crack formation and propagation in ultra-high performance concrete (UHPC)" (2018). *Graduate Theses and Dissertations*. 17238.
<https://lib.dr.iastate.edu/etd/17238>

This Thesis is brought to you for free and open access by the Iowa State University Capstones, Theses and Dissertations at Iowa State University Digital Repository. It has been accepted for inclusion in Graduate Theses and Dissertations by an authorized administrator of Iowa State University Digital Repository. For more information, please contact digirep@iastate.edu.

**Investigating micro-crack and local crack formation and propagation in ultra-high
performance concrete (UHPC)**

by

Christopher J. Levandowski

A thesis submitted to the graduate faculty
in partial fulfillment of the requirements for the degree of
MASTER OF SCIENCE

Major: Civil Engineering (Structural Engineering)

Program of Study Committee:
Sri Sritharan, Major Professor
Behrouz Shafei
Kejin Wang

The student author, whose presentation of the scholarship herein was approved by the program of study committee, is solely responsible for the content of this thesis. The Graduate College will ensure this thesis is globally accessible and will not permit alterations after a degree is conferred.

Iowa State University

Ames, Iowa

2018

Copyright © Christopher J. Levandowski, 2018. All rights reserved.

TABLE OF CONTENTS

LIST OF FIGURES	v
LIST OF TABLES	xi
ACKNOWLEDGMENTS	xii
ABSTRACT	xiii
CHAPTER 1: INTRODUCTION	1
1.1 Overview	1
1.2 Tensile Behavior of UHPC	2
1.3 Research Scope and Objectives	4
1.4 Thesis Layout	4
CHAPTER 2: LITERATURE REVIEW	6
2.1 Definition of UHPC	6
2.2 UHPC Composition	10
2.3 Applications of UHPC	12
2.3.1 Pedestrian Bridges	13
2.3.2 UHPC Bridge Beams	14
2.3.3 Bridge Overlay	18
2.3.4 Other Structural/Durability Applications	19
2.3.5 Architectural Applications	24
2.4 Material Properties	25
2.4.1 Compressive Behavior	25
2.4.2 Flexural Behavior	27
2.4.3 Modulus of Elasticity	29
2.4.4 Poisson's Ratio	29
2.4.5 Thermal Properties	30
2.4.6 Bond Strength	30
2.4.7 Impact Resistance	31
2.4.8 Creep	31
2.4.9 Shrinkage	31

2.5 Tensile Behavior	32
2.5.1 Tensile Test Methods.....	33
2.5.2 Tension Tests by Others.....	36
CHAPTER 3: EXPERIMENTAL INVESTIGATION OF UHPC TENSILE BEHAVIOR	51
3.1 Experimental Procedure.....	51
3.1.1 Test Matrix.....	51
3.1.2 Casting of Specimens.....	52
3.1.3 Test Setup and Specimen Dimensions.....	53
3.1.4 Data Collection Methods	55
3.1.5 Loading Procedures	56
3.1.6 Comparison of Sensory Data	56
3.1.7 UHPC Mix Types	57
3.2 Data Quantification.....	58
3.2.1 Strain.....	58
3.2.2 Stress.....	59
3.2.3 Fracture Energy.....	59
3.2.4 Characteristic Length.....	61
3.3 Experimental Results and Discussion.....	62
3.3.1 Definitions.....	63
3.3.2 Comparison of Global Results with Results from Others.....	64
3.3.3 Influence of Fiber Type	66
3.3.4 Comparison of Proposed Tension Model with Models Proposed by Others.....	72
3.3.5 Influence of Fiber Content.....	74
3.3.6 Supplier 1 – 2% Fiber	79
3.3.7 Supplier 1 – 1% Fiber	88
3.3.8 Supplier 2 – 2% Fiber	90
3.3.9 Supplier 3 – 2% Fiber	92
3.3.10 Variation between Different Specimens	94
3.3.11 Variation within a Specimen.....	97
3.3.12 Contribution of Micro-cracks to Global Specimen Displacement.....	100
3.3.13 Fracture Energy.....	104
3.3.14 Characteristic Length.....	105
3.3.15 Stress and Strain Limits	107

CHAPTER 4: CONCLUSIONS	109
4.1 Summary	110
4.2 Conclusions	111
4.2.1 Influence of Fiber Type	111
4.2.2 Proposed UHPC Tensile Behavior Model	112
4.2.3 Influence of Fiber Content	113
4.2.4 Contribution of Micro-crack to Overall Displacement	114
4.2.5 Fracture Energy and Characteristic Length	115
4.2.6 Stress and Strain Limits	115
REFERENCES	117

LIST OF FIGURES

Figure 1: View of the finished Sherbrooke Pedestrian Bridge (FHWA, 2013).....	13
Figure 2: View of the Seonyu “Footbridge of Peace” in South Korea (Lafarge, 2009).....	14
Figure 3: Road Bridge at Bourg-les-Valences. Central pier during placing of pi-shaped beams (Vergoossen, 2008).....	15
Figure 4; Photo of the completed Mars Hill Bridge (FHWA, 2013).....	16
Figure 5: Picture of the Jakway Bridge (FHWA, 2013).....	17
Figure 6: Cross-section of pi-shaped girder used in Jakway Park Bridge (FHWA, 2013).....	17
Figure 7: Construction being performed on the Chillon Viaducts (Source: Ductal).....	18
Figure 8: Experimental precast pile made of UHPC (Source: Iowa State University).....	19
Figure 9: UHPC waffle deck panel with formwork removed - panel upside down (Heimenn, 2013).....	20
Figure 10: Setting the UHPC Waffle Deck panels (Heimenn, 2013).....	21
Figure 11: Picture of finished Mission Bridge pier jacking (Source: Ductal).....	22
Figure 12: Picture of Caderousse Dam (Source: Ductal).....	23
Figure 13: Conceptual design for building a 100 m and taller Hexcrete wind turbine tower (Sritharan, 2015).....	24
Figure 14: UHPC lattice facade and footbridge MUCEM (Photo by Rudy Ricciotti).....	25
Figure 15: Load-deflection responses for each series of beams - beams with 1% fiber.....	28
Figure 16: Load-deflection responses for each series of beams - beams with 2% fiber.....	29
Figure 17: Sample direct tensile test specimen dimensions and gripping method (Graybeal and Baby, 2013).....	37
Figure 18: Testing of a 17 inch (431.8 mm) long specimen (Graybeal and Baby, 2013).....	38

Figure 19: Idealized uniaxial tensile mechanical response of UHPC (Graybeal and Baby, 2013)	39
Figure 20: Uniaxial tensile stress-strain response from specimen (Graybeal and Baby, 2013) ...	39
Figure 21: Post-cracking facial strain disparity from specimen data (Graybeal and Baby, 2013)	40
Figure 22: Geometry of direct tensile specimen, test setup, and load application method (Wille, et. al, 2011)	41
Figure 23: Steel fiber types used in this research, a) straight smooth fiber (S), b) hooked fiber (H), c) high twisted fiber (T1), d) high twisted fiber zoomed-in (T1), and e) low twisted fiber zoomed-in (T2) (Wille, et. al, 2011)	42
Figure 24: Direct tensile response of UHPC with twisted steel fibers, a) 1.0% high twist fiber, b) 1.5% low twist, and c) 2.0% high twist fiber, d) Comparison of average curves for twisted steel fiber (Wille, et. al, 2011)	43
Figure 25: Direct tensile response of UHPC with smooth steel fibers, a) 1.5% by volume, b) 2.5% by volume, and c) Comparison of average curves for smooth steel fiber (Wille, et. al, 2011)	44
Figure 26: Direct tensile response of UHPC with hooked steel fibers, a) 1.0% by volume, b) 2.0% by volume, and c) 2.5% Comparison of average curves for hooked steel fiber (Wille, et. al, 2011)	44
Figure 27: Comparison of direct tensile response of UHPC with different fiber types, a) 1.0% fiber by volume, b) 1.5% fiber by volume, and c) 2.0% fiber by volume (Wille, et. al, 2011)	45
Figure 28: Dog-bone shaped specimens used in previous research (Wille, et. al, 2014)	47

Figure 29: Un-notched prism/cylinder specimens used in previous research (Wille, et. al, 2014)	48
Figure 30: Notched prism/cylinder specimens used in previous research (Wille, et. al, 2014)....	48
Figure 31: Direct tensile test setup used by Wille, et. al (2014).....	49
Figure 32: Analytical procedure for sample series of tests (Wille, et.al, 2014)	50
Figure 33: Comparison of bi-linear model for all specimens including unloading line (Wille, et. al, 2014)	50
Figure 34: Specimen Naming Convention.....	52
Figure 35: Specimen Dimensions and Photographs of Data Collection Methods.....	55
Figure 36: Comparison of LED and LVDT Data - Stress vs. Average Axial Strain.....	57
Figure 37: Sample Curve Used to Calculate Fracture Energy - Stress vs. Local Crack Displacement.....	61
Figure 38: Comparison of Global Results with FHWA Test Result (FHWA 2013).....	65
Figure 39: Comparison of Global Results with Average Wille et. al Data.....	65
Figure 40: Comparison of Brittle and Ductile UHPC Responses.....	66
Figure 41: Effect of Fiber Type on Micro-crack Strain Response.....	68
Figure 42: Stress vs. Average Axial Strain for Specimens Exhibiting Ductile Behavior.....	71
Figure 43: Stress vs. Average Axial Strain for Specimens Exhibiting Ductile Behavior - Zoomed In.....	71
Figure 44: UHPC Tensile Stress-Strain Response Model Proposed by Alkaysi, M. and El-Tawil, M.....	72
Figure 45: UHPC Tensile Stress-Strain Response Model Proposed by FHWA.....	73
Figure 46: Micro-cracking in Supplier 1 - 2% Fiber Specimen.....	75

Figure 47: Micro-cracking in Supplier 1 - 2% Fiber Specimen - with marks	75
Figure 48: Micro-cracking in Supplier 1 - 1% Fiber Specimen.....	76
Figure 49: Micro-cracking in Supplier 1 - 1% Fiber Specimen - with marks	76
Figure 50: Stress vs. Average Axial Strain - 4" Gage Length - 0% Fiber	77
Figure 51: Effect of Fiber Content - Stress vs. Average Axial Strain – 4” Gage Length.....	78
Figure 52: Effect of Fiber Content Zoomed In - Stress vs. Average Axial Strain.....	78
Figure 53: Effect of Fiber Content on Micro-crack Strain - Stress vs. Average Micro-crack Strain.....	79
Figure 54: Supplier 1 - 2% Type A Fiber - Stress vs. Average Axial Strain – 4” Gage Length ..	80
Figure 55: Supplier 1 - 2% Type A Fiber - Stress vs. Average Micro-crack Strain.....	81
Figure 56: S11.A20 Stress, Local crack Strains, and Average Micro-crack Strains vs. Time	82
Figure 57: Cross-section of failure S11.A20	83
Figure 58: S12.22.A20 Stress, Local crack Strains, and Average Micro-crack Strain vs. Time..	84
Figure 59: Cross-section of failure S12.A20	85
Figure 60: S13.A20 Stress, Local crack Strains, and Average Micro-crack Strains vs. Time	87
Figure 61: Cross-section of failure S13.A20	87
Figure 62: Supplier 1 - 1% Type A Fiber - Stress vs. Average Axial Strain.....	89
Figure 63: Supplier 1 - 1% Type A Fiber - Stress vs. Average Axial Strain Zoomed In	89
Figure 64: Supplier 2 - 2% Type A Fiber - Stress vs. Average Axial Strain – 4” Gage Length ..	91
Figure 65: Supplier 2 - 2% Type A Fiber - Stress vs. Average Micro-crack Strain.....	91
Figure 66: Stress vs. Average Axial Strain - Supplier 3 - 2% Combined of Type A and E Fiber	92

Figure 67: Stress vs. Average Axial Strain - Supplier 3 - 2% Combined of Type A and E Fiber - Zoomed In	93
Figure 68: Stress vs. Average Micro-crack Strain - Supplier 3 - 2% Combined of Type A and E Fiber	93
Figure 69: High Variation in Micro-cracking Behavior - Supplier 1 - 2% Type A Fiber	95
Figure 70: Low Variation in Micro-cracking Behavior - Supplier 1 - 1% Type A Fiber	96
Figure 71: Variation in Average Axial Strain Responses – Supplier 1 – 2% Type A Fiber	96
Figure 72: Variation within a Specimen - Micro-crack Strains at One-Inch Intervals – S13.A20	98
Figure 73: Variation within a Specimen - Average of Left and Right Micro-crack Strains at One-Inch Intervals – S13.A20	99
Figure 74: Variation within a Specimen – Average Micro-crack Strain +/- StdDev - S13.A20	99
Figure 75: Variation within a Specimen - Micro-crack Strain Range - Min, Max, and Average Micro-crack Strains - S13.A20.....	100
Figure 76: Contribution of Micro-cracks to Overall Displacement - S12.A20 Stress vs. Displacement.....	101
Figure 77: Contribution of Micro-cracks to Overall Displacement - S12.A20 Stress vs. Displacement - Zoomed In.....	102
Figure 78: Contribution of Micro-cracks to Overall Displacement - S11.A20 Stress vs. Displacement.....	102
Figure 79: Contribution of Micro-cracks to Overall Displacement - S11.A20 Stress vs. Displacement – Zoomed In.....	103

Figure 80: Contribution of Micro-cracks to Overall Displacement - S11.A10 Stress vs. Displacement.....	103
Figure 81: Contribution of Micro-cracks to Overall Displacement - S11.A20 Stress vs. Displacement - Zoomed In.....	104
Figure 82: Fracture Energies for Supplier 1 Specimens	105
Figure 83: Characteristic Lengths for Supplier 1 Specimens	106

LIST OF TABLES

Table 1: UHPFRC Categories - EPFL Recommendations	9
Table 2: Canadian Standards Association Proposed UHPC Classifications	9
Table 3: Typical UHPC Components	11
Table 4: Components for Three UHPC Mixes - R. Yu et. al.....	11
Table 5: Test Matrix.....	52
Table 6: UHPC mix constituents	58
Table 7: Descriptions of Fiber Type	58
Table 8: Fracture Energy Values - Supplier 1 - 2% Type A Fiber	105
Table 9: Fracture Energy Values - Supplier 1 - 1% Type A Fiber	105
Table 10: Characteristic Length Values - Supplier 1 - 2% Type A Fiber.....	106
Table 11: Characteristic Length Values - Supplier 1 - 1% Type A Fiber.....	106

ACKNOWLEDGMENTS

First and foremost, I would like to thank my supervisor, Dr. Sri Sritharan, for his immense support throughout my graduate studies. His valued input and guidance were essential to the completion of this thesis, and without his assistance, I would not have been able to successfully complete my graduate research.

I would like to thank the American Society of Civil Engineer for the financial support received through the Freeman Fellowship. The opportunity to work under this Fellowship was greatly appreciated. All Ultra-High Performance Concrete material was donated by UHPC suppliers available in the United States market. The substantial financial investment and professional assistance of all suppliers involved are appreciated.

I greatly appreciate all the help from the laboratory personnel of Structural Engineering Research Lab at Iowa State University, particularly Owen Steffens and Doug Wood. I would also like to thank Satish Jain, Sameer Pachalla, and Liang Zhong for their contributions to the experimental research performed in this study. I would also like to express my appreciation to Dr. Kejin Wang and Dr. Behrouz Shafei for serving on my program of study committee.

Finally, I would like to thank my family and friends for their love and support throughout my graduate studies, particularly my mother and father. I could not have achieved this accomplishment without them.

ABSTRACT

Ultra-High Performance Concrete (UHPC) is a unique structural material growing in use in the United States and throughout the world. Its increased use is due to its many benefits, including high compressive and tensile strengths, resistance to chloride ingress, freeze-thaw durability, and increased bond strength with reinforcement. However, the tensile behavior of UHPC, particularly regarding the micro-cracks that form under tensile stress, is not well understood. Properly understanding the tensile behavior of UHPC is essential for design of UHPC structures subjected to flexural and shear action. As flexural or shear action are present in a vast majority of structural members, fully understanding the tensile behavior of UHPC is of the utmost importance to ensure the design of safe and efficient UHPC structures.

The micro-cracks that form in UHPC under tensile load are regarded by many researchers as essential to UHPC ductility allowing UHPC to reach significantly higher strains before reaching its maximum tensile stress. Additionally, UHPC is assumed to remain durable, even past its maximum stress value, as micro-cracks widths are typically small enough to prevent damaging chloride penetration. However, when defining tensile behavior, traditional tensile test methods measure displacement over a gage length. These test methods do not directly measure UHPC micro-cracking behavior under tensile loads, instead grouping the micro-cracking behavior with the global tensile behavior over this chosen gage length. Therefore, results regarding micro-cracking behavior in UHPC are derived from these tests based on assumptions rather than measured directly during testing.

The primary goal of this research is to directly quantify micro-cracking behavior in UHPC specimens under tensile loading in order to fully understand UHPC tensile behavior. In particular, this research focuses on understanding the role of UHPC mix type, fiber type, and fiber content on tension and micro-cracking behavior through the testing of over 30 dog-bone shaped specimens. Specimens in this study are composed of UHPC from three different suppliers available in the United States market and included combinations of five different fiber types dosed at various fiber contents ranging from 0% to 2.75% by volume.

By separating the micro-cracking behavior from the global tensile behavior of UHPC, the relationship between the formation and propagation of micro-cracks and local cracks is investigated in this study. Furthermore, the effect of UHPC mix, fiber type, and fiber content on overall tensile behavior is explored. Two potential tensile responses observed during testing are explained in this thesis. These responses include a brittle response in which specimens reach their maximum strength before failing suddenly and a ductile response in which specimens exhibit post-cracking behavior. A four-stage model for the tensile behavior of UHPC exhibiting a ductile response is proposed based on test results. The contribution of micro-crack displacement to total displacement, variations in tensile behavior, and relative brittleness of UHPC exhibiting ductile behavior are also explored. Characteristic length values are also calculated and show that UHPC with 1% fiber is more ductile than UHPC with 2% fiber under tensile loads. Additionally, stress and strain recommendations are provided for various UHPC applications based on test results from this study. Based on test results, stress and strain limits for UHPC with 2% fiber by volume are 1000 psi and 0.25 me to prevent local crack formation and 1300 psi and 0.5 me

to prevent local crack growth. Stress and strain limits for UHPC with 1% fiber by volume are 500 psi and 0.1 me to prevent local crack formation and 900 psi and 0.8 me to prevent local crack growth.

CHAPTER 1: INTRODUCTION

1.1 Overview

Ultra-High Performance Concrete (UHPC) is a relatively new material with properties that vary significantly from existing conventional and high strength concrete materials. Significant research has been performed to define the properties of UHPC, and many properties of the material, including compression behavior, creep, and shrinkage have been well defined through research efforts. However, the tensile behavior of UHPC, which is critical for design of members subject to flexural and shear action, is not fully understood.

Per the Federal Highway Administration (FHWA), UHPC is a new class of cementitious composite that meets the following characteristics: “freeze-thaw durability, scaling resistance, abrasion resistance, chloride penetration, high compressive strength, modulus of elasticity, shrinkage, and creep.” The American Concrete Institution’s definition of UHPC is pending approval, but the proposed definition requires that a material shall have a minimum compressive strength of 150 MPa and meet any “specified durability, tensile ductility, and toughness requirements.” It also states that fibers are generally included. Other researchers define UHPC by its large compressive strength which reaches a magnitude of 21.8 to 30 ksi (150-207 MPa) according to Vande Voot (2008). However, the value of compression strength varies as the American Society for Testing Materials (ASTM) defines 17 ksi (117 MPa) as the minimum compressive strength for a material to be considered as UHPC (ASTM International, 2017).

The benefits of using UHPC in structural applications are numerous. Its durability, resistance to harsh weather conditions, and strong compressive strength make it an appealing material for structures that must be able to withstand harsh conditions for long periods of time without failure. Additionally, since UHPC is significantly stronger than conventional concrete in compression and tension, much less UHPC material is required to meet the same structural capacity as conventional concrete. This enables structures built out of UHPC to be significantly lighter. The higher compression capacity of UHPC compared to conventional and high strength concrete is due to the small and purposefully graded particles used in the mix. These particles fit together to form a dense cementitious matrix. The higher tensile capacity of UHPC is primarily due to the fiber reinforcement typically included in its composition. These fibers, typically composed of steel, enable the UHPC to have a post-cracking tensile strength larger than its pre-cracking strength according to many researchers. However, issues regarding UHPC tensile behavior still exist.

1.2 Tensile Behavior of UHPC

Though the basic requirements of UHPC tensile behavior such as ductility and post-cracking strength have been defined, gaps in knowledge still exist on the subject. The primary issue with the current understanding of UHPC's tensile properties lies in the data collection methods used during testing and the application of results from such tests. Though typical tensile testing methods adequately define the tensile behavior of a specimen from a global perspective, they do not adequately determine the formation and propagation of micro-cracks during tensile loading or their relationship to the formation and propagation of the localized crack(s). Current direct tensile testing methods provide results in the form of average cross-section stress in the

specimen versus strain over a gage length. This strain is calculated from displacement data collected by Linear Variable Differential Transformers (LVDTs) or similar measurement tools. Since displacement data is collected over a gage length, micro-cracking behavior is lumped in with the local cracking behavior throughout testing. Therefore, the true nature of micro-crack formation and propagation and its relationship to local crack formation and propagation is inferred from global strain results rather than being captured.

The primary goal of this study is to fully understand the formation and propagation of micro-cracks and local cracks that occur in UHPC under tensile loads. To determine these properties, over 30 specimens with various combinations of UHPC mixes, fiber types, and fiber contents were loaded in direct tension until failure. Displacement data was collected along specimens at regular intervals throughout the testing with the Optotrak Certus HD System. This system uses a camera to capture the x-y-z coordinates of Light-Emitting Diodes (LEDs) attached to the specimens. Data from these LEDs were then used to determine micro-crack and local crack strains which were used to investigate micro-crack formation and propagation and their relationship to local crack formation and propagation. Based on these results, stress and strain limits to prevent local crack formation and local crack growth are proposed for UHPC with different fiber contents. Additionally, fracture energy and characteristic length values are calculated and compared for relevant specimens.

1.3 Research Scope and Objectives

The research goals for this thesis include:

- Investigate the formation and propagation of micro-cracks and local cracks and determine the relationship between the two under tensile loading
- Determine the effect of fiber type and content on UHPC tensile behavior
- Discuss variation observed in test results
- Examine the contribution of micro-cracks to total axial displacement over a gage length
- Compare fracture energy and characteristic length results for different fiber contents
- Stress and strain limits for UHPC are proposed to prevent local crack formation and local crack growth

1.4 Thesis Layout

This thesis is comprised of four chapters including the general introduction presented in this chapter. The second chapter consists of a literature review focused on the definition of UHPC, UHPC's current applications to bridges and other structures, and UHPC's properties. The tensile behavior of UHPC is discussed in detail including various tensile behavior models, tensile testing methods, and previous experimental investigations relevant to UHPC tensile behavior. The following chapter, Chapter 3, details the experimental procedure for the direct tensile tests conducted in this study and a comparison of test results to tensile tests conducted in similar experimental investigations. Additionally, the relationship between micro-crack and local crack strains is investigated with an emphasis on directly quantifying micro-cracking behavior. The results of direct tensile tests performed in this study are presented in terms of micro-crack strains

and average axial strains. Fracture energy and characteristic length results are also discussed.

Chapter 4 presents conclusions from the study regarding UHPC tensile behavior.

CHAPTER 2: LITERATURE REVIEW

An extensive review of literature related to Ultra-High Performance Concrete constituents, applications, properties, and current understanding of tensile behavior was undertaken as part of this study. The first section of the chapter provides an overview of UHPC definitions provided by various researchers and entities. This is followed by a description of typical UHPC mix constituents and their ratios within sample UHPC mix designs. Various UHPC applications are then outlined with an emphasis placed on the innovative applications of the material. A brief summarization of UHPC's general properties is provided in the following section. Finally, the tensile behavior of UHPC is discussed in depth with an emphasis placed on tensile test methods used to define UHPC tensile behavior and the results of various tensile tests conducted in experimental investigations by other researchers.

2.1 Definition of UHPC

The general properties of UHPC, such as high compressive strength, high tensile strength relative to conventional concrete, and a densely packed cementitious matrix are widely accepted. However, the specific values for Ultra-High Performance Concrete vary greatly between definitions proposed by different entities and researchers. Many define UHPC by its compressive strength and/or the tensile strength. Others define UHPC by its tensile behavior, requiring strain hardening or categorizing UHPC based on its tensile response. Meanwhile, some definitions do not require the inclusion of fiber or post-cracking strength to occur. This high variance in the definition of UHPC displays the lack of consensus on what classifies a material as Ultra-High Performance Concrete. The remainder of this section is a summarization of UHPC definitions

provided by various entities followed by the definition of UHPC used for the purposes of this study.

Standards, codes, and guides for UHPC began development in several countries in the late 1990's. The first published guide was France's first UHPC Design Guide introduced in 2001. An updated version of this design guide released in 2013 defines UHPC, known as Ultra-High Performance Fiber-Reinforce Concrete (UHPRFC) in France, as "materials with a cement matrix and a characteristic compressive strength of more than 150 MPa and a maximum [compressive strength] of 250 MPa" (FGAC, 2013). It also requires that UHPC materials exhibit ductile tensile behavior and high post-cracking strength greater than 7 MPa, obtained through the use of a high fiber dosage of 2% or more by volume. This design guide also requires UHPRFC to have high durability (FGAC, 2013). Similar to the French Design Guide, the Japanese Recommendations published by the Japanese Society of Civil Engineers require UHPC, known as High Performance Fiber Reinforced Cementitious Composite (HPRFRC) in Japan, to exhibit ductile tensile behavior. Moreover, these recommendations require HPRFRC to be a cement-based matrix containing short reinforcing fibers which ensure the material exhibits multiple fine cracks and pseudo strain-hardening characteristics in tension (JSCE, 2008). The Japanese document is the only document to require strain hardening in order for a material to be classified as UHPC.

The Federal Highway Administration (FHWA), defines UHPC as a relatively new class of advanced cementitious composite materials that contain discontinuous fiber reinforcement. Additionally, UHPC is defined as having a compressive strength above 21.7 ksi (150 MPa) with a range of 21.7 ksi to 30 ksi (150 MPa to 207 MPa), pre-and post-cracking tensile strengths above

0.72 ksi (5 MPa), and meeting the following criteria: “freeze-thaw durability, scaling resistance, abrasion resistance, chloride penetration, high compressive strength, modulus of elasticity, shrinkage, and creep” (FHWA, 2013). However, the American Society for Testing and Materials (ASTM) International recently published standards for testing UHPC in compression. This document defines the minimum compressive strength of UHPC as 17 ksi (120 MPa) making this the new standard minimum compressive strength in the United States (ASTM International, 2017).

The Maintenance Construction Sécurité – École Polytechnique Fédérale de Lausanne (MCS-EPFL) Recommendation on UHPFRC from Switzerland characterizes UHPC by its tensile behavior, compressive behavior, and several other properties. For a material to be considered UHPC according to the EPFL Recommendations, the material must have a maximum tensile strength of approximately 1.0 – 2.2 ksi (7-15 MPa), elastic limit stress of 1.0 – 1.75 ksi (7-12 MPa), and specific fracture energy of approximately 4-12 ft-lb/in² (8-25 kJ/m²). Compressive strengths of 17-29 ksi are required and recommendations for a variety of other parameters including Modulus of Elasticity, Poisson’s ration, thermal expansion coefficient, shrinkage, and density are provided. The different types of UHPFRC are specified according to Table 1 in this definition. Potential compressive strength classes that may be specified on projects are also defined. These are classes U120, U160, and U200 which require minimum compressive strengths of 17.4 ksi, 23.3 ksi, and 29.0 ksi (120 MPa, 160 MPa, and 200 MPa) respectively (EPFL, 2016).

Table 1: UHPFRC Categories - EPFL Recommendations

Type	U0	UA	UB
f_{Utek} MPa	$\geq 7,0$	$\geq 7,0$	$\geq 10,0$
f_{Utuk} / f_{Utek}	$> 0,7$	$> 1,1$	$> 1,2$
ϵ_{Utu} ‰	$> 1,5$	$> 1,5$	$> 2,0$
f_{Uck} MPa	≥ 120	≥ 120	≥ 120

The American Concrete Institution (ACI) definition of UHPC is pending approval, but the proposed definition requires that a material shall have a minimum compressive strength of 21.7 ksi (150 MPa) and meet any “specified durability, tensile ductility, and toughness requirements.” It also states that fibers are generally included, meaning that a dense cementitious matrix meeting all other requirements could not have fiber within the matrix and still be considered UHPC (Perry, V. et. al, 2016). The Canadian Standards Association (CSA) are also developing a definition and standard for UHPC. The current CSA proposal defines several categories to be used to classify UHPC. The properties that define a UHPC’s category according to their system are the compressive strength, tensile strength, and tensile response. Table 2 displays these proposed categories. (Perry, V. et. al, 2016)

Table 2: Canadian Standards Association Proposed UHPC Classifications

Class		H	S	N
Mechanical properties		Strain Hardening Tensile Properties	Strain Softening Tensile Properties	Non-Fibre Matrices
	1	$f_c > 120$ MPa $f_t > 5.0$ MPa other mechanical & durability properties		
	2	$f_c > 120$ MPa 3.0 MPa $< f_t < 5.0$ MPa other mechanical & durability properties		
	3	$f_c > 120$ MPa $f_t =$ not required other mechanical & durability properties	-	-

Based on the aforementioned definitions of UHPC, the following definition was chosen for the purposes of this study: Ultra-High Performance Concrete is a material composed of purposefully graded fine particles which create a dense cementitious matrix. This dense cementitious matrix typically includes fiber. For the purposes of determining the effect of fibers on UHPC, some specimens were tested with no fiber. However, UHPC used in the field must include fibers or an alternative method of reinforcement as both the tensile and compressive failure modes are brittle and catastrophic without reinforcement that provides ductility. The minimum compressive strength for UHPC for the purposes of this study is 17 ksi (117 MPa). Tensile post-cracking behavior is not required for a material to be considered UHPC in this study as some UHPC's on the market may not achieve this behavior. However, UHPC without post-cracking strength should not be used for structural purposes without appropriate reinforcement and/or unless adequate testing has been performed.

2.2 UHPC Composition

Mix constituents of a typical Ultra-High Performance Concrete mix design include sand, cement, silica fume, crushed quartz, superplasticizer, water, and fiber reinforcement. According to the Vande Voort, these components are typically added by weight at the ranges seen in Table 3 (Vande Voort, 2008). Additionally, recipes for three UHPC's developed by R. Yu et. al in an experimental study can be found in Table 4 (R. Yu, et. al 2014). As can be seen in these tables, coarse aggregates are typically not included in UHPC mix designs. Instead, only fine aggregates are included in the dry mix constituents. These well-graded fine aggregates are combined to create a dense, purposefully-packed particle matrix (Vande Voort 2008). This matrix, which is designed through optimized particle packing models such as the modified Andreasen and Andersen packing

model, provides UHPC with its high compressive strength and durability characteristics (Yu, R. et. al 2014). Many commercial UHPC mix designs provide pre-portioned dry-mix constituents, simplifying the batching of such UHPCs.

Table 3: Typical UHPC Components

Component	Typical Range of Weight (Mass) per ft ³ (m ³)
Sand	31 - 87 lb (490 - 1390 kg)
Cement	38 - 67 lb (610 - 1080 kg)
Silica Fume	3.1 - 21 lb (50 - 334 kg)
Crushed Quartz	0 - 26 lb (0 - 410 kg)
Fibers	2.5 – 15.5 lb (40 - 250 kg)
Superplasticizer	0.6 – 4.5 lb (9 - 71 kg)
Water	7.9 – 16.3 lb (126 - 261 kg)

Table 4: Components for Three UHPC Mixes - R. Yu et. al

Component	UHPC 1 (kg/m ³)	UHPC 2 (kg/m ³)	UHPC 3 (kg/m ³)
CEM I 52.5 R	874.9	612.4	699.9
Limestone	0	262.5	0
Quartz	0	0	175.0
Microsand	218.7	218.7	218.7
Sand 0-2	1054.7	1054.7	1054.7
Micro-silica	43.7	43.7	43.7
Water	202.1	202.1	202.1
Superplasticizer	45.9	45.9	45.9
Water/cement ratio	0.23	0.33	0.29

2.3 Applications of UHPC

As UHPC has grown in use in the United States and throughout the world, the variety of structures UHPC is applied to has grown as well. Its primary application to date has been bridges, including application to bridge beams, decks, connections, and overlays. In addition to bridge applications, UHPC has been used for structural strengthening, retrofitting, and architectural applications. Many of these applications are designed to fully utilize one or more of the beneficial properties of the material including high compressive strength, tensile strength, durability, and bond to reinforcing bars.

According to the Federal Highway Administration, UHPC has been used in over 100 bridges in the United States and over 80 bridges in Canada. The most common application of UHPC in these bridges is in deck-level and composite connections with over 150 applications of UHPC in bridge connections. Other applications for which UHPC has been used on multiple projects include bridge beams/girders, pedestrian bridges, and overlays. Additionally, a variety of applications have explored optimizing UHPC for a particular design solution. These include applications of UHPC to waffle deck bridge solutions and seismic retrofit pier jackings. Many countries outside of North America are also using UHPC on projects varying from pedestrian bridges to complex architectural projects. The applications of UHPC discussed in this section demonstrate the successful use of UHPC in innovative ways that maximize the beneficial properties of the material.

2.3.1 Pedestrian Bridges

Sherbrooke Footbridge

The Sherbrooke pedestrian bridge was opened in Sherbrooke, Canada in 1997 and was the first application of UHPC in the world. The bridge is a 10-foot (3 m) deep open-web truss spanning 197 feet (60 m), and the design used Reactive Powder Concrete (RPC) which is an earlier term for UHPC. This RPC material was used in the deck which acted as the top chord of the truss and in the double beam which was used as the bottom chord. (Vande Voort 2008). The bridge consisted of precast, prestressed RPC members connected by diagonal members composed of RPC filled Steel tubes. As the first bridge composed of UHPC, it was very innovative in its use of UHPC. This especially true for the diagonal members which, due to heat treatment and confinement by steel tubes, exhibited RPC compressive strengths of 50 ksi (Blais and Couture, 1999). Figure 1 shows a picture of the finished bridge.



Figure 1: View of the finished Sherbrooke Pedestrian Bridge (FHWA, 2013)

Seonyu Footbridge

Also known as the Bridge of Peace, this slender arch bridge was constructed in Seoul, South Korea and opened in 2002. The bridge used a 394 foot (120 m) arch consisting of 6 RPS precast segments. These segments were joined using grouted post-tensioning to create a unique aesthetic that could not be achieved using conventional concrete. (Lafarge, 2009). Figure 2 contains a picture of the finished bridge.



Figure 2: View of the Seonyu “Footbridge of Peace” in South Korea (Lafarge, 2009)

2.3.2 UHPC Bridge Beams

Bourg-les-Valence Road Bridges

The Bourg-les-Valence Road Bridges in France were the first road bridges to be built with UHPC. The two bridges were built using five pre-tensioned pi-girders composed of UHPC with each bridge having two span lengths of 72.2 ft (22 m). These girders were connected using cast-in-place UHPC joints. Although not the first bridge composed of UHPC, as the first road bridge,

it paved the way for the UHPC applications that followed (Lewin, T. et. al 2010). Figure 3 shows a picture of the central pier of the bridge during construction.



Figure 3: Road Bridge at Bourg-les-Valences. Central pier during placing of pi-shaped beams (Vergoossen, 2008)

Mars Hill Bridge

The Mars Hill Bridge was constructed in Wapello County, Iowa in 2006. It was the first highway bridge constructed out of UHPC in North America and consisted of three 110-foot (33.5-m) long precast, prestressed beams. The beams used were a modified version of the standard 45-inch (1.14-m) deep Iowa bulb-tee beam. The modified beam section was designed to optimize the tensile and compressive properties of UHPC, allowing for a smaller cross-section and, thereby, a lighter member compared to conventional concrete. Additionally, the beams were designed with no rebar stirrups for shear purposes, instead relying on the superior tensile strength provided by the fiber to handle all shear loads. This bridge design was innovative in many ways and set the

stage for UHPC growth in bridge applications in the United States (Lewin, 2010). Figure 4 shows a photograph of the completed Mars Hill Bridge.



Figure 4; Photo of the completed Mars Hill Bridge (FHWA, 2013)

Jakway Bridge

The Jakway Bridge was built in Buchanan County, Iowa in 2008 and used prestressed UHPC pi-girders specifically optimized for UHPC. It was a 112.3 foot (34.2 m) long three-span bridge with each span containing three girders. The central span was composed of UHPC girders while the others were composed of conventional concrete. Therefore, three UHPC girders were used on the project. It is notable that no stirrups were needed in this pi-shaped girder as the fibers provided adequate shear capacity for the structure (FHWA, 2013). Figure 5 shows a picture of the finished bridge and Figure 6 shows the cross-section of the pi-shaped girder used for the project.



Figure 5: Picture of the Jakway Bridge (FHWA, 2013)

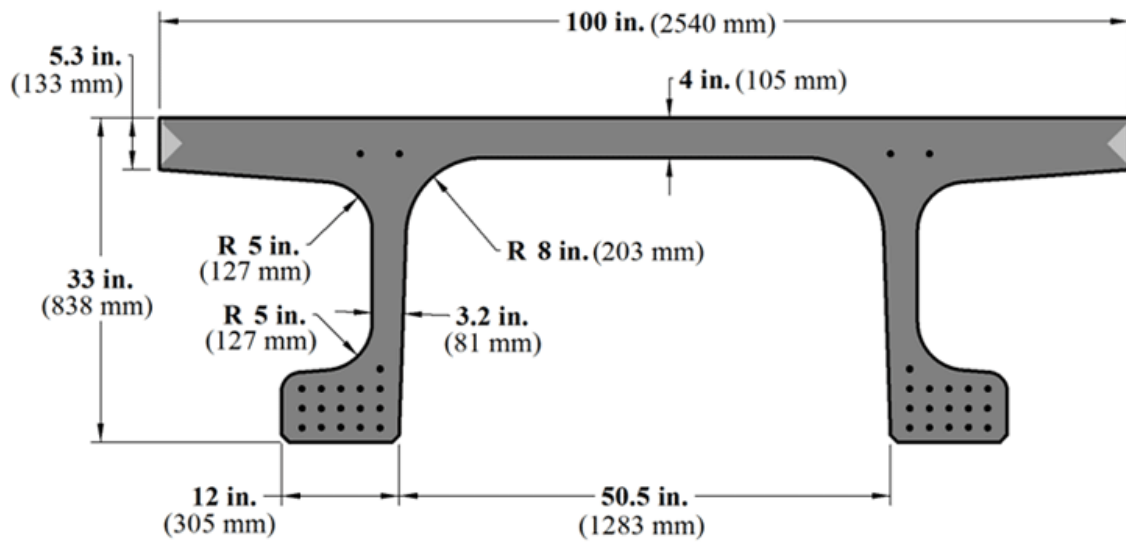


Figure 6: Cross-section of pi-shaped girder used in Jakway Park Bridge (FHWA, 2013)

2.3.3 Bridge Overlay

Chillon Viaducts

The Chillon Viaducts are two parallel reinforced concrete highway bridges near Montreux in Switzerland and are considered to have high cultural value and economic importance in the region. These 2120 m bridges were opened to traffic in 1969 and during rehabilitation in 2012, early signs of alkali-aggregate reaction were discovered in the structure. As this condition can lead to deterioration of concrete compressive strength over time, a solution involving rehabilitation and strengthening was required. It was determined that an application of UHPC overlay with reinforcing bars would efficiently waterproof and reinforce the existing structure. The key innovation in this project was the use of a paver capable of placing a UHPC in a thin layer, allowing the construction to be completed more quickly while significantly reducing labor. Additionally, this was the first UHPC overlay completed in Europe. Figure 7 shows a picture of the viaducts during construction.



Figure 7: Construction being performed on the Chillon Viaducts (Source: Ductal)

2.3.4 Other Structural/Durability Applications

H-shaped UHPC piles

In an effort to increase the durability of foundations, a tapered, H-shaped, precast, prestressed UHPC pile was developed at Iowa State in 2008. This pile was designed to replace steel H-shaped piles in order to increase the longevity of bridge foundations. The designed UHPC pile performed well under applied loads during testing and was determined to be an adequate replacement for steel H-piles. After achieving success in the initial testing stage, a UHPC H-pile was placed in a bridge in Iowa and monitored over time. Thus far, the pile has performed well and has proven that UHPC piles are a viable solution when pile durability is key. Figure 8 shows the initial test UHPC pile being tested in the field (Sritharan, 2015).



Figure 8: Experimental precast pile made of UHPC (Source: Iowa State University)

Little Cedar Creek Bridge

The Little Cedar Creek Bridge is a full-depth precast UHPC waffle deck bridge constructed in Wapello County, IA in 2011 as part of the FHWA's Highways for LIFE program. This unique bridge design was chosen in order to optimize the high compressive strength, high tensile strength, and durability of UHPC. One of the primary advantages of applying UHPC to bridge deck applications is that UHPC's high durability resulting from its dense cementitious matrix prevents chloride penetration and early deck deterioration that can result from de-icing salts applied in the wintry months (Sritharan, 2015). Additionally, the thin, ribbed waffle deck design innovatively utilized UHPC's high compressive and tensile strength in a way that significantly reduced the self-weight of the structure while maintaining adequate strength capacity. All connections between the waffle deck and bridge girders utilized UHPC. Although the initial costs were too high to make it a viable solution in most situations (Heimenn, 2013), this bridge inspired the idea of a UHPC overlay which uses much less material and is more cost effective (Sritharan, 2015). Figure 9 shows a picture of a waffle deck panel and Figure 10 shows the bridge during construction.



Figure 9: UHPC waffle deck panel with formwork removed - panel upside down (Heimenn, 2013)



Figure 10: Setting the UHPC Waffle Deck panels (Heimenn, 2013)

Mission Bridge

The Mission Bridge was completed in British Columbia, Canada in 1973. Located in a high seismic zone, the bridge required retrofitting to bring the bridge piers in compliance with current seismic standards. After considering many solutions, an innovative UHPC pier-jacketing design was developed to address this issue. In order to retrofit the bridge piers, dowels were added into the existing concrete and an approximately 9-inch layer of UHPC material was poured to create a jacket around the existing column. This jacket extended from the base of the pier to a height of 10.5 feet. In addition to the innovation of seismic retrofitting with UHPC, the project also used ready-mix trucks to complete the project. Figure 11 shows a photograph of the finished UHPC pier retrofit.



Figure 11: Picture of finished Mission Bridge pier jacketing (Source: Ductal)

Caderousse Dam

The Caderousse Dam in Vaucluse, France is a storage reservoir on the Rhône River. Originally opened in 1975, the dam was experiencing erosion on the wearing course of the floor slab due to abrasion by solid materials, and enough concrete had eroded that the structural reinforcement could be seen. UHPC was applied to the affected area to remedy the situation and provide long-term durability to the floor slab. This application displays how UHPC's durability makes it an ideal fit for rehabilitation of hydraulic structures. Figure 12 shows a view of the floor slab rehabilitated with UHPC.

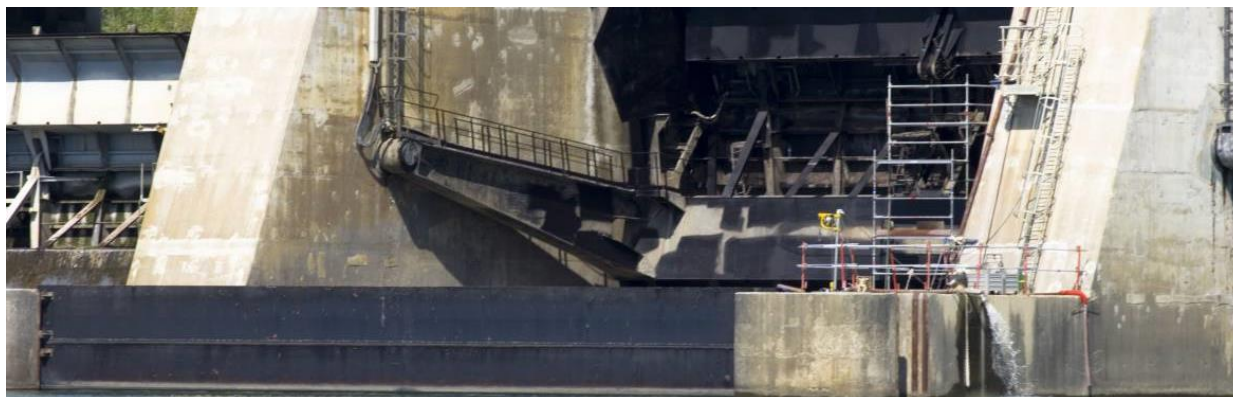


Figure 12: Picture of Caderousse Dam (Source: Ductal)

Wind turbine towers

As the wind turbine industry goes towards taller wind turbine towers to harvest the higher wind speeds that occur at those heights, logistical issues arise with the steel turbine towers traditionally used. Therefore, a tall UHPC wind turbine tower design was developed at Iowa State University to overcome this challenge. This tower design, termed Hexcrete, is a hexagonally shaped wind turbine tower and is comprised of segments of six concrete columns and six concrete panels. In the proposed design, the columns are composed of high strength concrete and the panels are composed of UHPC. This innovative use of UHPC is still in the design phase, but it could significantly impact the wind energy industry and the way UHPC is utilized in structures. Figure 13 contains concept drawings of this tower (Sritharan, 2015).

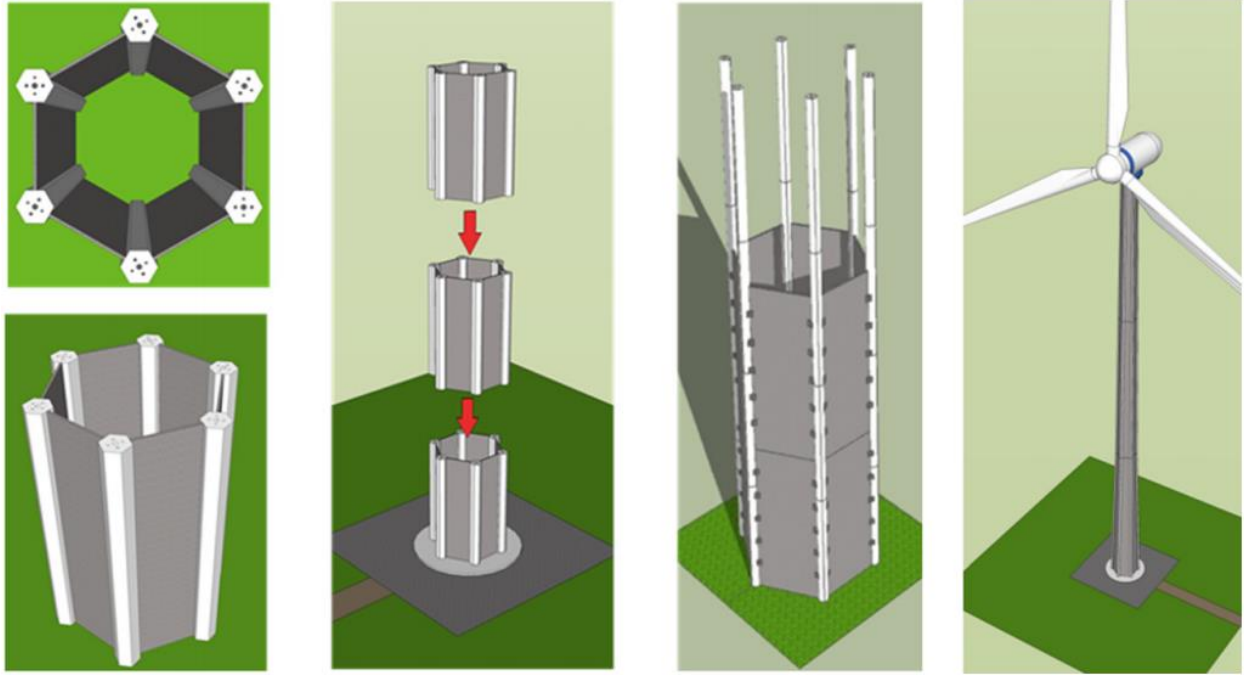


Figure 13: Conceptual design for building a 100 m and taller Hexcrete wind turbine tower (Sritharan, 2015)

2.3.5 Architectural Applications

Museum of European and Mediterranean Civilizations

The Museum of European and Mediterranean Civilizations (MUCEM) is one of the most advanced applications of UHPC in the world. This building includes UHPC in its columns, 115 m and 69 m pedestrian bridges, brackets, and most innovatively, in its tree-like façade. It is the first building in the world to make such extensive use of UHPC (Gu, C. et. al 2015). All UHPC members were prefabricated off site. Though there are many other architectural applications of UHPC that have been constructed, this was the first building to extensively use UHPC, and its lattice structure was very innovative (Mazzacane, P. et. al, 2013). A picture of the finished building can be found in Figure 14.



Figure 14: UHPC lattice facade and footbridge MUCEM (Photo by Rudy Ricciotti)

2.4 Material Properties

The general material properties of UHPC, such as high compressive strength, high tensile strength relative to conventional concrete, and high durability, are widely accepted. However, the exact recommended values for these properties vary as discussed in the UHPC Definition section. Therefore, this section will focus on the general material properties of UHPC with relevant experimental investigation used to define typical ranges of values. The tensile behavior of UHPC will be discussed in depth in a separate section as it is the primary focus of this study.

2.4.1 Compressive Behavior

The compression strength of conventional concrete is an essential property in defining the material. This remains true for UHPC as the high compressive strength due to the dense

cementitious matrix is one of the most significant benefits the material provides. Typical UHPC compressive strengths range from 17.4 – 29.0 ksi (120 - 200 MPa) according to the EPFL (2016) and ASTM defines the minimum compressive strength of UHPC as 17 ksi..

Many UHPC definitions set a minimum compressive strength for a material to be considered UHPC, such as the FHWA, ACI, ASTM, and the French UHPC Recommendations. It is noteworthy that a standard compression test method for UHCP has been released by ASTM. This standard requires UHPC 3” x 6” cylinders, and in order for a material to be considered UHPC, it must have a compressive stress greater than 17 ksi. The compressive strength of UHPC is largely gained by its dense, well-graded dense cementitious matrix and low water-to-binder ratio. However, other factors, such as addition of fibers, curing conditions, and confinement affect the compressive strength as well.

Without fibers, UHPC exhibits nearly pure linear-elastic behavior under compression. When 70-80% of the peak stress is reached, the modulus of elasticity becomes nonlinear (Fehling, 2004). UHPC with no fibers results in a sudden, explosive failure with little warning due to the high compressive strength of the material and lack of fibers to hold the specimen together at failure. While fibers are typically added to UHPC to increase its tensile ductility, these fibers also have a significant effect on its compressive strength. According to Vande Voort (2008), the average compressive strength gained by adding 2% steel fiber by volume to a UHPC mix is 30%. Other researchers report a lower strength gain due to fiber, such a Fehling (2004) who reported report a strength gain of only 15% due to 2% steel fiber by volume.

Another factor affecting UHPC compressive behavior is the curing condition applied to the material. In order to increase the compressive capacity of UHPC, heat treatment or confining pressure during curing may also be applied. With heat treatment, strength is gained primarily through the reduction of the UHPC's porosity. When a standard heat treatment of 190 °F for 48 hours was applied to UHPC, an increase in average compressive strength of 33% was observed based on 5 different studies (Vande Voort, 2008). Confining of UHPC is another way the compressive strength of the material can be significantly increased. Confinement can either be applied during curing of the concrete or through mechanical methods such as use of steel tubes. Heat treatment and confinement can be combined if large increases in compressive strength are desired. Both of these techniques were used in the diagonal members of the Sherbrooke Bridge (See Section 2.3.1), resulting in 50 ksi (350 MPa) compressive strength. This represents a 67% increase versus the non-confined UHPC used in the bridge (Vande Voort, 2008). The compressive stress-strain curve for UHPC is very similar in shape to the compressive stress-strain curve for conventional concrete. As with conventional concrete, age of concrete has a significant effect on the compressive strength and behavior of UHPC.

2.4.2 Flexural Behavior

In general, flexural tests are performed on concrete sections as an alternative way to characterize tensile behavior. For UHPC, these flexural tests provide valuable insight into the post-cracking behavior of UHPC. Tests conducted by the FHWA explored the cracking of lightly reinforced UHPC beams in flexure by counting and measuring cracks that occurred in a beam with a digital microscope (Meade, 2010). Figure 15 and Figure 16 contain results from these flexural

tests. In each graph, the first number denotes the percent fiber by volume and the second number denotes rebar configuration.

From the load-displacement figures, it is clear that the flexural behavior of fiber-reinforced UHPC is initially linear elastic until cracking begins to occur. After this point, the behavior becomes nonlinear and the applied load continues to increase. After the ultimate load is reached, the applied load gradually drops until fiber or rebar fracture occurs in the beams. As mentioned previously, fibers bridge the micro-cracks that form in UHPC and allow for loading past the cracking point. Beam S2-0 in Figure 16 shows a load-displacement graph for a UHPC beam with fiber dosed at 2% by volume and no reinforcing bar. This graph displays the engagement of fibers to bridge micro-cracks and enable nonlinear behavior in the beam, thereby preventing brittle failure.

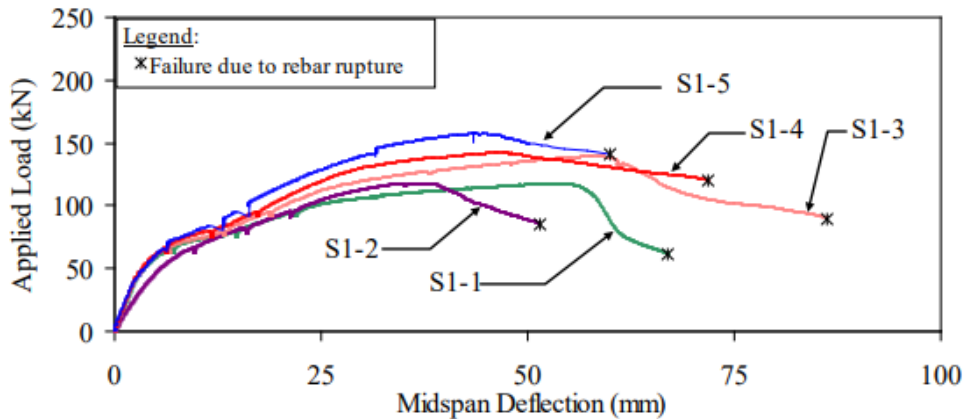


Figure 15: Load-deflection responses for each series of beams - beams with 1% fiber

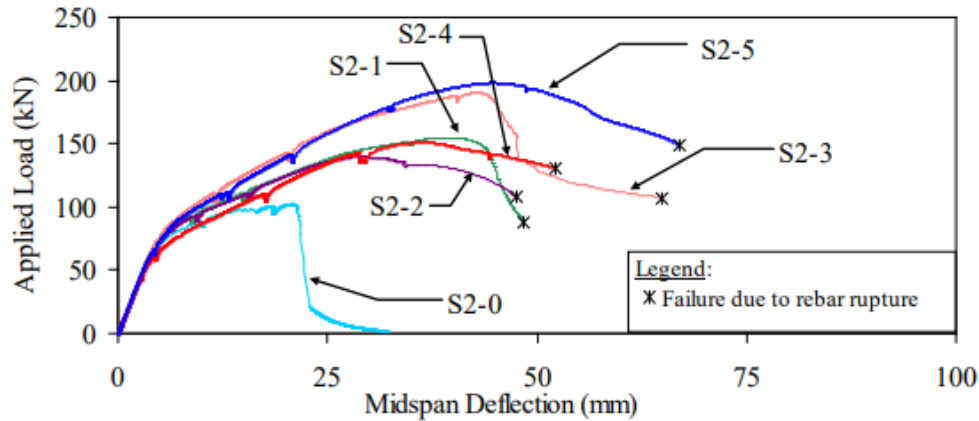


Figure 16: Load-deflection responses for each series of beams - beams with 2% fiber

2.4.3 Modulus of Elasticity

The Modulus of Elasticity for UHPC is 7,250 ksi (51.9 MPa) for steam cured specimens and 6,200 ksi (47.6 MPa) for specimens cured in laboratory conditions according to the FHWA (2013). However, no standardized equations exist for calculating the modulus of elasticity for UHPC. Significant research has been performed to develop equations for determining the modulus of elasticity for UHPC, and equations have been proposed by several different researchers. Some equations proposed by various researchers can be found on the next page.

$E = 50,000 \cdot \sqrt{f'_c}$	$(E = 4150 \cdot \sqrt{f'_c})$	(Sritharan et al. 2003)
$E = 46,200 \cdot \sqrt{f'_c}$	$(E = 3840 \cdot \sqrt{f'_c})$	(Graybeal 2007)
$E = 2,373,400 \cdot \ln(f'_c) - 468,910$	$(E = 16,364 \cdot \ln(f'_c) - 34,828)$	(Ma et al. 2002)
$E = 525,000 \cdot \sqrt[3]{f'_c}$	$(E = 19,000 \cdot \sqrt[3]{f'_c/10})$	(Ma et al. 2004)

2.4.4 Poisson's Ratio

According to the FHWA (2013), Poisson's Ratio for UHPC varies slightly based on author.

The values proposed by various researchers are in the range of 0.16 to 0.21. However, all but one

value is in between 0.18 to 0.21 with the average reported value equal to 0.19. The EPFL Recommendations provide a value of 0.2 for Poisson's ratio (EPFL, 2016). Based on these results a value of 0.19 or 0.2 should be used for Poisson's Ratio for UHPC.

2.4.5 Thermal Properties

Thermal properties of UHPC must be considered when high thermal fluctuations are expected. Coefficients of thermal expansion (COTE) have been investigated by various researchers with results giving values ranging from 5.6-8.7 millionths/°F. The average COTE value from results summarized by the FHWA is 7.2 millionths/°F (FHWA, 2013). The French Recommendations state a value of 6.1 millionths/°F if no other value can be determined (FGAC, 2013).

2.4.6 Bond Strength

UHPC has a significantly higher bond strength with reinforcing bar compared to conventional concrete. This higher bond strength allows the development length for reinforcing bar to be much lower in UHPC. This in turn allows UHPC to be extremely beneficial in precast bridge connections as rebar bends which are typically required for other materials, such as conventional concrete and grouts, are not required for UHPC to fully develop the strength of the bar. This leads to much less congestion in joints in the field which in turn makes construction significantly easier (FHWA, 2014).

2.4.7 Impact Resistance

Results from investigations on impact resistance performed by Bindiganvile et. al showed that UHPC is two to three times stronger in flexure than conventional steel Fiber Reinforced Concrete (FRC) under quasi-static loading. Additionally, UHPC absorbed three times greater energy than conventional FRC under quasi-static loading. This difference in flexure strength and absorbed energy increases even further under impact loading. UHPC is twice as strong as conventional FRC and dissipates three to four times as much under impact loading (FHWA, 2013).

2.4.8 Creep

Concrete creep is a measure of the change in length over time in a specimen subjected to constant loading. Investigations performed by Graybeal were conducted by subjecting specimens to a constant axial stress in accordance with ASTM C512. These tests determined that creep coefficients after one year ranged from 0.29 to 0.78 for 4-in diameter UHPC specimens loaded at ages 4, 21, and 28 days depending on the method of curing. The specific creep, which is a measure of creep strain/applied stress, ranged from 0.04 to 0.15 millionths/psi. Specific creep values for conventional concrete are in the range of 0.25 to 1.0 millionths/psi (FHWA, 2013).

2.4.9 Shrinkage

Two types of shrinkage may occur in Ultra-High Performance Concrete including drying shrinkage caused by the loss of moisture from the material and autogenous shrinkage caused by a decrease in volume as hydration of the cementitious material occurs. The ASTM standard test method is designed to measure drying shrinkage. Therefore, other methods must be used to determine autogenous shrinkage. Shrinkage tests conducted by FHWA resulted in an ultimate

shrinkage value of 555 millionths for untreated specimens. Results from test conducted by other researchers varied slightly with the highest shrinkage value being 900 millionths (FHWA, 2013).

2.5 Tensile Behavior

The tensile strength of conventional concrete in design is assumed to be zero for reinforced concrete structures and $6\sqrt{f_c'}$ in prestressed concrete structures. However, the tensile strength of UHPC is much higher than conventional and high strength concrete due to the discontinuous fiber reinforcement generally included within the matrix. This fiber typically provides substantial post-cracking strength in UHPC, bridging micro-cracks and providing ductility to the material, even without the presence of reinforcing bar.

The tensile behavior of UHPC has been the subject of intense experimental investigation over the past several years and continues to be a major subject of research within the UHPC community. One of the significant roadblocks to determining a definition for the tensile behavior of UHPC is the lack of a standardized test method. This lack of standardized test method results in a wide variety of tensile test methods being used to determine tensile behavior. Additionally, the complexity of testing a concrete material containing discontinuous fiber reinforcement in tension makes defining the tensile behavior of UHPC difficult. Adding complexity is the variation in fiber distribution and orientation that must be accounted for in field applications. This section discusses the various tensile testing methods conducted by researchers to determine the behavior of UHPC. It also discusses relevant investigations into UHPC tensile behavior performed by other researchers including the specific testing methods used, tensile results observed, and tensile behavior models proposed by such researchers.

2.5.1 Tensile Test Methods

Many researchers have studied the best way to obtain the tensile behavior of UHPC. However, no consensus exists on the best way to determine the tensile behavior of UHPC and no standardized test method has been implemented as a variety of tensile test methods are currently being recommended by entities from several different countries. The tension test methods used for determining the tensile behavior of UHPC can be split into two primary categories: direct tensile tests and indirect tensile tests. Each category has its advantages and disadvantages, and due to these, the debate over which tensile test method should be used is ongoing.

Direct Tensile Test Methods

Direct tensile testing methods subject a specimen to direct tension forces in order to determine the tensile behavior of the material. These testing methods are desirable because they directly and accurately provide the tensile behavior of the material. However, no standardized testing method exists for direct tensile testing of UHPC resulting in specimens with many different sizes and shapes being tested. Furthermore, direct tensile tests require specific laboratory testing equipment not commonly found in the concrete industry. This equipment is commonly used for testing of steel specimens, but appropriate adjustments must be made to this equipment for testing of UHPC. Specimen preparation and test execution for direct tension tests is difficult to perform due to challenges in obtaining evenly distributed stresses across the cross-section and controlling a stable load versus displacement response. Additionally, direct tension tests require significant time and effort to perform (Wille, et. al., 2014).

Several variations of direct tensile tests have been performed by researchers, and within these variations, distinct categories can be defined. Direct tensile test specimens typically have one of three shapes according to Wille et. al (2014): unnotched, notched, and tapered. Each specimen shape has its benefits, but the tapered “dog-bone” specimens are often used because they allow for approximately uniform stress to be applied throughout the tapered portion of the specimen. Notched specimens simplify the test setup by forcing cracking to occur at the location of the notch in the specimen, thereby making data collection easier. However, notched specimens are not appropriate for characterizing elastic or strain hardening behavior as the predetermined plane of failure and sudden change in cross-section results in stress localization which causes earlier crack initiation. Furthermore, multiple cracks are not able to form in such specimens due to the small height of the notch. Unnotched specimens with top glued ends are useful for determining the elastic behavior of the material but are not appropriate for capturing strain hardening behavior. Side glued unnotched specimens have successfully obtained strain hardening behavior. However, as the cross-section of failure could occur anywhere in the specimen during testing, it is difficult to accurately capture data from such specimens. This is because the measurement length should remain away from the ends of the specimens to avoid constraints provided by the supports. However, the cross-section of failure may occur near the supports making the local crack behavior potentially difficult captured for such specimens (Wille, et. al, 2014).

Specimen connections for direct tensile tests can be defined by three possibilities according to Dobrusky and Bernardi (2017): freely-rotating, fixed-ends, and active control for fixed supports. Freely-rotating connections allow the specimen to rotate freely at the ends, thereby prevent any bending moment from occurring in the specimen. This results in accurate cracking stress results

but inaccurate post-cracking behavior. The inaccurate post-cracking behavior observed in these tests is due to local inconsistencies in stiffness at the plane of the first crack resulting in rotation and fiber pullout at this crack prior to the generation of a full set of additional cracks (Bernardi, 2017).

Meanwhile, specimens with fixed-end connections prevent any rotation from occurring at the ends of the specimen. This results in specimens experiencing a bending moment if any accidental eccentricity exists in the test setup. Since some amount of accidental eccentricity is unavoidable, one side of the specimen will inevitably experience higher tensile stress, likely causing the specimen to crack first on that side. Therefore, the cracking stress observed in these tests is lower than the actual cracking stress of the UHPC. However, the post-cracking behavior of the UHPC is accurately captured for tests with fixed-ends, making it the preferred choice for many researchers, including the FHWA. The final connection type proposed by Dobrusky and Bernardi, active control for fixed supports, has yet to be conducted and is therefore theoretical (Bernardi, 2017).

Indirect Tensile Test Methods

Indirect tensile test methods are desirable because they are faster and easier to conduct than direct tensile tests. Indirect tensile tests require equipment that is already common within the concrete industry, and typical indirect tension test methods include flexural tests and split cylinder tests. However, these tests results require assumptions and high computational effort to determine the final tensile properties of the material. Additionally, final tensile properties calculated from flexural tests may significantly overestimate the tensile strength of the material due to differences

in the assumed moment curvature for tensile computations and actual moment curvature that occurs during testing (Wille, et. al, 2014).

2.5.2 Tension Tests by Others

Development of direct tension test method for Ultra-High Performance Fiber Reinforced Concrete - Graybeal and Baby (2013)

The tensile behavior model proposed by the FHWA was developed in an experimental investigation by Graybeal and Baby (2013). The focus of this test investigation was developing a practical direct tensile testing model for UHPC. The requirements set for this test method were that the method accurately capture the uniaxial tensile mechanical response of UHPC in tension from elastic behavior to formation of the localized crack. Therefore, rotation must be prevented at specimen end connections to ensure non-uniform localization of individual cracks so that post-cracking behavior may be accurately captured. Additionally, flexural strain in the specimen was to be minimized, and specimen preparation was to be kept as simple as possible to allow for relatively short testing times.

The recommended test method based on this investigation involved attaching tapered aluminum plates to prismatic specimens and gripping the specimen directly with an MTS tensile testing unit or equivalent to apply a tensile load. Specimens with various lengths were investigated to determine the effect of specimen length on test results. Additionally, tests were conducted with two different UHPC mixes and one UHPC mix was tested with 2% and 2.5% fiber by volume under two different curing conditions: steam cured and laboratory cured. The proposed tension test method uses four Linear Variable Transducers (LVDTs) to measure the displacements which are

used to calculate strain. One LVDT was placed on each of the four specimen sides. A figure of sample test specimen dimensions and tension test setup can be found in Figure 17 and Figure 18 respectively.

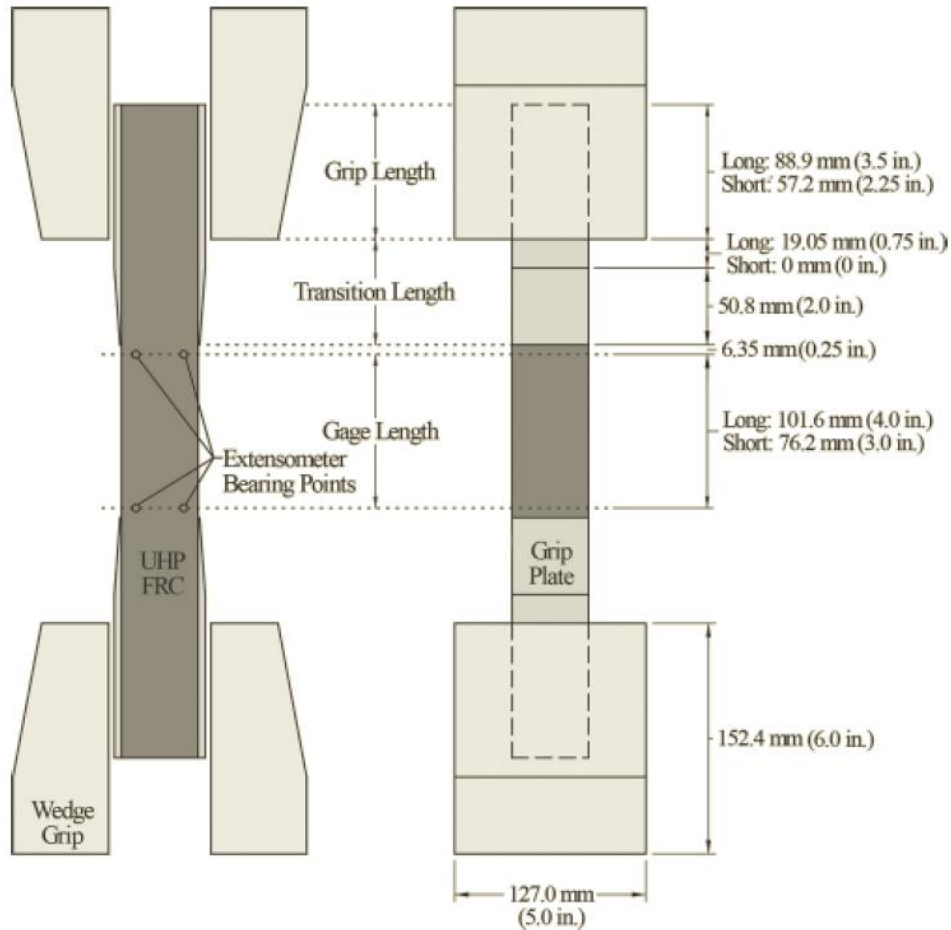


Figure 17: Sample direct tensile test specimen dimensions and gripping method (Graybeal and Baby, 2013)

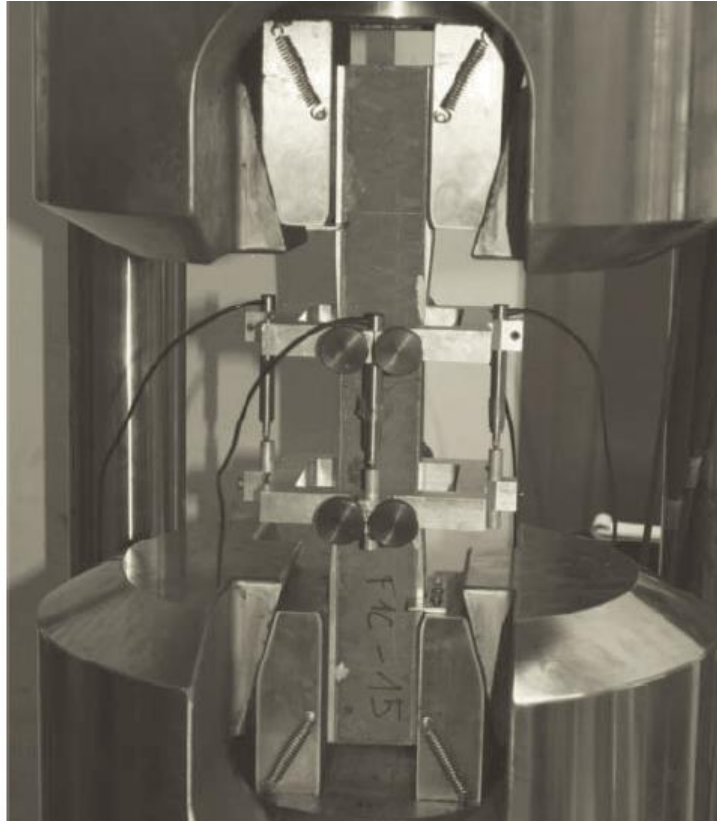


Figure 18: Testing of a 17 inch (431.8 mm) long specimen (Graybeal and Baby, 2013)

In this study, it was observed that first-cracking stress depended highly on curing method and slightly on the length of specimens. Average cracking stresses ranging from 900 psi to 1,300 psi (6.18 MPa to 9.09 MPa) were observed. Maximum tensile strength was observed to depend primarily on curing method and fiber content with specimen length also having a slight effect. Average maximum tensile strength values observed ranged from 1,240 psi to 1,675 psi (8.56 MPa to 11.56 MPa). The idealized tensile response model proposed by Graybeal and Baby based on results from this investigation can be found in Figure 19. Results from one specimen with labeled phases can be found in Figure 20. This model will be discussed further in Chapter 3.

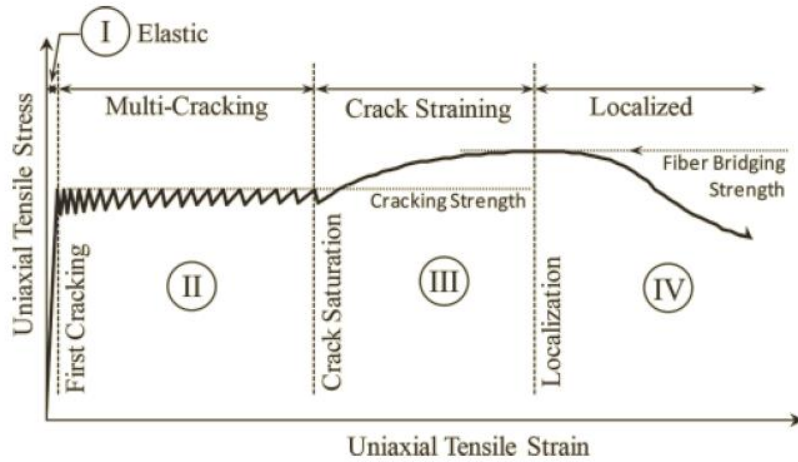


Figure 19: Idealized uniaxial tensile mechanical response of UHPC (Graybeal and Baby, 2013)

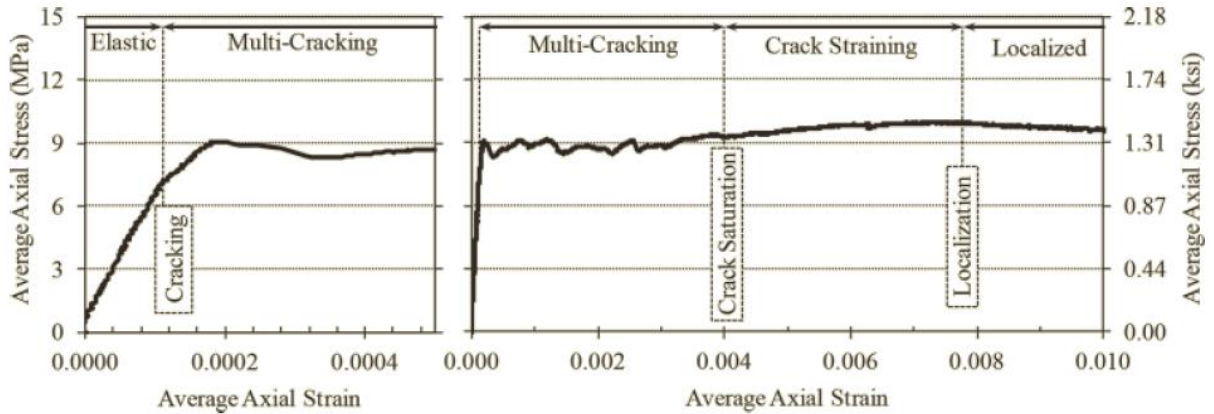


Figure 20: Uniaxial tensile stress-strain response from specimen (Graybeal and Baby, 2013)

It is noteworthy that tensile strain observed during testing varied based on the side from which the specimen data came. Due to the nature of UHPCs discontinuous fiber composition, variations in tensile cracking stress and maximum tensile capacity will occur across the cross-section of UHPC specimens. This will typically cause the specimen to crack on one side of the specimen first, whether there is a bending moment applied to the specimen or not. However, the

relatively high disparity in post-cracking facial strains from the average of the four facial strains suggests that bending moments may have been relatively large in these specimens. Figure 21 contains the facial strain disparity on the four sides of the specimen as reported by Graybeal and Baby (2013).

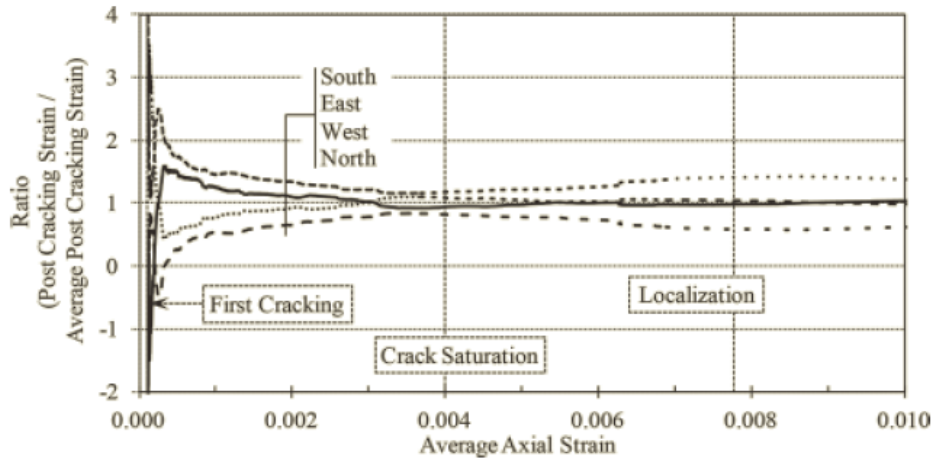


Figure 21: Post-cracking facial strain disparity from specimen data (Graybeal and Baby, 2013)

Strain-hardening UHP-FRC with low fiber contents - Wille, Kim and Naaman (2011)

This experimental investigation performed by Wille, Kim, and Naaman focuses on the optimization of UHPC strength and ductility under direct tensile loads. In this study, direct tensile tests were conducted on UHPC specimens containing four types of steel fiber at fiber contents varying from 1% to 2.5% by volume. Results from these tests show that 1% fiber by volume is adequate to trigger strain hardening behavior and multiple cracking for appropriate high strength steel fibers. This multi-cracking behavior is essential in achieving high ductility in UHPC according to the authors.

In this study, direct tensile loads were applied to dumbbell specimens with a middle cross-section of 1-inch by 2-inches (25.4 mm by 50.8 mm). Due to the thickness of the specimen and casting method, fibers tended to orient in the longitudinal direction, parallel to the direction of tensile loading. Specimens were attached to the tensile testing unit and loading was applied via the method in Figure 22. Displacement data was collected on two sides of the specimen via LVDTs over a gage length of 7 inches (177 mm). The load data from the load cell was combined with displacement data from the LVDT's to create the tensile stress-strain response of specimens.

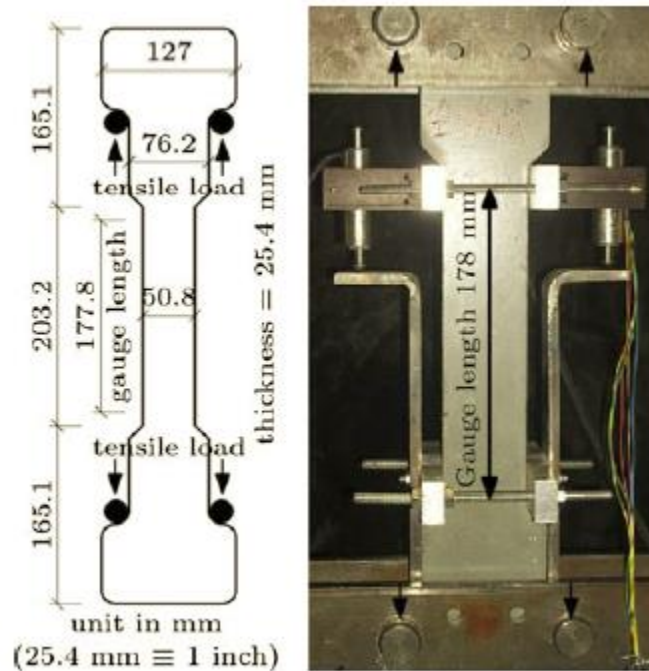


Figure 22: Geometry of direct tensile specimen, test setup, and load application method (Wille, et. al, 2011)

Direct tensile tests were conducted on specimens containing straight, smooth fibers, hooked fibers, fibers with high twist, and fibers with low twist at various fiber contents. Fiber contents ranged from 1% to 2.5 % by volume depending on fiber type. Pictures of all fiber types

used can be found in Figure 23. Results from these tests showed that increasing fiber content increased tensile cracking stress and maximum tensile strength for all fiber types. In these tests, fiber content was observed to have a greater effect on the average maximum tensile strength than on average cracking stress.

Average tensile cracking stress values ranged from 740 psi to 1070 psi (5.1 MPa to 7.4 MPa) with hooked fiber at 1% by volume exhibiting the lowest cracking stress and straight, smooth fiber at 2.5% by volume exhibiting the highest cracking stress. Average maximum tensile strength values ranged from 740 psi to 1070 psi (8.0 MPa to 14.9 MPa) with high twist fiber at 1% by volume exhibiting the lowest maximum tensile strength and high twist fiber at 2.0% by volume exhibiting the highest maximum tensile strength. Tensile results for each fiber type can be found in Figure 24 through Figure 27. Through this study, UHPC containing 1.5% low-twist fiber by volume achieved an average maximum tensile strength of 1.9 ksi (13 MPa) and maximum post-cracking strain of 0.6%.

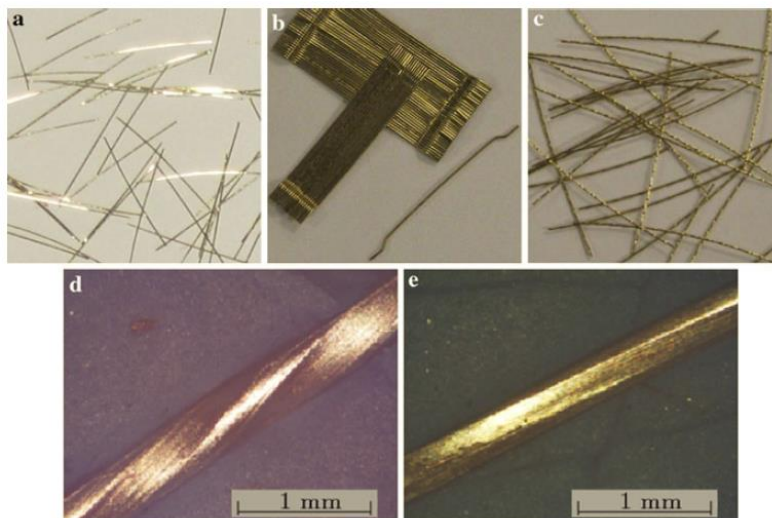


Figure 23: Steel fiber types used in this research, a) straight smooth fiber (S), b) hooked fiber (H), c) high twisted fiber (T1), d) high twisted fiber zoomed-in (T1), and e) low twisted fiber zoomed-in (T2) (Wille, et. al, 2011)

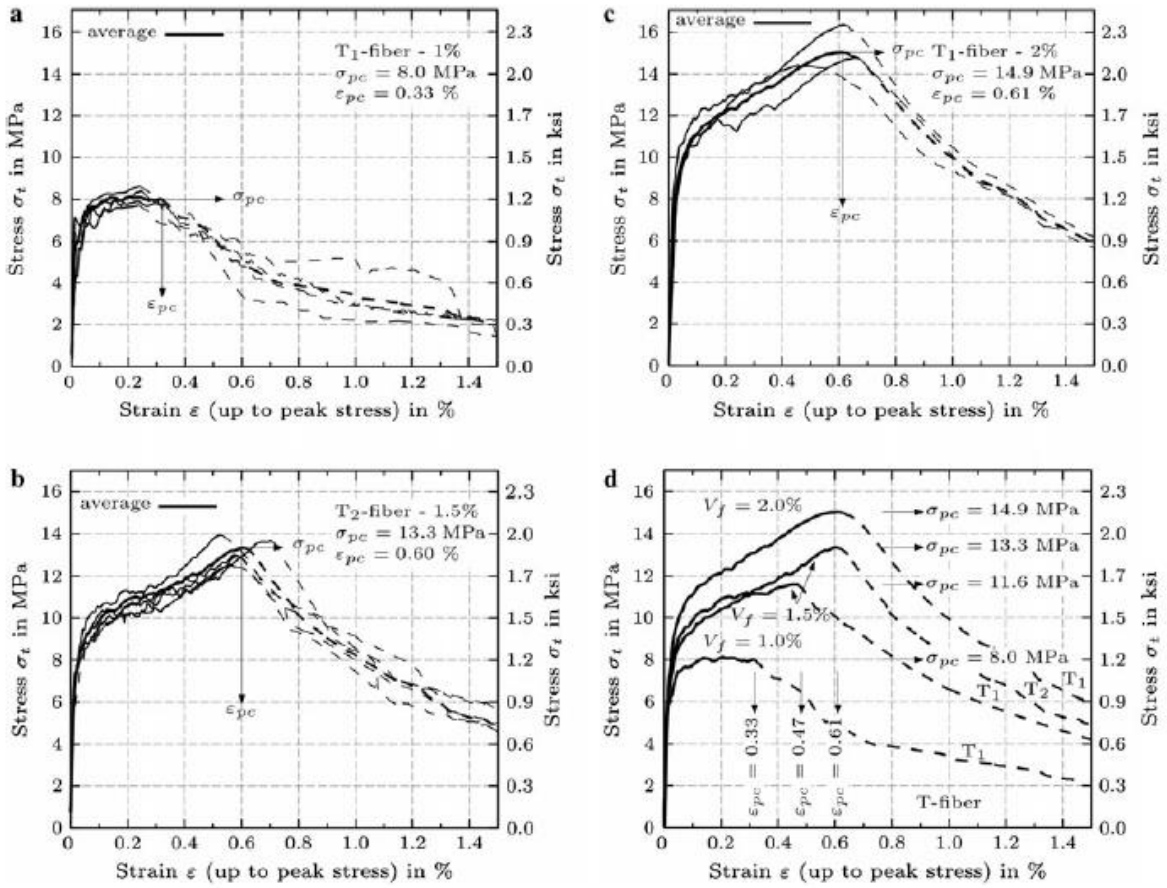


Figure 24: Direct tensile response of UHPC with twisted steel fibers, a) 1.0% high twist fiber, b) 1.5% low twist, and c) 2.0% high twist fiber, d) Comparison of average curves for twisted steel fiber (Wille, et. al, 2011)

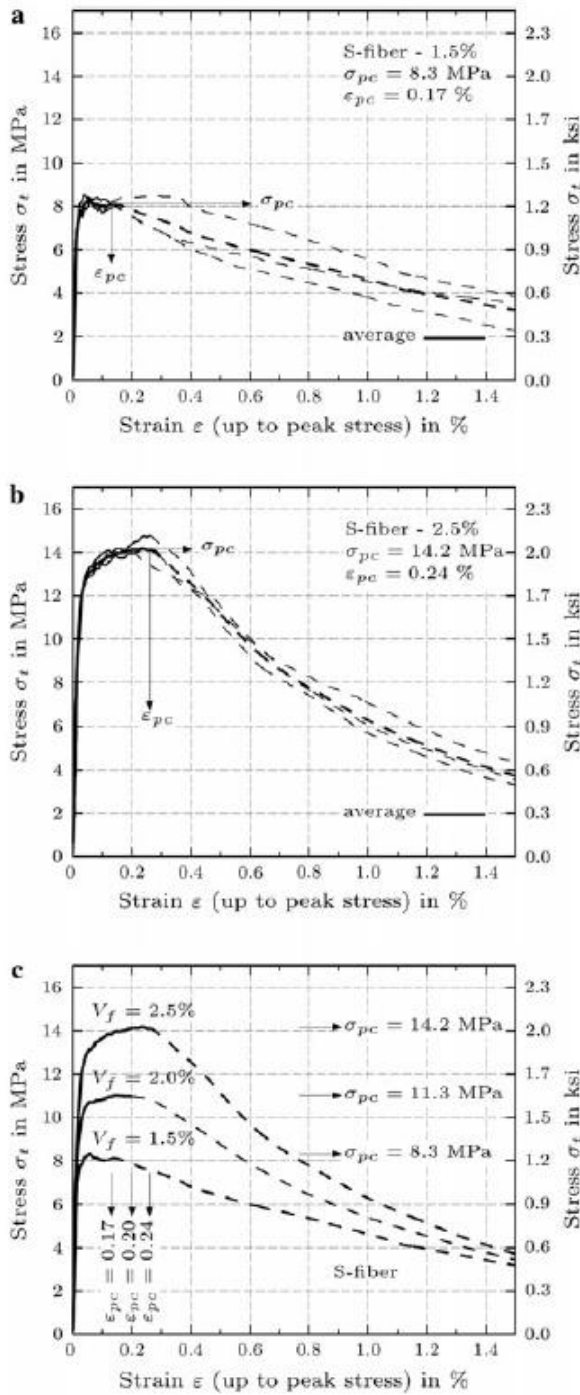


Figure 25: Direct tensile response of UHPC with smooth steel fibers, a) 1.5% by volume, b) 2.5% by volume, and c) Comparison of average curves for smooth steel fiber (Wille, et. al, 2011)

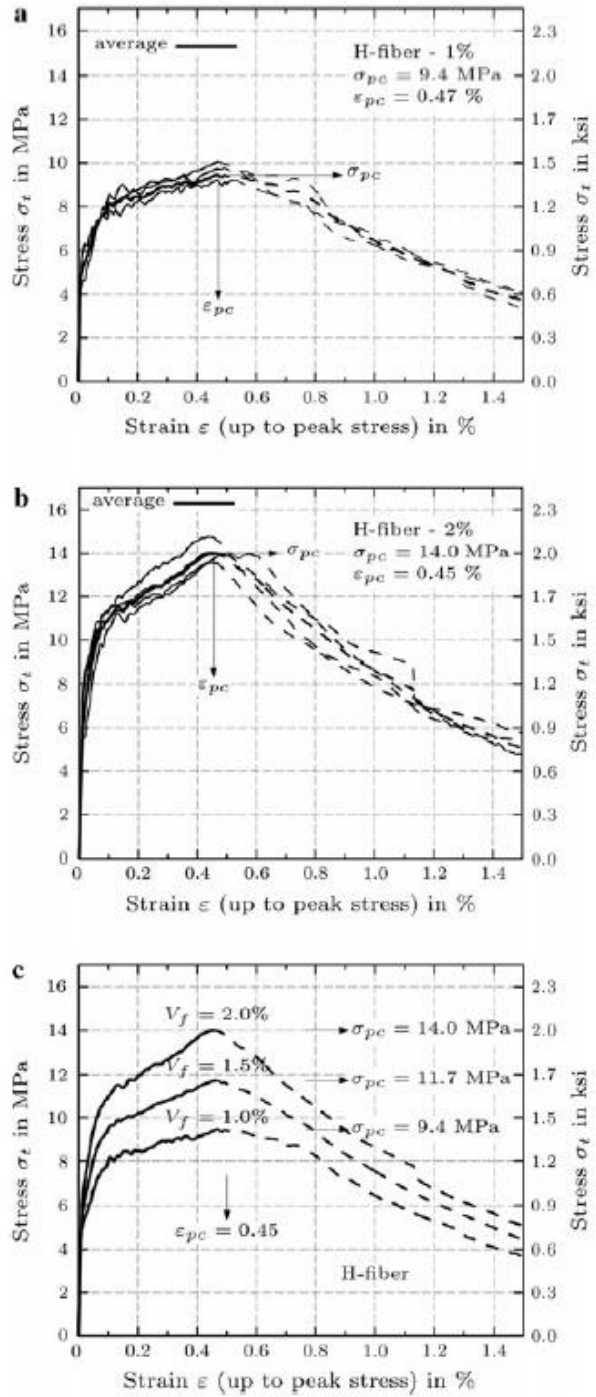


Figure 26: Direct tensile response of UHPC with hooked steel fibers, a) 1.0% by volume, b) 2.0% by volume, and c) 2.5% Comparison of average curves for hooked steel fiber (Wille, et. al, 2011)

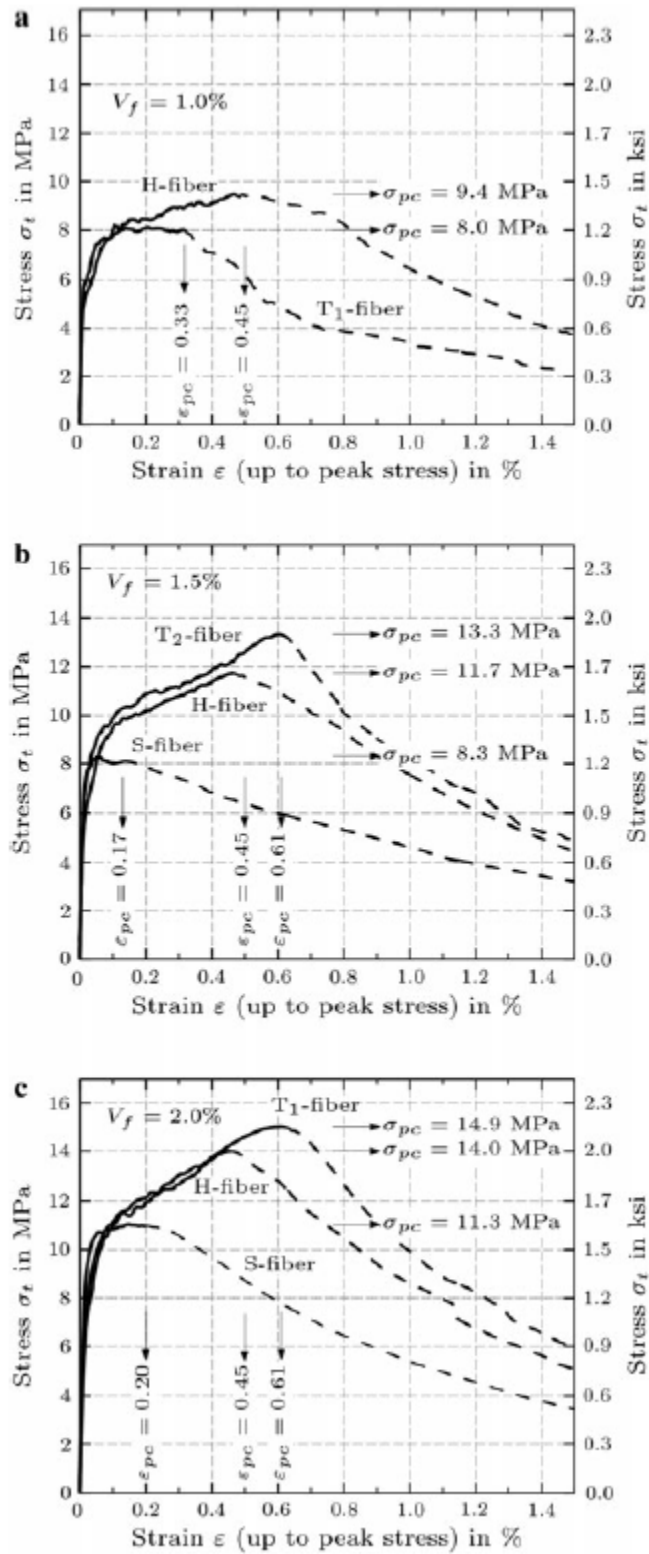


Figure 27: Comparison of direct tensile response of UHPC with different fiber types, a) 1.0% fiber by volume, b) 1.5% fiber by volume, and c) 2.0% fiber by volume (Wille, et. al, 2011)

Properties of strain hardening Ultra-High Performance Fiber-Reinforced Concrete (UHP-FRC) under direct tensile loading - Wille, El-Tawil and Naaman (2014)

This experimental investigation performed by Wille, El-Tawil, and Naaman focuses on determining the elastic, strain hardening, and strain softening tensile parameters of UHPC using a revised tensile test setup designed to obtain reliable results while minimizing the required preparation. Tests are conducted on UHPC specimens containing one of three steel fiber types, each dosed at three different volume fractions. Based on results from these tests, first cracking stress and strain, elastic and strain hardening modulus, composite strength, and energy dissipation capacity are characterized.

The paper begins with a discussion of a tensile performance classification system for UHPC. This tensile performance classification system categorizes tensile behavior from deflection softening to high energy absorbing. An overview of direct tensile test specimen shapes and boundary conditions conducted in previous experiments by others is then conferred. As previously discussed, specimen shapes include notched, un-notched, and dog-bone specimens. Specimen dimensions varied significantly between different experimental investigations with dog-bone shaped specimen cross-sections ranging from approximately 1" x 0.5" to 6" x 2" in the middle region of specimens. The various advantages and disadvantages of each general specimen shape and boundary condition are then discussed.

Figure 28 through Figure 30 display the various direct tension test specimens and boundary conditions used in tests by other researchers. After this overview, a specimen shape and test setup designed to ensure accurate results and minimize the required material and preparation is proposed. This test setup was used in the experimental investigation and can be found in Figure 31

Shape dogbone	Material (-)	Performance level (-)	Length, width and depth of constant area (total specimen) in (mm)			Diff. area	Grip/attachment	DOF ^a top-bottom
			L	W	D			
	UHP-FRC	4	80	30	13	50%	Fixed	0-0
	HPFRCC	3-4	80	24	40	60%	Fixed	0-0
	HPFRCC	4	152	38	76	50%	Self-clamping friction grip ^b	1-1
	HPFRCC	3	150	25	25	63%	Anchored/pinned	1-1
	HPFRCC	3	200	50	13	40%	Anchored/pinned	1-1
	UHP-FRC	3-4	178	51	25	41%	Anchored/pinned	1-1
	UHP-FRC	3-4	200	100	50	33%	Top glued/anchored	0-0
	UHP-FRC	3	250	100	35	50%	Side glued/pinned	1-1
	UHP-FRC	3	200	160	45	80%	Side glued + anchored (greased)	0-0
	HPFRCC	3-4	80	30	13/30	50%	Clamped/anchored/pinned	0/2-0/2
	Plain concrete	0	200	60	100	60%	Top glued	0-0
	Plain concrete	0	0 ^c	60 ^c	100 ^c	60%	Top glued/pinned	2-2
	Plain lightweight concrete	0	0	80 ^d	-	64%	Top glued/anchored	0-0

Figure 28: Dog-bone shaped specimens used in previous research (Wille, et. al, 2014)






Shape unnotched prism/cylinder	Material (-)	Performance level (-)	Length, width and depth of constant area (total specimen) in (mm)			Diff. area	Grip/attachment	DOF ^{top-bottom}
			L	W	D			
	FRC	<3	127	127	28	100%	Side glued/pinned	0-0
			(330)	(127)	(28)			
	FRC/ECC	3/4	205	76	13	100%	Side glued/pinned	0-0
			(305)	(76)	(13)			
	UHP-FRC	3	102	51	51	100%	Side glued + clamped /fixed	0-0
			(432)	(51)	(51)			
	UHP-FRC	3	160	70	70	100%	Top glued	0-0
			(160)	(70)	(70)			
	Plain concrete/UHP-FRC	0/3	200	100 ^b	-	100%	op glued	0-0
			(200)	(100) ^b				

Figure 29: Un-notched prism/cylinder specimens used in previous research (Wille, et. al, 2014)


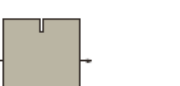


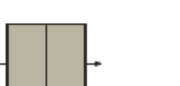

Shape notched prism/cylinder	Material (-)	Performance level (-)	Length, width and depth of constant area (total specimen) in (mm)			Diff. area	Grip/attachment	DOF ^{top-bottom}
			L	W	D			
	FRC	<3	2	51	51	44%	Top glued	0-0
			(152)	(76)	(76)			
	FRC	<3	3	42	50	70%	Top glued	0-0
			(55)	(60)	(50)			
	FRC	2	1	51	13	67%	Top glued	0-0
			(254)	(76)	(13)			
	UHP-FRC	3-4	~5	160	50	80%	Side glued + anchored (greased)	0-0
			(500)	(200)	(50)			
	FRC/UHP-FRC	2/3	2-5	135 ^a	-	81%	Top glued	0-0
			(150)	(150) ^b	-			
	UHP-FRC	3-4	2	44 ^b	-	35%	Top glued	0-0
			(60)	(74) ^b				

Figure 30: Notched prism/cylinder specimens used in previous research (Wille, et. al, 2014)

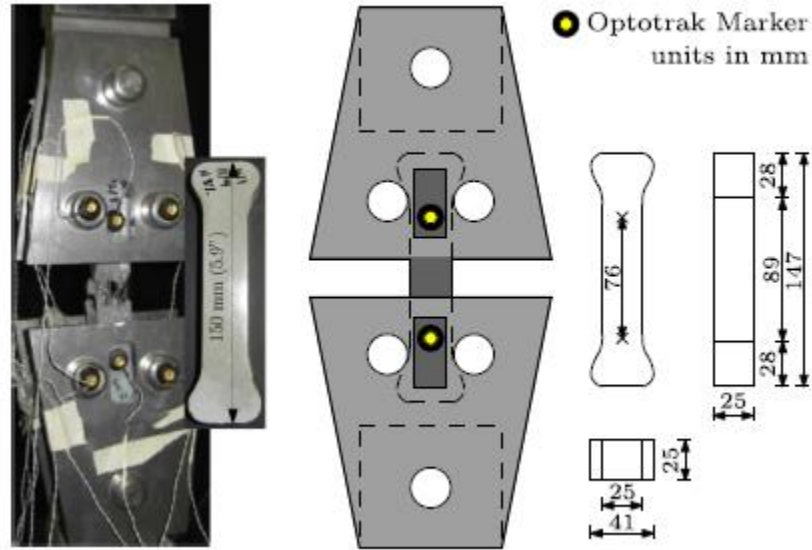


Figure 31: Direct tensile test setup used by Wille, et. al (2014)

In this study, the effects of smooth, hooked, and twisted fibers on UHPC tensile behavior were investigated. Results from these tests were analyzed to determine the idealized, bi-linear strain-hardening tensile behavior of specimens with each fiber dosed at three different fiber contents. Smooth fiber was observed to have a lower maximum tensile stress value than hooked and twisted fiber at a fiber content of 3% by volume. However, smooth fiber had the highest tensile strength by a small amount at 2% fiber by volume. The crack spacing observed at peak load ranged from 3 to 8 mm. Fracture energy values were also calculated for all specimens in this study. The progression used to analyze data can be found in Figure 32. The idealized strain-hardening curves for each fiber type can be found in Figure 33.

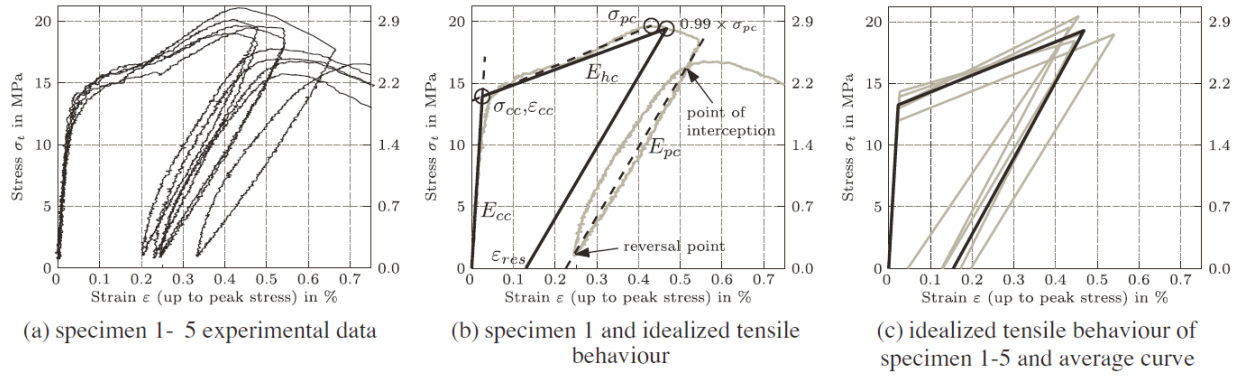


Figure 32: Analytical procedure for sample series of tests (Wille, et.al, 2014)

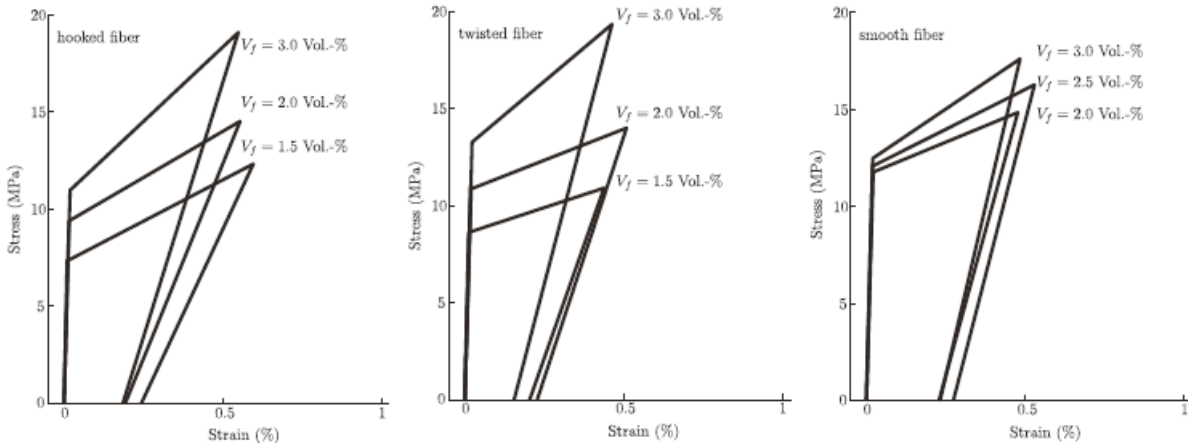


Figure 33: Comparison of bi-linear model for all specimens including unloading line (Wille, et. al, 2014)

CHAPTER 3: EXPERIMENTAL INVESTIGATION OF UHPC TENSILE BEHAVIOR

3.1 Experimental Procedure

3.1.1 Test Matrix

This section briefly details the specimens tested in this study. To determine UHPC micro-cracking behavior and the relationship between micro-crack and local crack formation and propagation, direct tensile tests were performed on over 30 dog-bone specimens. These specimens were composed of UHPC mixes provided by three different suppliers available in the United State market. Specimens contained various combinations of five different fiber types with fiber contents ranging from 0-2.75% by volume.

The naming convention used for these specimens denotes the supplier, specimen number, fiber type, and fiber content. The three suppliers who provided UHPC material for this study are designated as suppliers 1, 2, and 3. Specimens were numbered in the order in which they were tested. The various fiber types used were denoted with letters. If more than one fiber type was used in a specimen, multiple letters were included in the specimen name. Finally, the fiber content in each specimen was denoted with two numbers representing the percent by volume. The two numbers denoting fiber content represent the entire fiber content by volume. Therefore, if specimens contain more than one fiber type, the number representing fiber content in the specimen name denotes the total percent fiber, not the percent fiber of each type. The percent of each fiber type in specimens with more than one fiber type can be found in the results section. The numbering for fiber content is as follows: 25 = 2.5% fiber by volume, 20 = 2.0%, 10 = 1.0%, 00 = 0.0%.

Figure 34 explains this naming convention. Table 5 contains the various combinations of UHPC mix, fiber type, and fiber content that were tested in this experimental investigation.



Figure 34: Specimen Naming Convention

Table 5: Test Matrix

Specimen Name	Supplier	Percent Fiber	Fiber Type	Number of Specimens
S1X.22.A20	1	2	A	3
S1X.22.A10	1	1	A	3
S1X.22.X00	1	0	None	3
S2X.22.BC28	2	2.75	B, C	3
S2X.22.BC25	2	2.5	B, C	3
S2X.22.BD20	2	2	B, D	3
S2X.22.BD10	2	1	B, D	1
S2X.22.X00	2	0	None	2
S2X.22.D20	2	2	D	2
S2X.22.D10	2	1	D	2
S2X.22.A20	2	2	A	2
S3X.22.AE20	3	2	A, E	3
Total				31

3.1.2 Casting of Specimens

Specimens composed of UHPC from the same supplier and containing the same fiber type and fiber content were cast from the same batch of UHPC. The casting procedure for specimens involved pouring UHPC material into the higher side of dog-bone specimen molds placed at a

slight angle, allowing the UHPC to flow from one end of the mold to the other. This casting procedure allowed fibers to primarily align longitudinally within the specimen, parallel to the direction of flow.

Although, longitudinal alignment of fibers would not necessarily occur in a structure cast in the field, it is impossible to cast specimens in a way that applies to all field cast structures. This is because fiber orientation in the field depends highly on UHPC application and placement method. Even slight variations in casting procedure can have a notable effect on fiber orientation. Therefore, to capture the true tensile behavior of UHPC for field cast applications, specimens must be cast in the exact same way as the UHPC in the field. For these reasons, a casting method allowing fibers to align primarily in the longitudinal direction was chosen to ensure consistency. This allowed results from specimens composed of UHPC mixes from different suppliers and containing various fiber types and contents to be directly compared in this study. Additionally, it is the procedure used by researchers such as Wille, et. al and the FHWA. Therefore, using this casting procedure allowed results from this study to be compared to results from experimental investigations conducted by other researchers.

3.1.3 Test Setup and Specimen Dimensions

The tensile testing method chosen for this study was a direct tensile testing method. Although they are more time intensive, determining post-cracking tensile behavior of UHPC was significantly more important than ease of testing in this study. Additionally, the necessary testing equipment was readily available making direct tensile tests an attractive option for this study. It is noteworthy that the individuals working on developing code recommendations for UHPC in both

the United States and Canada have chosen direct tensile test methods as the required test methodology for the reasons previously listed.

Direct tensile tests were conducted on dog-bone shaped specimens using an MTS tensile testing unit. These dog-bone shaped specimens had wider cross-sections at the ends and thinner cross-sections in the middle, tapered region. The cross-section at the ends and middle portions of specimens were 2" x 6" and 2" x 2" respectively. The middle, tapered regions of specimens were 10" long. Dimensions for test specimens can be found in Figure 35a. Pictures of the test setup are also provided for reference in Figure 35b and Figure 35c. These specimens were loaded until failure with the goal of observing micro-crack and local crack formation and propagation throughout loading. Specimens were attached to the MTS for tensile loading using threaded bars which were anchored to T-shaped steel plates by steel nuts. These T-shaped steel plates were then gripped by the MTS tensile testing unit. These connections resulted in fixed-end boundary conditions in the plane passing through the threaded bars and a pinned-end boundary condition in the plane perpendicular to the fixed-end boundary condition plane. The fixed-end boundary conditions were observed to typically control the tensile behavior observed in specimens. This phenomenon is discussed further in Chapter 3 Section 3. LED's were attached to the front face of the specimen, and an LVDT was attached to the back face of the specimen for data collection purposes.

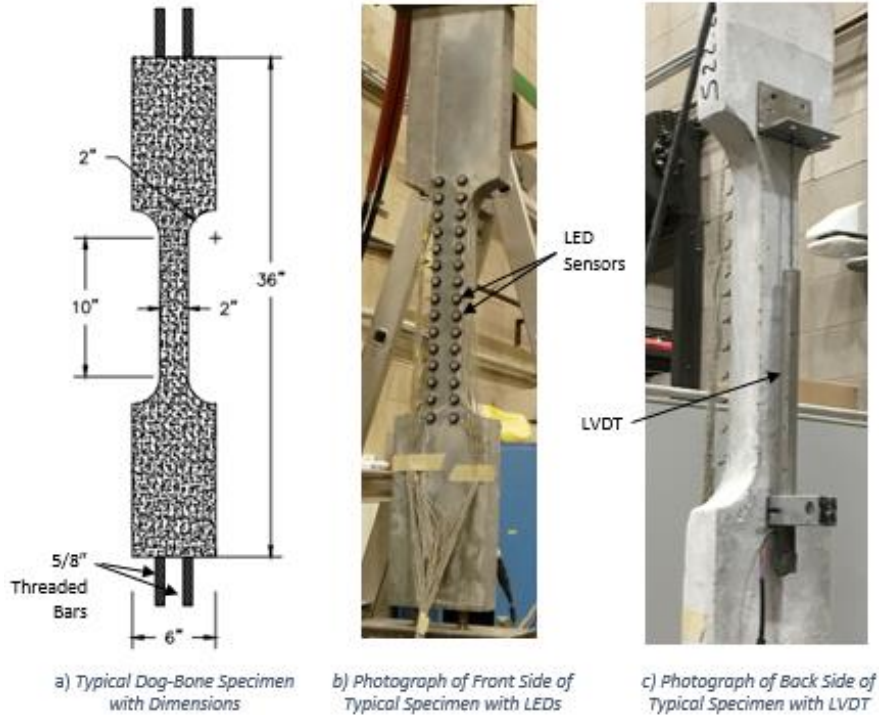


Figure 35: Specimen Dimensions and Photographs of Data Collection Methods

3.1.4 Data Collection Methods

Micro-crack and local crack data was collected using the NDI Optotrak LED system. In this system, each LED has coordinates in an x-y-z plane that are tracked via an Optotrak Certus HD camera. Each specimen was fitted with LEDs placed in pairs (one on the left and one on the right front face of the specimen) at one-inch spacings along the tapered portion of the specimen from the beginning to the end of the taper. Data collected from these LEDs was used to determine the total displacement at one-inch intervals along the specimen. In addition to the LEDs, load data from the MTS tensile testing unit and displacement data from an LVDT on the back side of the specimen was collected.

3.1.5 Loading Procedures

A displacement controlled loading procedure was used for testing specimens. Specimens that exhibited post-cracking strength were subjected to a three-part displacement controlled loading procedure of 0.05 inches/minute until 0.1 inches, 0.03 inches/minute until 0.2 inches, and 0.1 inches/minute until failure. The primary goal of this loading procedure was to make the three regions of the stress vs. micro-crack strain curve, the elastic, nonlinear, and unloading stages, occur over approximately equal time intervals for specimens exhibiting inelastic micro-crack strains. Specimens exhibiting inelastic micro-crack strains will be discussed in detail in Sections 3.3 of this document. Specimens exhibiting no post-cracking strength were loaded at 0.05 inches/minutes until specimen failure as these specimens failed during the first part of the three-part displacement controlled loading procedure.

3.1.6 Comparison of Sensory Data

LED and LVDT data were compared to determine the relative precision of the two data collection methods. Average axial stress vs. average axial strain results showed that results from LED data exhibited approximately the same precision as results from LVDT data. LVDT data was observed to have slightly higher precision, however, the difference in precision was not significant. Approximate precision values for LED and LVDT data were 0.0015 mm and 0.0013 mm respectively. Figure 36 shows the comparison of LED and LVDT data for a supplier 2 specimen.

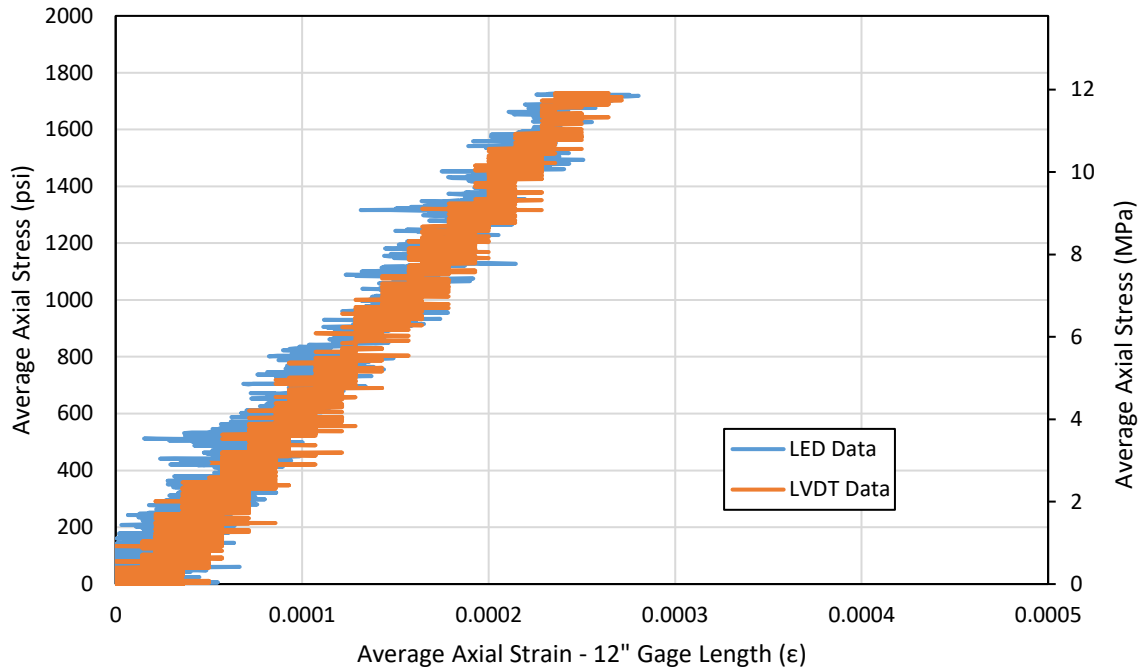


Figure 36: Comparison of LED and LVDT Data - Stress vs. Average Axial Strain

3.1.7 UHPC Mix Types

Mixes from three UHPC suppliers available in the United States market were used in this research. For each supplier, specimens were batched using appropriate mix constituents and mixing procedure, per the manufacturer's specifications. The basic mix constituents for each supplier are detailed in Table 6. Superplasticizers and other additives varied between suppliers and are not included in the table. Various fiber type combinations were used in batches of supplier 2 UHPC to determine the effect of fiber type on micro-cracking behavior.

Table 7 describes the fiber types used in this study.

Table 6: UHPC mix constituents

Supplier	Dry Constituents lb/ft ³ (kg/m ³)	Water lb/ft ³ (kg/m ³)	Fiber Type(s)
1	137 (2915)	7.49 (120.0)	A
2	135 (2162)	12.15 (194.6)	A, B, C, D
3	106 (1698)	9.08 (145.4)	A, E

Table 7: Descriptions of Fiber Type

Fiber Type	Material	Shape	Length (in)	Tensile Strength
A	Steel	Round	0.5	High
Low	Steel	Deformed	0.5	Low
C	PVA	Round	0.75	Low
D	Steel	Flat	0.75	Low
E	Steel	Round	0.75	High

3.2 Data Quantification

3.2.1 Strain

Strain values were the primary data used for quantification in this study. Strain values calculated include micro-crack, local crack, and average axial strain values. These values were calculated by determining the change in total length between two LEDs divided by the total length between these LEDs at zero stress. As LEDs were placed at approximately one-inch intervals, strains could be calculated at any whole-inch gage length (e.g. 1", 2", etc.). This allowed strain curves for various gage lengths to be developed and for these results to be compared to results from other studies. Equation 1 shows the equation used for calculating strains.

For strain analysis, it was assumed that the sample failure is controlled by tension, and therefore, torsion and shear do not contribute to sample failure. It was also assumed that cracking did not affect displacement of LEDs away from the local crack. This assumption only affected the strain between individual sets of LEDs. However, the primary analysis method used for micro-cracking was performed via an average of the micro-crack strains which accounts for this assumption.

$$\varepsilon = \frac{\Delta L}{L} \quad (1)$$

3.2.2 Stress

Stress was calculated by dividing MTS load values by the measured area at the cross-section of failure. Equation 2 shows the equation for calculating stress.

$$\sigma = \frac{F}{A} \quad (2)$$

3.2.3 Fracture Energy

Fracture energy, denoted as G_F , is the amount of energy required to completely fracture the cross-section of a material (O. Millon, et. al 2009). This energy is computed by measuring the subtended area in the stress-crack opening displacement (COD) curve in the strain softening region (post-peak stress) for conventional concrete (Caverzan, A. et. al 2012). There are many different test methods that can be used to determine the fracture energy of a material including three-point bending, spalling, and direct tensile testing. Therefore, fracture energy can be calculated using the direct tensile test results from this study.

The best way to determine fracture energy of UHPC from the direct tensile test stress-COD curve has not been established. Some researchers have calculated fracture energy for UHPC via the methodology used for conventional concrete by including only the area under the strain softening region of the curve. Other researchers have included the entire area under the stress-COD curve because the peak stress of UHPC is much higher and typically occurs at a much higher strain than it does in conventional concrete resulting in the pre-peak region of the curve being much larger for UHPC than for conventional concrete. Other methods used by researchers to determine fracture energy include subtracting the area of the elastic region from the total area under the curve and adding the area of the strain softening region to the area of the pre-peak region divided by the number of cracks (Tran, N., et. al 2015).

In this study, the entire area under the curve was used to calculate fracture energy as the area under the pre-peak region of the stress-COD curve is substantial for UHPC. The crack opening displacement curve is another name for the crack width curve for the localized crack. Therefore, the local crack width must be calculated from experimental results to calculate fracture energy. This was accomplished by calculating the displacement between the LEDs located on opposite sides of the localized crack. Although this does not consider cracks outside of the localized crack in the region between these LEDs, local crack displacement was observed to significantly larger than other crack displacements. Therefore, the displacement between the LEDs on opposite sides of the local crack was used as an approximation of local crack displacement for the purposes of this study. Equation 3 is a general equation that may be used to calculate the fracture energy of UHPC. Area 1 in Figure 37 is equal to the fracture energy for the sample curve in the figure.

$$G_F = \text{Area under the stress vs. COD curve} \quad (3)$$

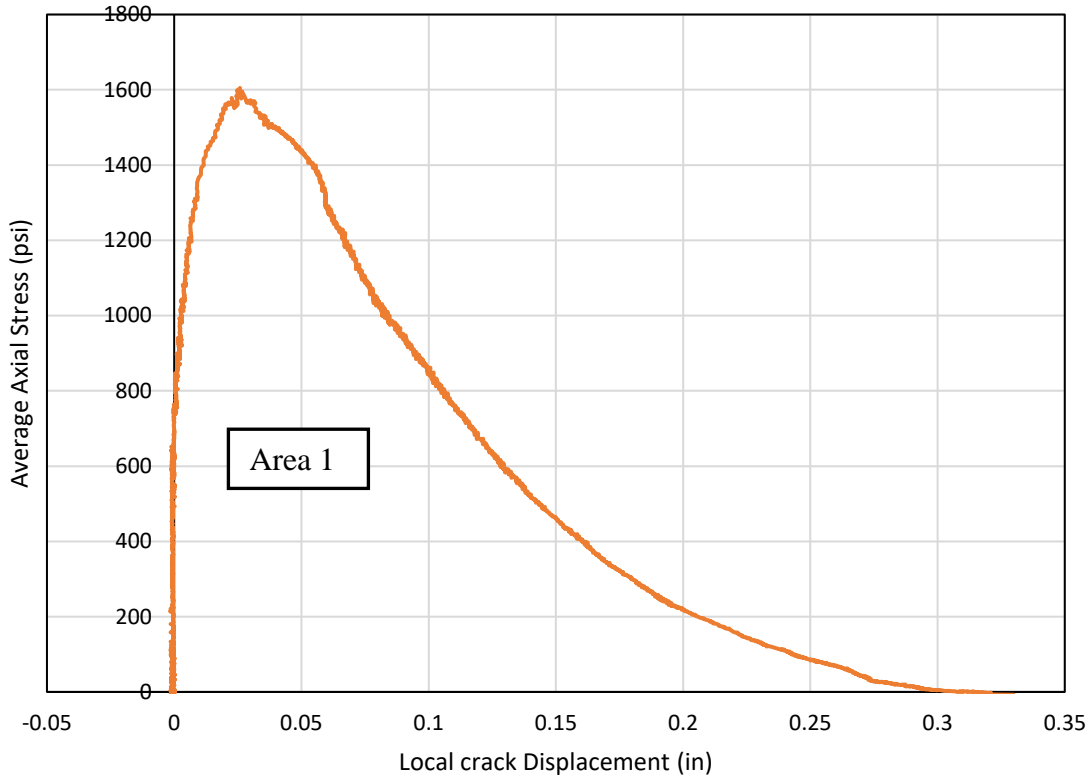


Figure 37: Sample Curve Used to Calculate Fracture Energy - Stress vs. Local Crack Displacement

3.2.4 Characteristic Length

Characteristic length is a material property of concrete that characterizes its brittleness. As characteristic length is a material property, specimen size and shape have no effect on it. According to Hillerborg (1988), the amount of deformation that is due to the stress-strain and the stress-COD portions of a tensile curve, in other words the pre-peak stress and post-peak stress portions of the curve, is of importance for a material. It is the relationship between these portions of a material's tensile curve that is of importance, and the primary way this relationship is defined is through characteristic length.

Characteristic length quantifies brittleness by comparing the pre-peak stress-strain curve and post-peak stress-displacement curve via a ratio which includes appropriate values from each portion of the curve. The value used from the pre-peak portion of the curve is f_t/E , and the value used from the post-peak portion of the curve is G_F/f_t . As previously discussed, G_F is the fracture energy of a material. The values f_t and E in these ratios represent the maximum tensile stress and modulus of elasticity respectively. These values are then combined to form the ratio known as characteristic length. This ratio can be found in Equation 4. It has been shown that concrete with low characteristic length values are more brittle than concrete with high characteristic length values (Hillerborg, 1988). Therefore, brittleness of UHPC with various fiber contents was compared via characteristic length values in this study.

$$l_{ch} = \frac{E \times G_F}{f_t^2} \quad (4)$$

3.3 Experimental Results and Discussion

Under direct tensile loads, the formation and propagation of micro-cracks and local cracks in UHPC were measured and compared. Based on the test results, it was determined that the tensile behavior of UHPC depended primarily on two factors: fiber type and fiber content. UHPC mix type influenced tensile behavior, but that effect was observed to be small when compared to the effects of fiber type and content. Therefore, results were evaluated to determine the effects of fiber type and fiber content on micro-crack and local crack formation and propagation.

3.3.1 Definitions

Average micro-crack strain

Average of strains between each interval of LEDs in micro-cracking regions.

Average axial stress

Value calculated by dividing the load by the measured cross-section area at the location of specimen failure. Hereafter referred to as “Stress.”

Formation

Formation is the point at which micro-cracks and local cracks begin to occur.

Propagation

Propagation is the spreading of a crack across the specimen cross-section. It is used in reference to local cracks but not micro-cracks as differentiating the propagation and growth stages of micro-cracks is difficult with the collected data. Local crack growth occurs after local crack formation.

Growth

Growth is used in reference to micro-cracks and local cracks and is the increasing of crack width for both crack types. This occurs after propagation for local cracks. Growth is used to describe both propagation and growth in micro-cracks as it is difficult to separate the two during testing.

3.3.2 Comparison of Global Results with Results from Others

Though global results do not capture the micro-cracking behavior of UHPC, they are the primary method that has been used to quantify UHPC tensile behavior to date. Therefore, to compare results from this study with results from other researchers, a comparison of global test results must be conducted. Since data was collected at one-inch intervals, results from this study can be calibrated and compared to results from other institutions, even post local crack formation. Figure 38 and Figure 39 display comparisons of tensile tests performed in this study with those conducted by other researchers. As can be seen in these figures, results from this study are very similar to results from tests conducted at other research facilities. Specimen shape and boundary conditions were different in each test, but UHPC mix and fiber type and content were the same. The tensile test curve published by the FHWA (2013) from one test performed by Graybeal and Baby (2013) is located between tensile curves from direct tensile tests performed in this study. Graybeal and Baby used 17” long prismatic specimens with 2” x 2” cross-sections and tapered aluminum plates attached to the specimen ends via an adhesive. These specimens were then gripped by a tensile testing unit to create a fixed-end boundary condition. Average test results from Wille et. al (2011) are very similar to results from the specimen in this study with the highest peak stress. Specimens in tests conducted by Wille, et. al were dumbbell-shaped specimens with 1” x 2” cross-sections and boundary conditions similar to those in this study.

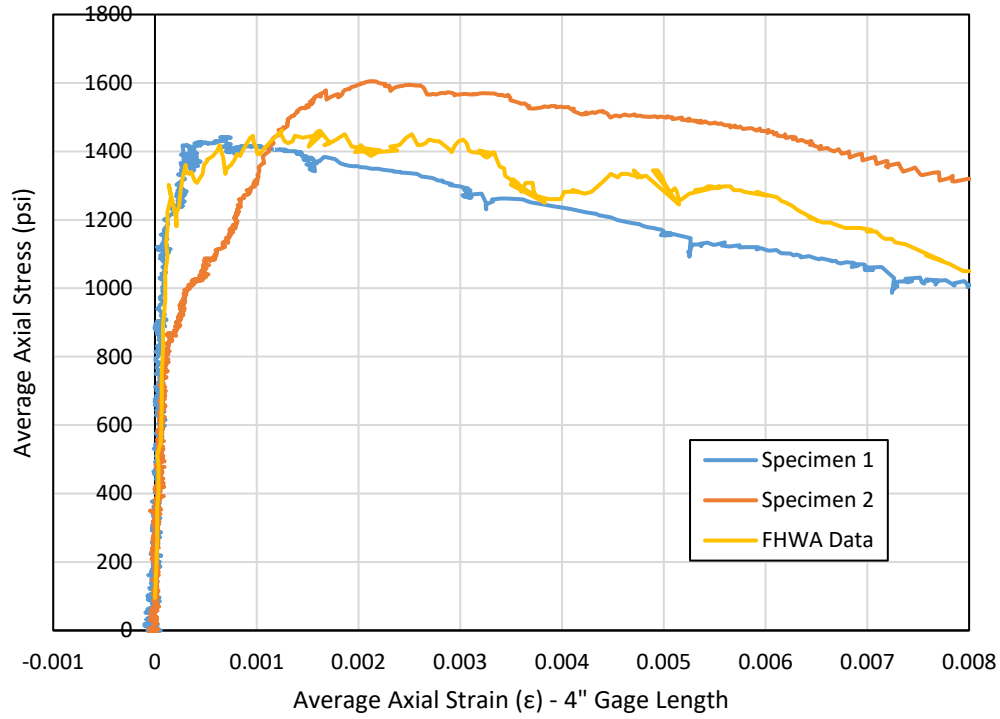


Figure 38: Comparison of Global Results with FHWA Test Result (FHWA 2013)

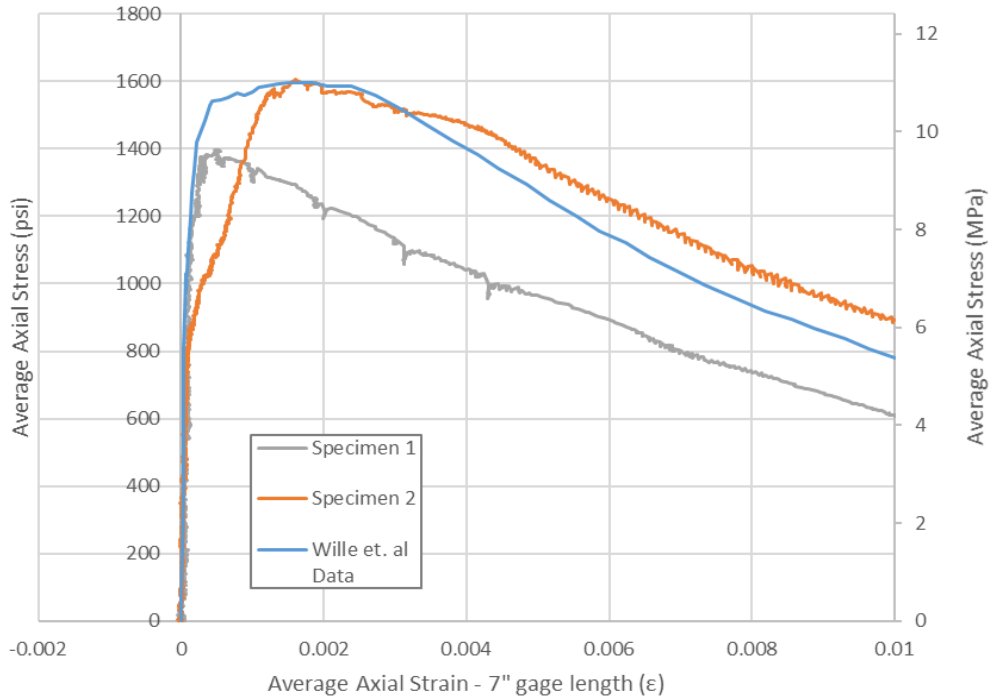


Figure 39: Comparison of Global Results with Average Wille et. al Data

3.3.3 Influence of Fiber Type

Two different types of responses were observed during tensile testing in this study. The first type of response, a brittle response, occurred in specimens which exhibited no post-cracking strength. In this response, specimens exhibited a linear elastic response until the peak stress was reached, at which point the specimen experienced brittle failure. This response can be seen in the results from specimens S21.E20 and S22.BC25 in Figure 40. The second observed response, a ductile response, occurred for specimens which exhibited post-cracking strength, such as specimens S12.A20 and S31.AE20. The results of these tests in Figure 40 display UHPC ductile behavior under tensile load. Fiber type was observed to be the primary variable that affects whether a UHPC will exhibit post-cracking strength. Specimens containing fiber types B, C, and D exhibited brittle tensile behavior. Specimens containing fiber types A and E exhibited ductile behavior.

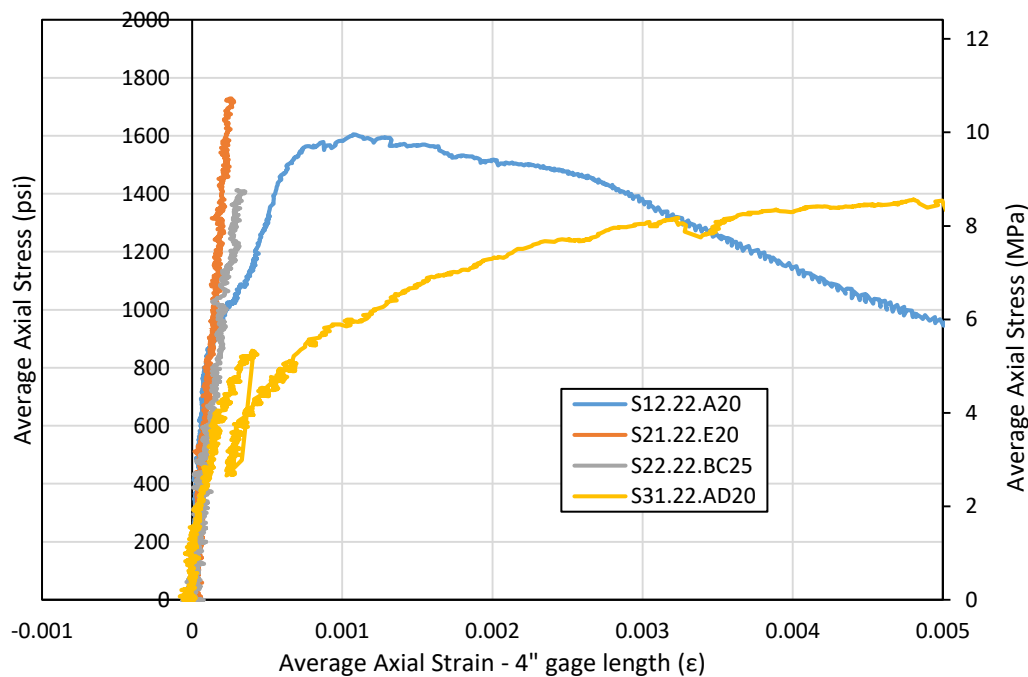


Figure 40: Comparison of Brittle and Ductile UHPC Responses

Fiber type was also observed to affect micro-crack responses in specimens. Specimens with fiber Types B, C, and D experienced no micro-cracking as they failed in a brittle manner before micro-cracking could occur. Fiber types A and E, which resulted in ductile behavior, were observed to have varying micro-crack strain responses. The maximum average micro-crack strain value observed in specimens with Type A fiber at 2% by volume was 2.79 me. The maximum average micro-crack strain value observed in specimens with a combination of Type A and E fiber at 1% by volume of each (a total of 2% by volume) was 5.46 me. This suggests that Type E fiber increases micro-cracking strains in UHPC when compared to Type A fiber. However, significant variation was observed in specimens with Type A fiber and in specimens with a combination of Type A and Type E fiber. Additionally, fiber Type E was used only in combination with Type A fiber in three specimens; it was never used on its own. Therefore, further testing must be completed to determine if fiber Type E increases micro-crack strain capacity for UHPC in tension. Variation is discussed further later in this thesis.

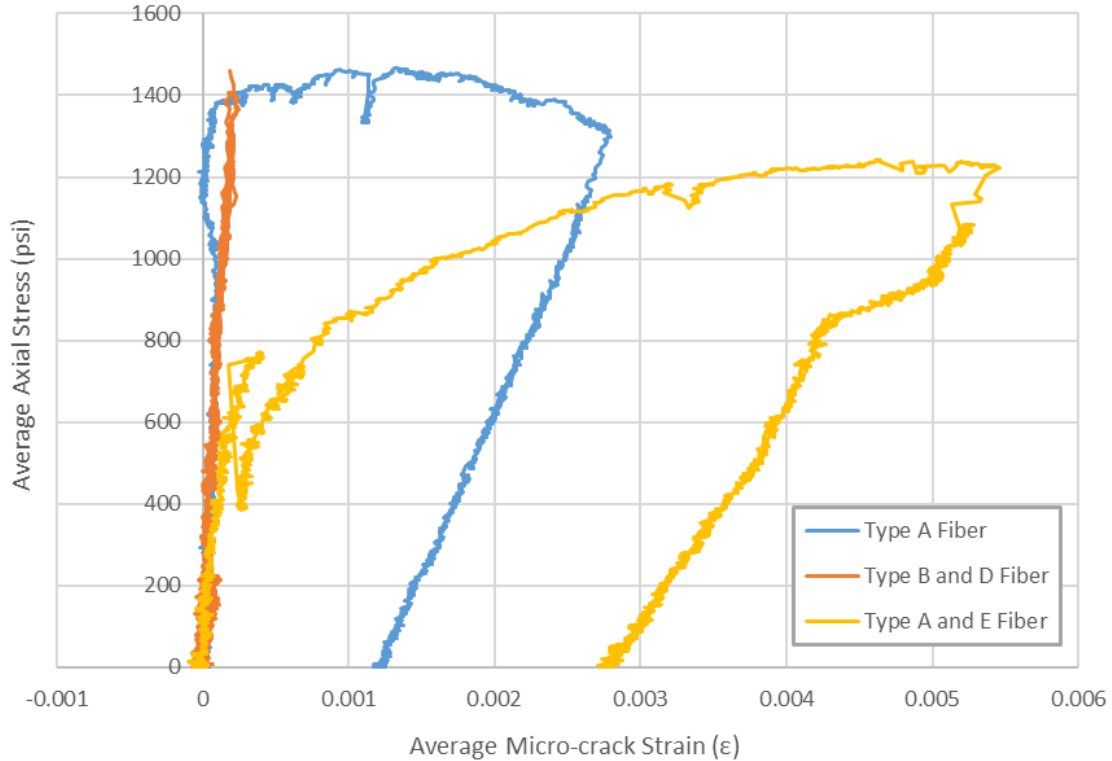


Figure 41: Effect of Fiber Type on Micro-crack Strain Response

Responses exhibiting brittle behavior

Responses exhibiting brittle behavior occur when the fiber tensile strength capacity at a cross-section is lower than the maximum tensile strength of the UHPC cementitious matrix. The fiber strength capacity at a cross section is highly reliant on maximum tensile strength of the fiber used, the bond strength between the UHPC and fiber, and the fiber content. In tests exhibiting brittle behavior, no post-cracking strength was observed. Due to the low tensile strength of the fibers used in these specimens, the fiber strength at the cross-section was less than the strength of the cementitious material resulting in brittle fiber fracture at first cracking. This failure due to fiber fracture was confirmed by observation of fibers at the cross-section of failure after testing.

Brittle responses are undesirable due to the lack of post-cracking strength and sudden nature of failure. Additionally, the definition of UHPC according to many researchers requires the material to exhibit post-cracking strength, such as the definition from the FHWA which requires UHPC to have a post-cracking strength above 0.72 ksi. Therefore, all UHPCs should utilize fiber types that ensure ductile behavior occurs in tension or include other methods of reinforcement appropriately.

Responses exhibiting ductile behavior

For specimens exhibiting ductile behavior, the relationship between the formation and propagation of micro-cracks and local cracks remained the same, even for specimens with different fiber types and contents. This behavior can be characterized by defining four stages of testing: the elastic stage, the micro-crack formation stage, the local crack formation and propagation stage, and the softening stage. These four stages are applicable to all tensile tests with fixed-end connections and can be modified slightly to apply to tests with pinned-end connections. Figure 42 and Figure 43 display two specimens exhibiting ductile behavior.

The first stage of testing is the elastic stage. During this stage, a specimen experiences small tensile strains as the applied load increases, but the UHPC does not crack. The second stage of testing is the micro-crack formation stage. During this stage, a specimen experiences increasing micro-crack strains as stress continues to increase. This stage begins with first cracking, and micro-cracks form throughout it. It was observed that specimens experienced greater micro-crack strains on one side, suggesting that a bending moment due to the fixed end test setup induced higher tensile stress on that side.

The third stage of testing consists of the formation and propagation of the local crack. In all applicable cases, the local crack formed on the side that experienced higher micro-crack strains, providing further evidence of higher tensile stress on that side of the specimen. The stress value at which local crack formation began varied based primarily on fiber content. As the local crack formed and proceeded to propagate across the cross-section, micro-cracks on the same side as the local crack plateaued or decreased. Conversely, micro-cracks on the opposite side began to increase, suggesting a shift in the load path through the specimen. As the local crack formed and propagated across the section, the stress in the specimen initially increased before reaching its maximum value. After this point, stress decreased. Complete propagation of the local crack occurred during this stress decrease, and typically occurred shortly after the maximum tensile stress was reached. The end of local crack propagation coincided approximately with the maximum average micro-crack strain.

Stage four of tensile testing is the softening stage and consists of local crack growth and decreasing micro-crack strains. Since the stress capacity of the cross-section decreases as the local crack grows, stress decreases more rapidly in this stage. This decrease in stress leads to a decrease in micro-crack strains. If fiber bridging micro-cracks in the specimen experienced inelastic deformation or bond slippage during testing, residual micro-crack strains were observed. If fiber bridging micro-cracks remained in the elastic region, micro-crack strains returned to approximately zero. This stage continues until specimen failure.

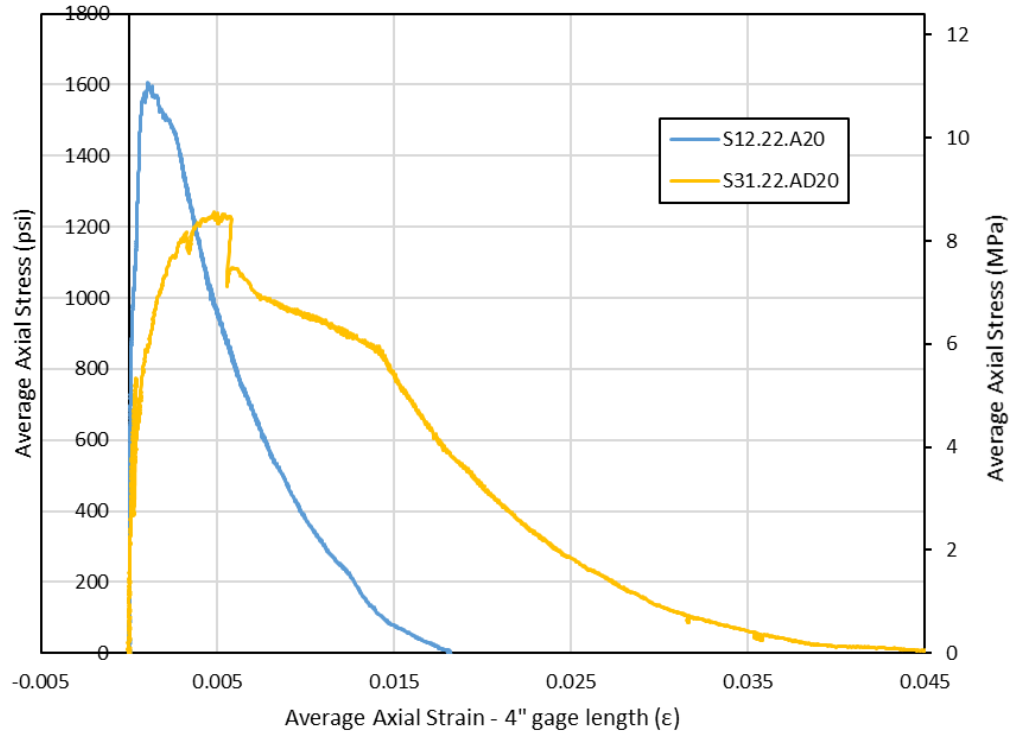


Figure 42: Stress vs. Average Axial Strain for Specimens Exhibiting Ductile Behavior

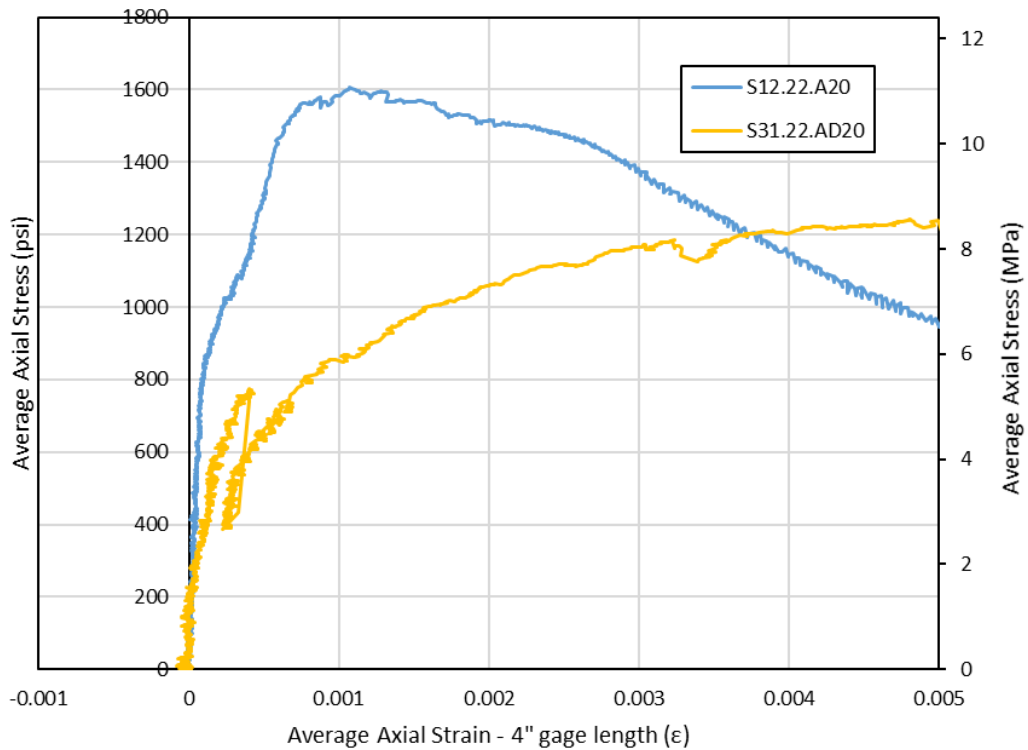


Figure 43: Stress vs. Average Axial Strain for Specimens Exhibiting Ductile Behavior - Zoomed In

3.3.4 Comparison of Proposed Tension Model with Models Proposed by Others

The four-stage UHPC Tensile Behavior Model proposed in this study is similar to the three-stage model proposed by Alkaysi and El-Tawil in Figure 44. The two models share the elastic stage and the strain softening stage, and the hardening stage defined in Alkaysi and El-Tawil's model is divided into the micro-crack growth and the local crack formation and propagation stages of the model proposed in this study. The primary difference between these two models is the division of the hardening stage in their model into the micro-crack formation stage and the local crack formation and propagation stage in the model proposed in this study. The use of only LVDT's makes differentiating the micro-crack formation stage and local crack formation and propagation stage difficult for other models. However, the LEDs used in this study allow for these two stages to be well defined.

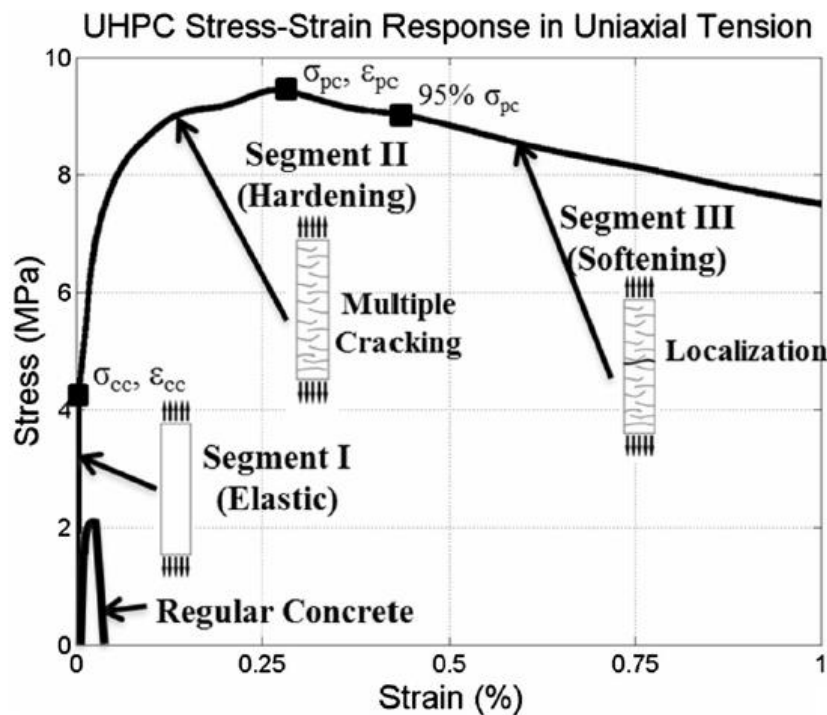


Figure 44: UHPC Tensile Stress-Strain Response Model Proposed by Alkaysi, M. and El-Tawil, M.

The primary difference between the model proposed in this study and the model proposed by the FHWA shown in Figure 45 is that the micro-cracking stage as shown in the FHWA model was not observed in results from this study. The micro-cracking stage in FHWA's model includes a significant increase in strain during this portion of testing, as well as rapid fluctuations in stress as strain increases. However, results from tests in this study did not display rapid fluctuations in stress or the corresponding significant increases in strain during the micro-crack stage as displayed in the FHWA model. Instead, results from this study showed relatively small increases in strain as stress gradually increased during the micro-cracking stage.

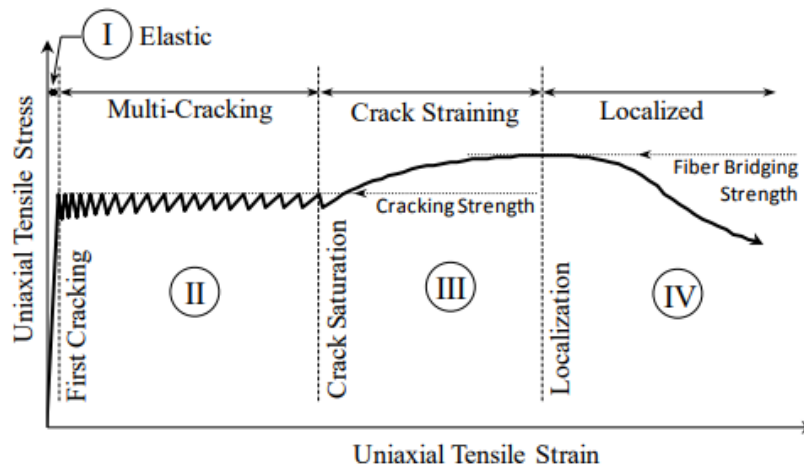


Figure 45: UHPC Tensile Stress-Strain Response Model Proposed by FHWA

3.3.5 Influence of Fiber Content

Supplier 1 specimens were tested with Type A fiber at dosages of 0%, 1%, and 2% fiber by volume to determine the effect of fiber content. Type A fiber was chosen to determine the influence of fiber content because it consistently displayed a ductile tensile response in direct tensile tests. From these tests, it was determined that the effect of fiber content on both local crack and micro-crack formation and propagation was significant.

Supplier 1 specimens with no fiber (0% fiber) experienced no post-cracking strength due to the brittle nature of cementitious material fracture once the maximum tensile strength was reached. Therefore, no micro-cracking was observed in these specimens. Variation in the maximum tensile stress observed for specimens with 0% fiber can be largely attributed to the bending moment induced by the test setup. As discussed in Chapter 2, the cracking stress for UHPC is not necessarily accurate for tests with fixed end boundary conditions and will vary based on any induced bending moment. Therefore, since the cracking stress for UHPC with no fiber is the maximum tensile stress of the material, the maximum tensile stress of UHPC with no fiber observed is expected to have some variation.

Specimens with 1% fiber exhibited post-cracking strength and micro-cracking behavior. However, no inelastic micro-crack deformation was observed for specimens with 1% fiber. Specimens with 2% fiber experienced post-cracking strength and micro-cracking. Additionally, two of the three specimens with 2% fiber experienced inelastic deformation in micro-cracking regions while one specimen did not. The tensile behavior of supplier 1 UHPC with 2% fiber and 1% fiber is discussed in more detail in Sections 3.3.6 and 3.3.7 respectively. Figure 46 and Figure

47 show pictures of micro-cracking in specimens with 2% after testing was completed. Figure 48 and Figure 49 show pictures of micro-cracking in specimens with 1% after testing was completed. Figure 50 shows stress vs. average axial strain results for specimens with 0% fiber.



Figure 46: Micro-cracking in Supplier 1 - 2% Fiber Specimen



Figure 47: Micro-cracking in Supplier 1 - 2% Fiber Specimen - with marks



Figure 48: Micro-cracking in Supplier 1 - 1% Fiber Specimen

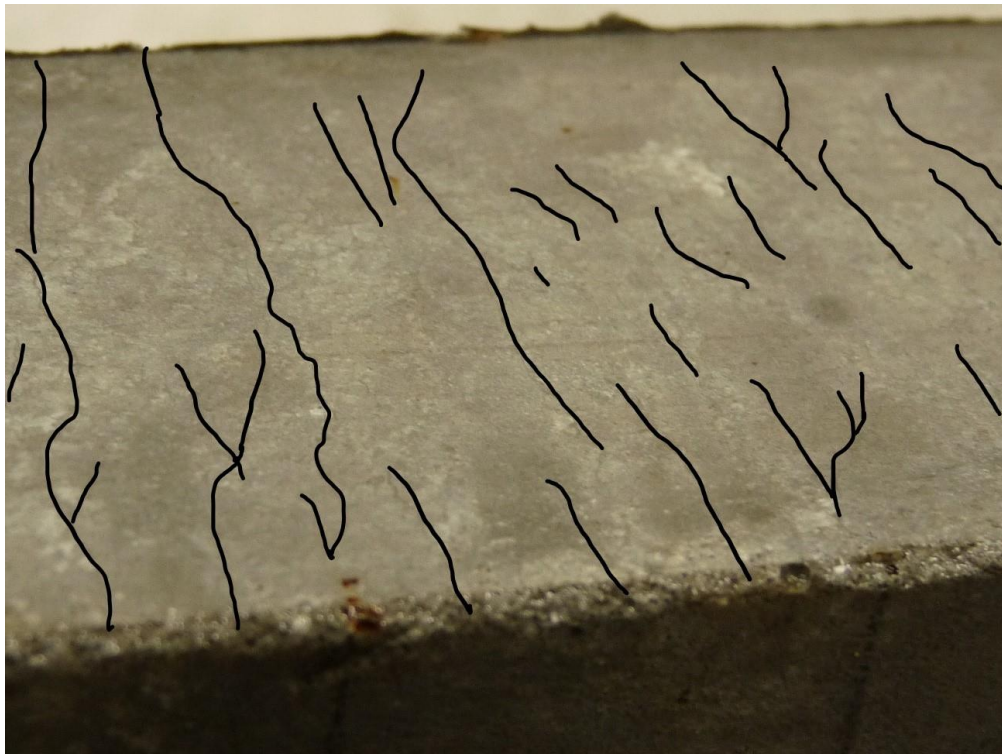


Figure 49: Micro-cracking in Supplier 1 - 1% Fiber Specimen - with marks

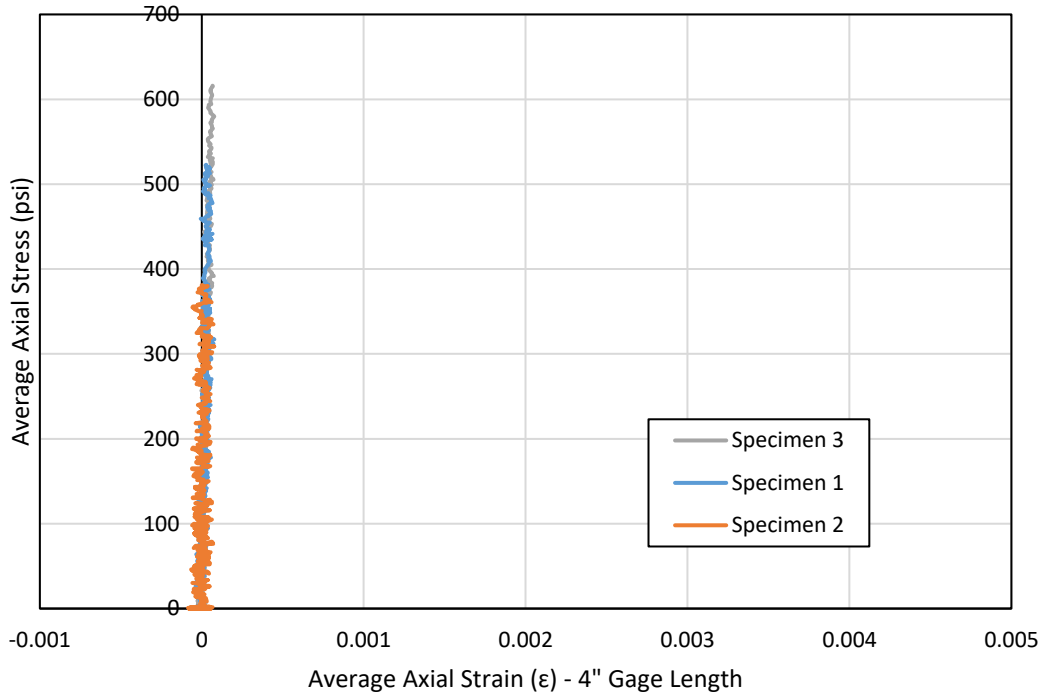


Figure 50: Stress vs. Average Axial Strain - 4" Gage Length - 0% Fiber

The average cracking stress values for supplier 1 specimens were 503 psi, 728 psi, and 940 psi for fiber contents of 0%, 1%, and 2% by volume, respectively. Likewise, the average maximum stress values were 503 psi, 1072 psi, and 1497 psi and the average strain values at maximum stress were 0.0789 me, 3.17 me, and 0.973 me. The average maximum average micro-crack strain values were 0.268 me for 1% fiber and 1.61 me for 2% fiber. High variation was observed for strain values at maximum stress in specimens with 1% and 2% fiber while high variation in maximum average micro-crack strain values were only observed in specimens with 2% fiber. Figure 51 and Figure 52 display the effect of fiber content on global stress-strain behavior over a 4" gage length. Figure 53 displays the effect of fiber content on micro-crack strains.

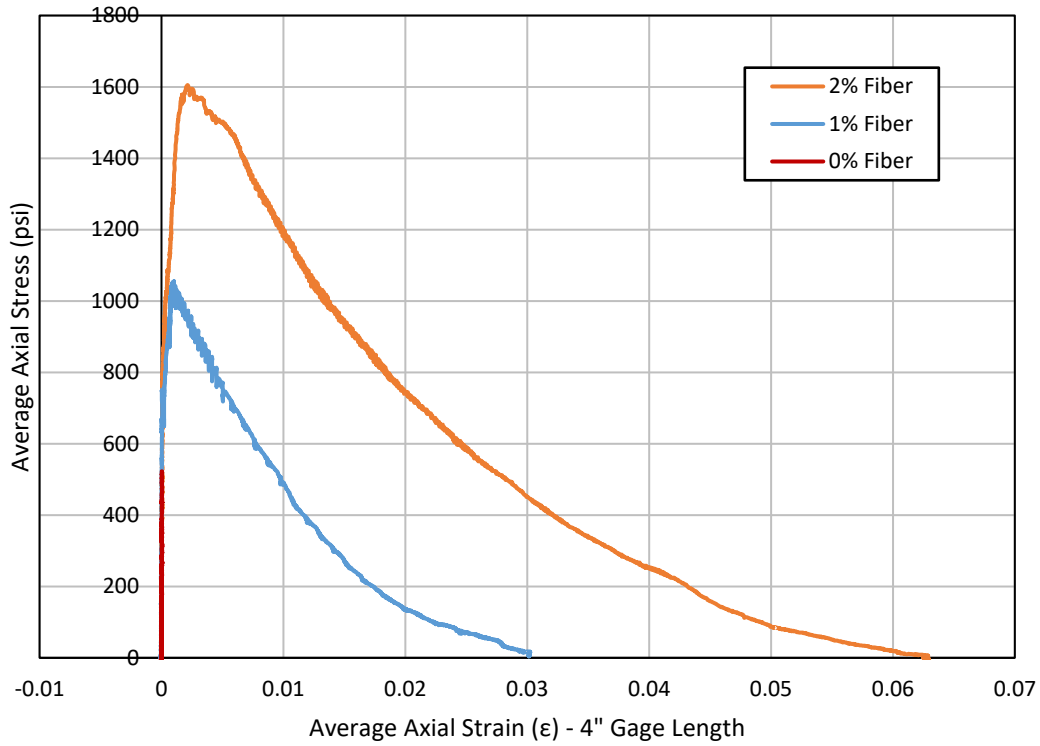


Figure 51: Effect of Fiber Content - Stress vs. Average Axial Strain – 4" Gage Length

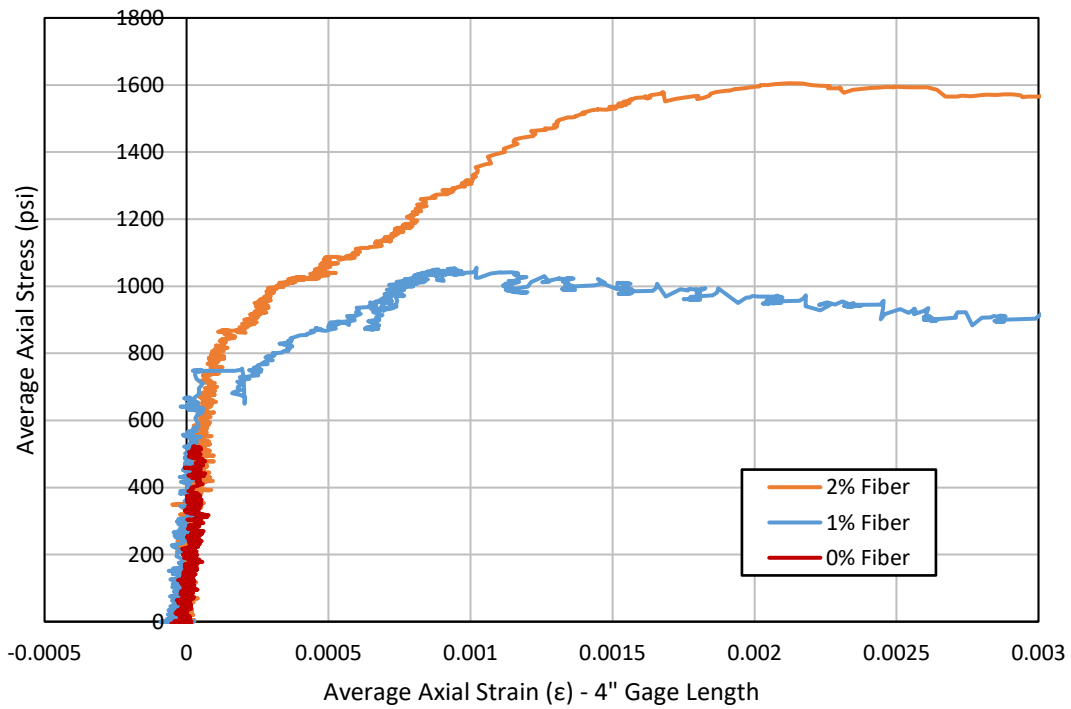


Figure 52: Effect of Fiber Content Zoomed In - Stress vs. Average Axial Strain

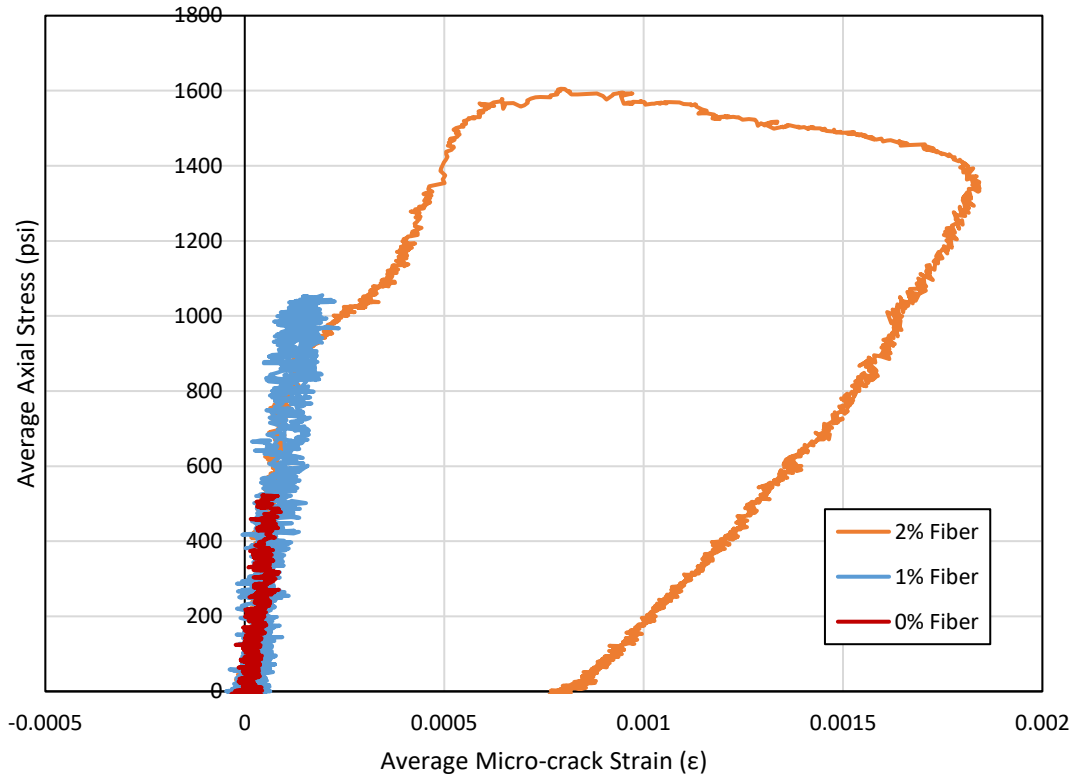


Figure 53: Effect of Fiber Content on Micro-crack Strain - Stress vs. Average Micro-crack Strain

3.3.6 Supplier 1 – 2% Fiber

Three specimens of supplier 1 UHPC with 2% Type A fiber were tested in this study. Similarities in the local crack, micro-crack, and stress results were observed between these specimens. However, notable variation was observed as well. All three specimens exhibited ductile behavior.

Local crack formation occurred after a tensile stress of 1000 psi was reached in all specimens. At a tensile stress of approximately 1300 psi, all specimens had micro-crack strain values in the mille-strain range. All micro-crack strains at this time were less than 0.0006, and one

was lower than 0.0002. This occurred after local crack formation but before the maximum tensile stress was reached. After this point, local crack formation began and observed micro-crack strains began increasing rapidly in two of the three specimens. Figure 54 shows the stress vs. average axial strain curves for the three specimens with strains measured at a 4" gage length. Figure 55 displays stress vs. average micro-crack strain curves for the specimens.

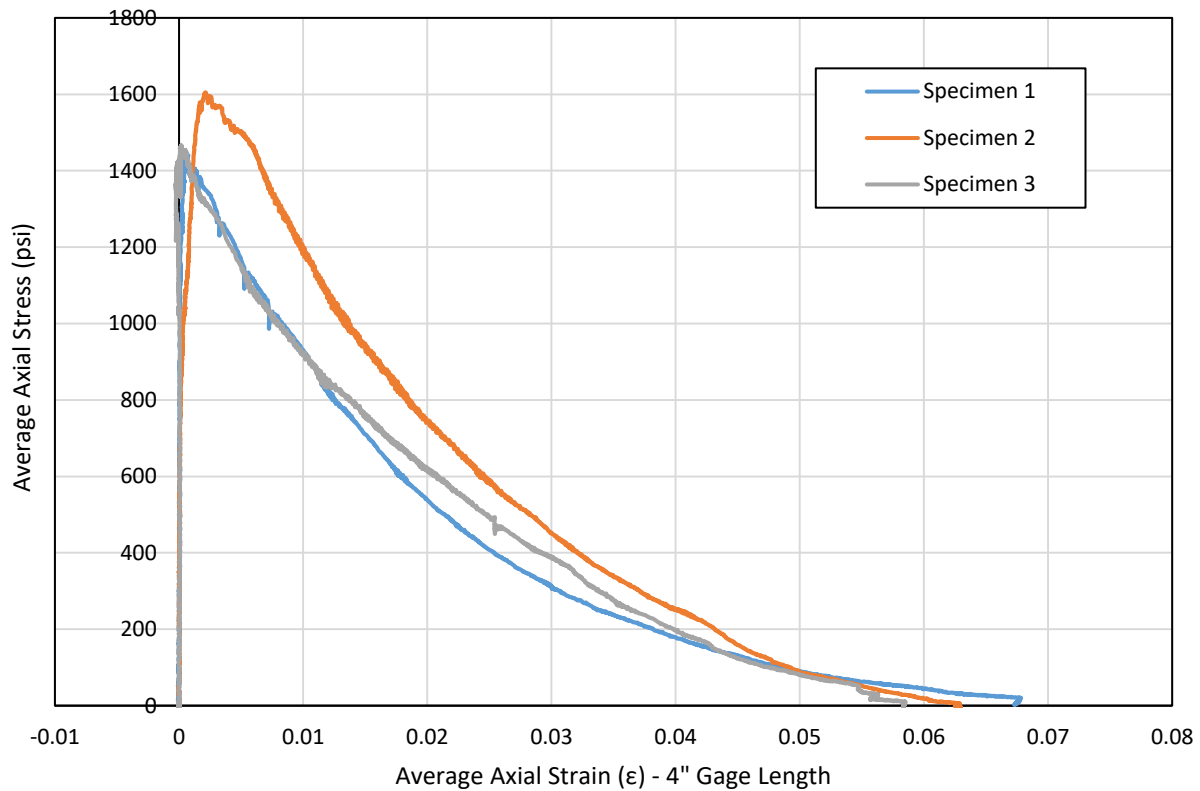


Figure 54: Supplier 1 - 2% Type A Fiber - Stress vs. Average Axial Strain – 4" Gage Length

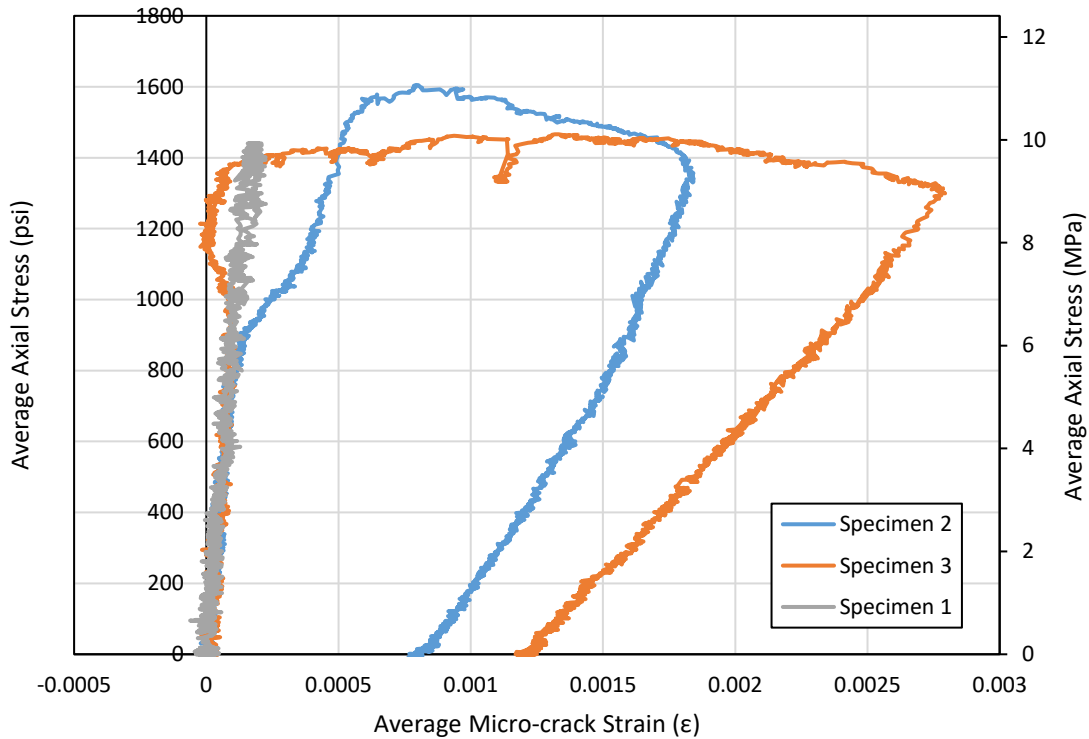


Figure 55: Supplier 1 - 2% Type A Fiber - Stress vs. Average Micro-crack Strain

Supplier 1 -2% fiber - specimen 1

Specimen 1 exhibited first cracking and local crack formation on the left side of the specimen, with respect to the front face. As previously discussed, direct tensile test setups with fixed-end connections induce some moment in the specimen. First cracking and local crack formation occurred on the left side of the specimen suggesting higher tensile stresses were present in this side. This suggests that a bending moment was induced in the specimen by the fixed-end boundary condition previously discussed, and therefore, the fixed-end boundary condition controlled for this specimen. At the initiation of local crack formation, micro-crack strains plateaued on the left side and began to increase on the right side. This occurred at a stress value of

1342 psi. Local crack propagation across the entire cross-section occurred after the maximum average cross-section tensile stress of 1441 psi was reached. The maximum values for average left and right micro-crack strains were observed slightly before and after the max tensile stress occurred, respectively. The maximum average micro-crack strain value observed was 0.23 me. This low value suggests that micro-cracks had minimal opportunity to grow. This is perhaps due to the cross-section stress being too low to engage the fibers inelastically outside of the local crack region. Visual observation showed that fiber orientation was less oriented in the longitudinal direction than Specimens 2 and 3. The less oriented fiber at the cross-section of failure may be the cause of the lower stress value observed which may in turn have caused the maximum average micro-crack value observed. Figure 56 displays stress, micro-crack, and local crack values for specimen S11.A20. A picture of the cross-section of failure can be found in Figure 57.

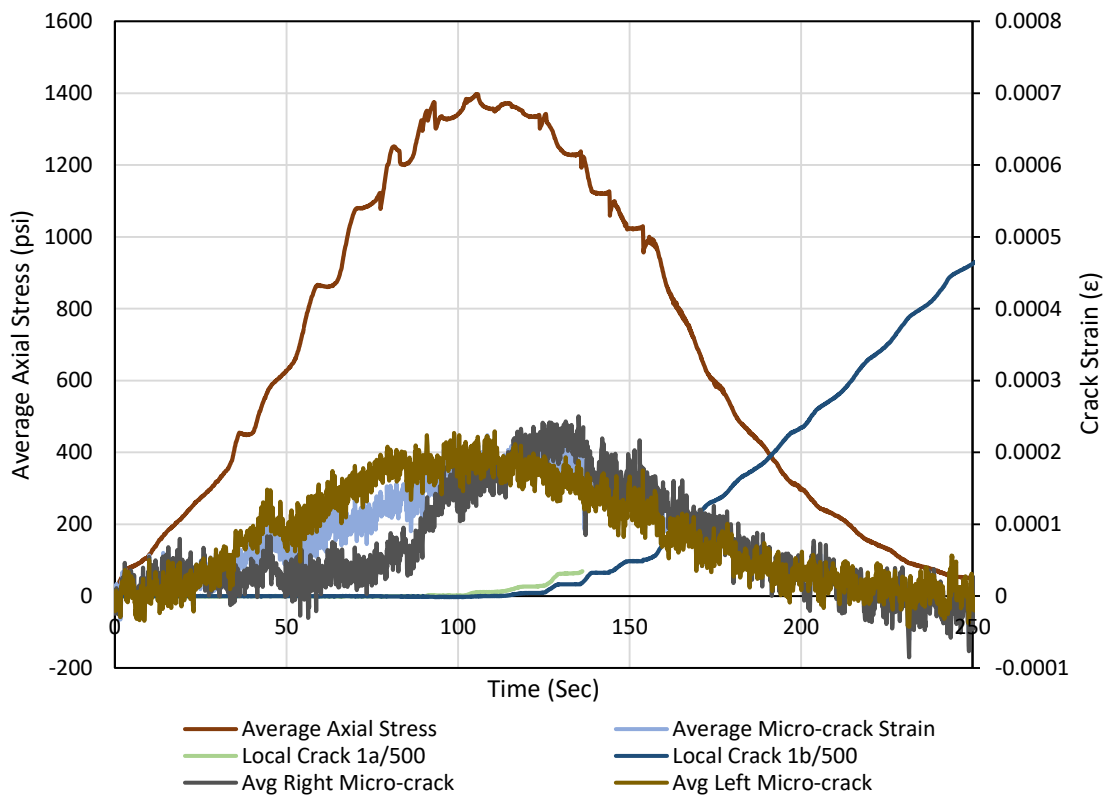


Figure 56: S11.A20 Stress, Local crack Strains, and Average Micro-crack Strains vs. Time



Figure 57: Cross-section of failure S11.A20

Supplier 1 -2% fiber - specimen 2

Specimen 2 exhibited first cracking and local crack formation on the right side of the specimen suggesting higher tensile stress was experienced on that side due to the bending moment induced by the test setup. This suggests the fixed-end boundary condition previously discussed controlled for this specimen. At the beginning of local crack formation, micro-crack strains plateaued on the right side and began to increase on the left side. This occurred at a stress value of 1416 psi. Local crack propagation across the entire cross-section occurred after the maximum average cross-section tensile stress of 1605 psi was reached. The maximum values for average right and left micro-crack strains were observed slightly before and after the max tensile stress occurred, respectively. The maximum average micro-crack strain value observed was 1.84 me.

The difference between the average left and right micro-crack strains was large during portions of testing and was observed to be significantly larger than what was observed in the other two specimens with 2% Type A fiber by volume. This suggests that bending effects may have been larger in this specimen than in the other specimens. This specimen reached a higher maximum stress value and larger micro-crack strains than Specimen 1, suggesting that the local crack region where specimen failure occurred had higher strength than the local crack region in Specimen 1. Visual observation showed that fiber orientation at the cross-section of failure was better oriented longitudinally than in Specimens 1 and 3. Figure 58 displays stress, micro-crack, and local crack values for specimen S12.A20. A picture of the cross-section of failure can be found in Figure 59. The well-orientated fiber in this specimen may have caused the higher stress values observed which may have, in turn, caused the higher average micro-crack strain values observed.

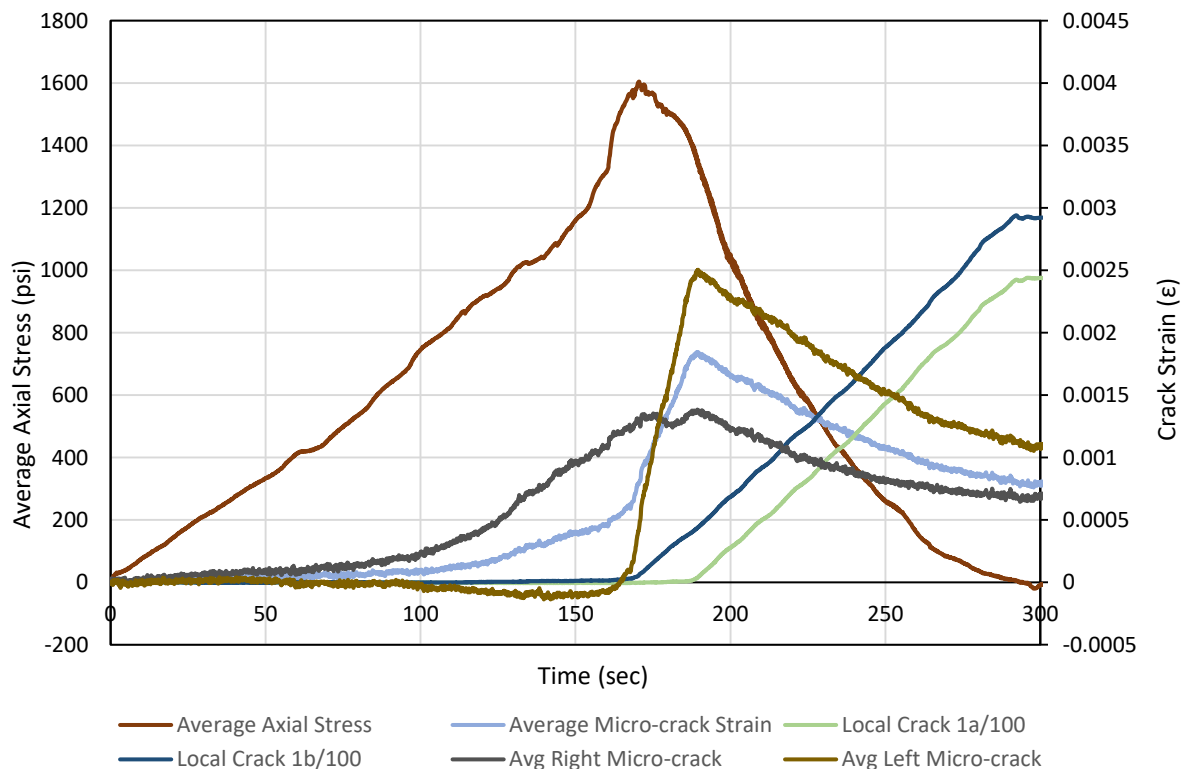


Figure 58: S12.22.A20 Stress, Local crack Strains, and Average Micro-crack Strain vs. Time



Figure 59: Cross-section of failure S12.A20

Supplier 1 -2% fiber - specimen 3

Specimen 3 exhibited first cracking and local crack formation on the back side of the specimen. As previously discussed, the test setup provides a pinned-end connection condition in one direction and fixed-end connection condition in the other. Formation of the local crack on the back side of the specimen suggests that there was minimal bending moment induced in this specimen, causing it to behave like a specimen with pinned-end boundary conditions. Further evidence of the pinned-end boundary conditions controlling for this specimen can be found by observing the value of the average left and right micro-crack strains in the specimen. The value of the average left and right micro-crack strains throughout this test were very close in value, suggesting very little bending moment was induced in the specimen. Therefore, the observed micro-crack strains were approximately equal at the beginning of local crack formation which

occurred at a stress value of 1311 psi. Local crack propagation across the entire cross-section occurred after the maximum average cross-section tensile stress of 1466 psi was reached.

The maximum values for average micro-crack strains were observed after the max tensile stress occurred. However, by applying results from other tests to this specimen, it can be deduced that the maximum average micro-crack strain on the back side of the specimen occurred before the maximum tensile stress was reached. The maximum average micro-crack strain observed using LEDs on the front face of the specimen was 2.79 me. It is suspected that the strains on the back side of the specimen may have been higher. However, no data that is able to confirm or disprove this hypothesis was collected. Visual observation showed that fiber at the cross-section of failure was more oriented in the longitudinal direction than specimen 1 and less oriented than specimen 2. This may have caused the maximum stress value observed as the value observed in this specimen was between the maximum stress values for specimens 1 and 2. However, it is difficult to determine what caused the higher average micro-crack strains to occur as these were the highest micro-crack strains observed. Figure 60 displays stress, micro-crack, and local crack values for specimen S11.A20. Figure 61 contains a photograph of the cross-section of failure after testing

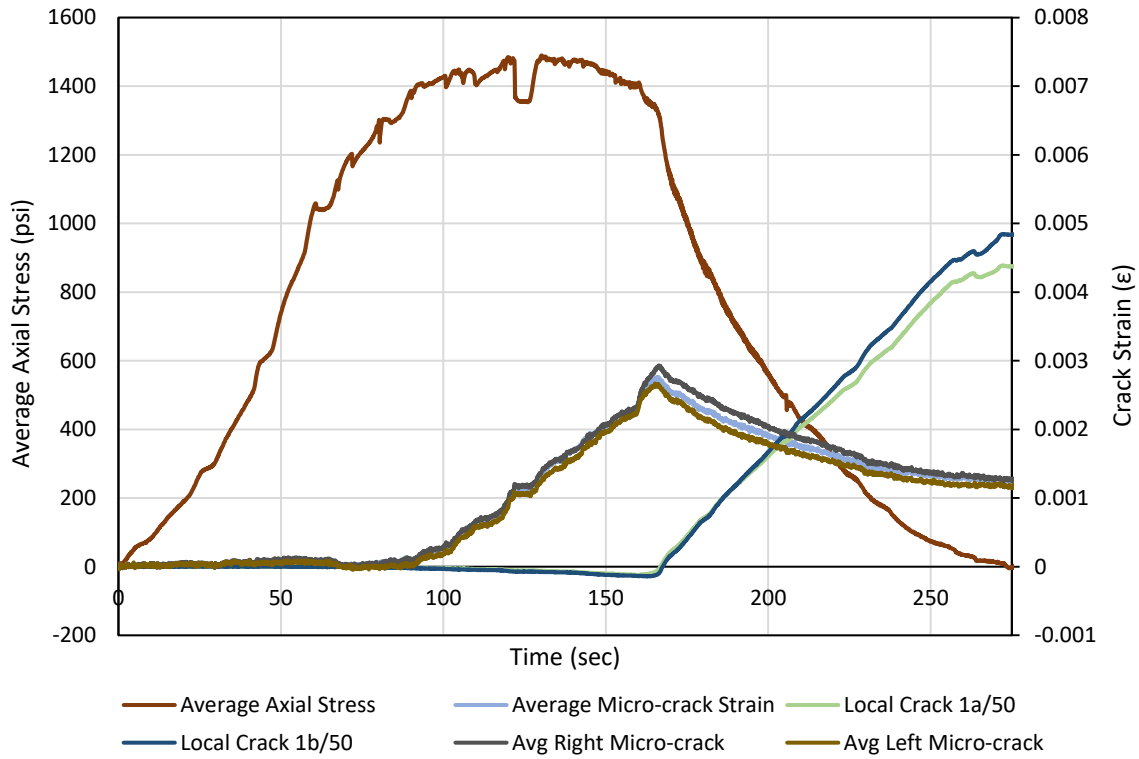


Figure 60: S13.A20 Stress, Local crack Strains, and Average Micro-crack Strains vs. Time



Figure 61: Cross-section of failure S13.A20

3.3.7 Supplier 1 – 1% Fiber

Three specimens of supplier 1 UHPC with 1% Fiber were tested in this study, and all exhibited ductile behavior. During the initial stages of testing, strain in the specimen increased elastically. During the next stage, micro-cracks began to form. Local crack formation occurred once a stress value of 450-675 psi was reached. All specimens also experienced micro-crack strain values in the mille-strain range throughout testing with maximum average micro-crack strains of approximately 0.0002 for all specimens.

Specimens with 1% fiber experienced very little variation in micro-crack strains. However, variation in overall tensile behavior was observed due to variations in the local crack behavior. Variation in local crack behavior is expected as fiber distribution and orientation at the cross-section of failure will vary slightly between specimens, even when they are batched in the same way. However, the variations in local crack behavior did not translate to notable variation in micro-crack behavior for these specimens. As with 2% fiber, higher strains were observed on one side of the specimen prior to local crack formation in each test, providing evidence of the bending moment induced by the test setup. The global and micro-crack behavior of all supplier 1, 1% fiber specimens can be found in Figure 62 and Figure 63. Cracking stress values for specimens 1, 2 and 3 were 747, 978, and 460 psi respectively. Likewise, maximum stress values were 1055, 1179, and 982 psi, strains at maximum stress for a 4" gage length were 2.38 me, 1.50 me, and 5.63 me and maximum average micro-crack strain values were 0.232 me, 0.255 me, and 0.318 me.

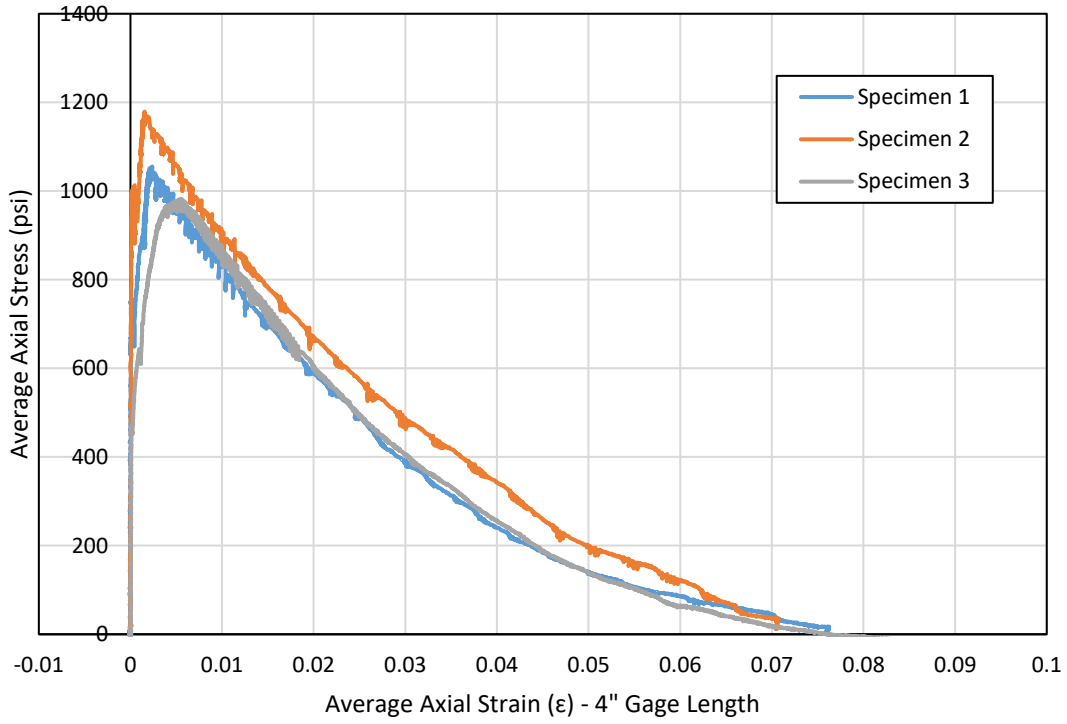


Figure 62: Supplier 1 - 1% Type A Fiber - Stress vs. Average Axial Strain

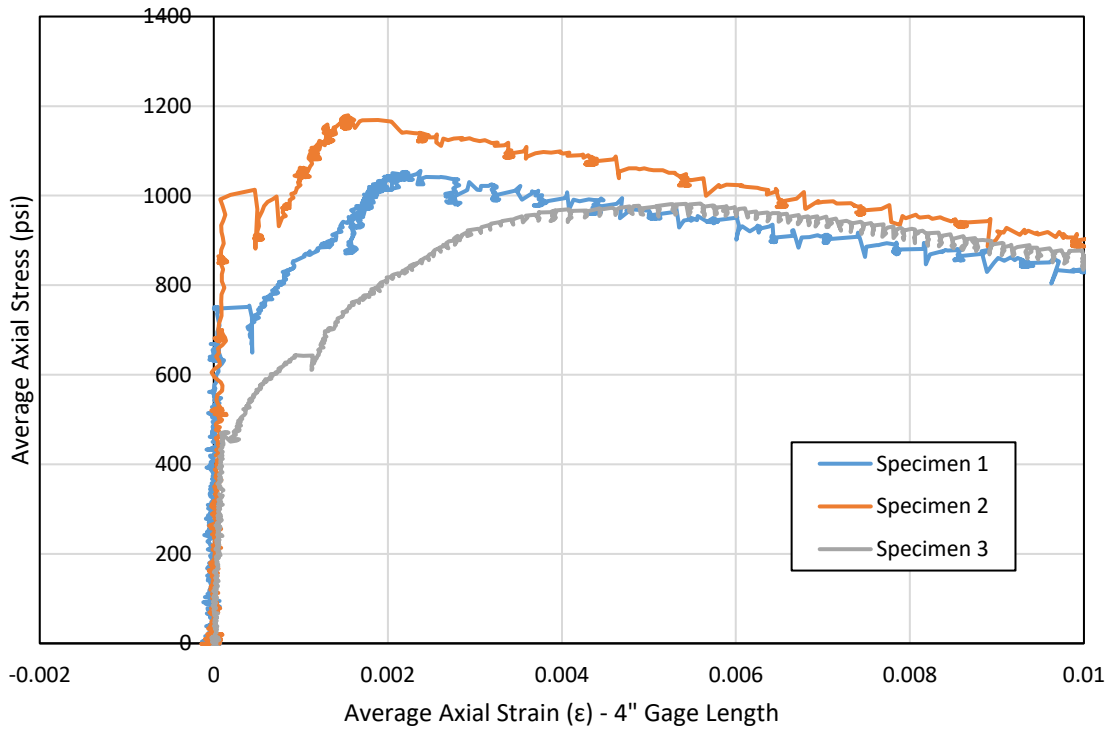


Figure 63: Supplier 1 - 1% Type A Fiber - Stress vs. Average Axial Strain Zoomed In

3.3.8 Supplier 2 – 2% Fiber

For supplier 2, various tests were conducted using fiber types A, B, C, and D. Tests with fiber types B, C, and D resulted in brittle failure primarily due to fiber strength. However, tests conducted on two specimens with Type A fiber dosed at 2% by volume exhibited ductile responses similar to supplier 1 with 2% fiber. Supplier 2 results with various fiber combinations show that use of proper fiber type is essential in ensuring UHPC without additional reinforcement exhibits ductile behavior.

Cracking stress values for specimens 1 and 2 were 433 and 469 psi respectively. Likewise, maximum stress values were 1697 and 1841 psi, strains at maximum stress for a 4” gage length were 5.64 me and 1.41 me, and maximum average micro-crack strain values were 0.478 me and 1.65 me. As with supplier 1, notable variation was observed in micro-cracking behavior between specimens. Specimen 1 did not exhibit inelastic deformation in micro-cracking regions while specimen 2 did exhibit inelastic deformation in these regions. During testing, specimen 1 experienced testing equipment stoppage that may have affected results, and specimen 2 experienced significant load fluctuations that were observed only during that test. This stoppage for specimen 1 may have cause the stress vs. average micro-crack strain curve observed in Figure 65. Therefore, additional testing must be performed to confirm stress and strain values for supplier 2 specimens. The results of these two specimens can be found in Figure 64 and Figure 65

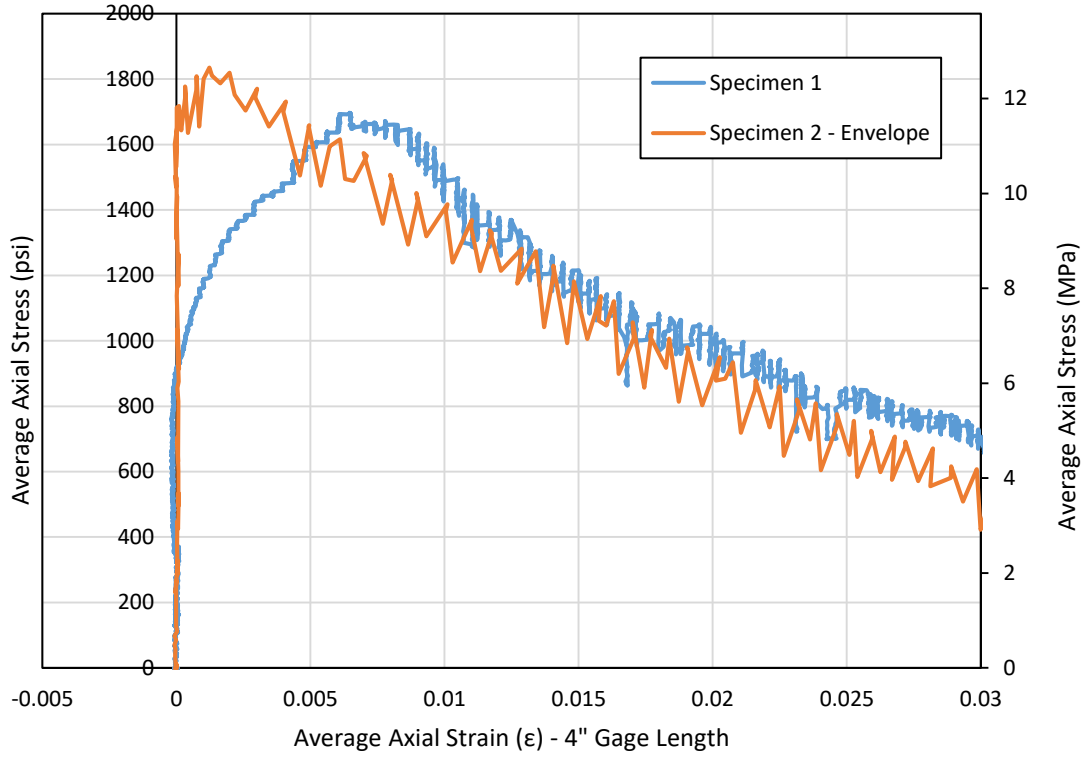


Figure 64: Supplier 2 - 2% Type A Fiber - Stress vs. Average Axial Strain – 4” Gage Length

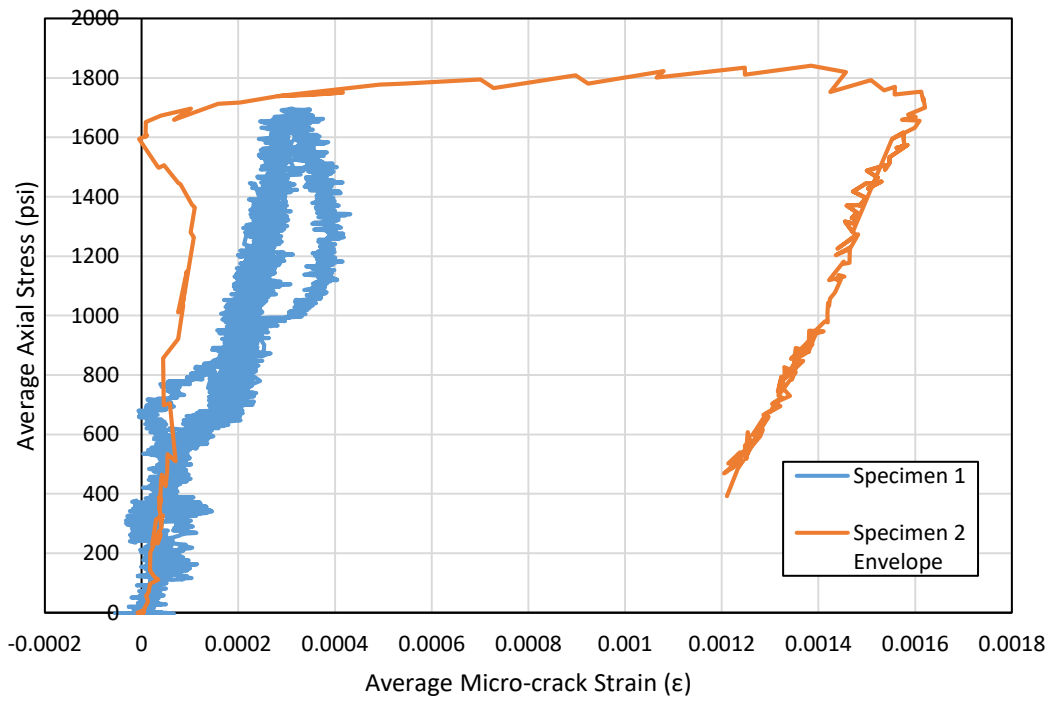


Figure 65: Supplier 2 - 2% Type A Fiber - Stress vs. Average Micro-crack Strain

3.3.9 Supplier 3 – 2% Fiber

Three supplier 3 tests were conducted using a combination of fiber types A and E. Each fiber type was dosed at 1% for a total fiber content of 2% by volume. All three specimens exhibited ductile behavior. Cracking stress values for specimens 1, 2, and 3 were 773, 796, and 684 psi respectively. Likewise, maximum stress values were 1242, 1168, and 1039 psi, strains at maximum stress for a 4" gage length were 5.72 me, 5.37 me, and 4.81 me and maximum average micro-crack strain values were 5.46 me, 1.02 me, and 1.77 me. As with the other suppliers, notable variation was observed in micro-cracking behavior between specimens. All specimens experienced inelastic micro-crack deformation. However, the amount of residual average micro-crack strain observed ranged significantly between specimens. The average axial strain and average micro-crack strain results of these three specimens can be found in Figures Figure 66, Figure 67, and Figure 68.

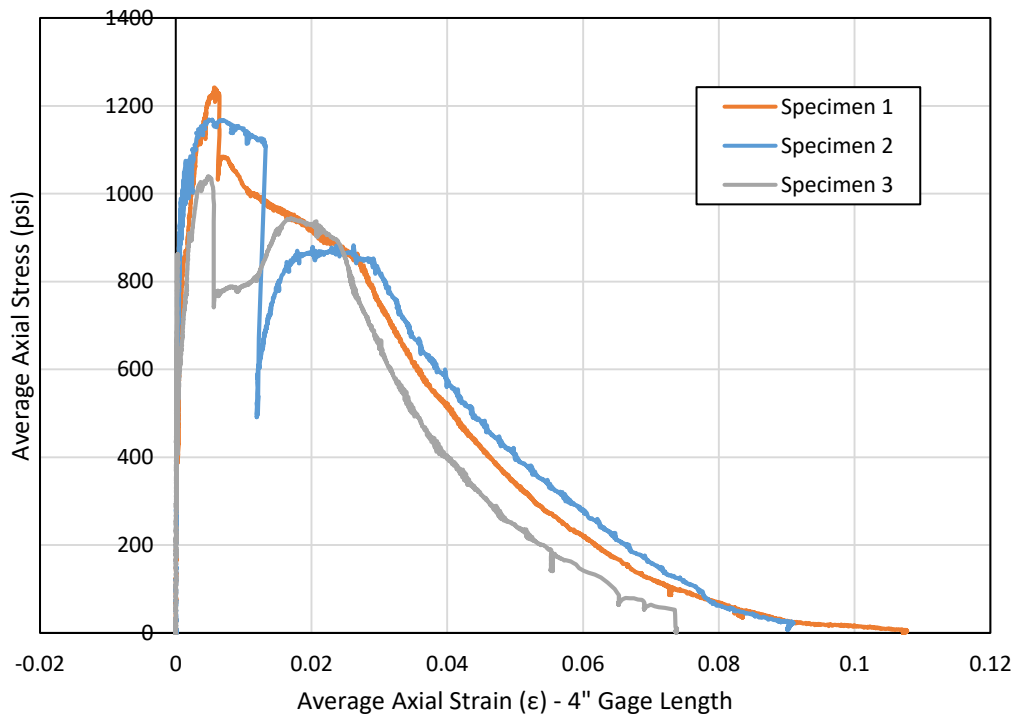


Figure 66: Stress vs. Average Axial Strain - Supplier 3 - 2% Combined of Type A and E Fiber

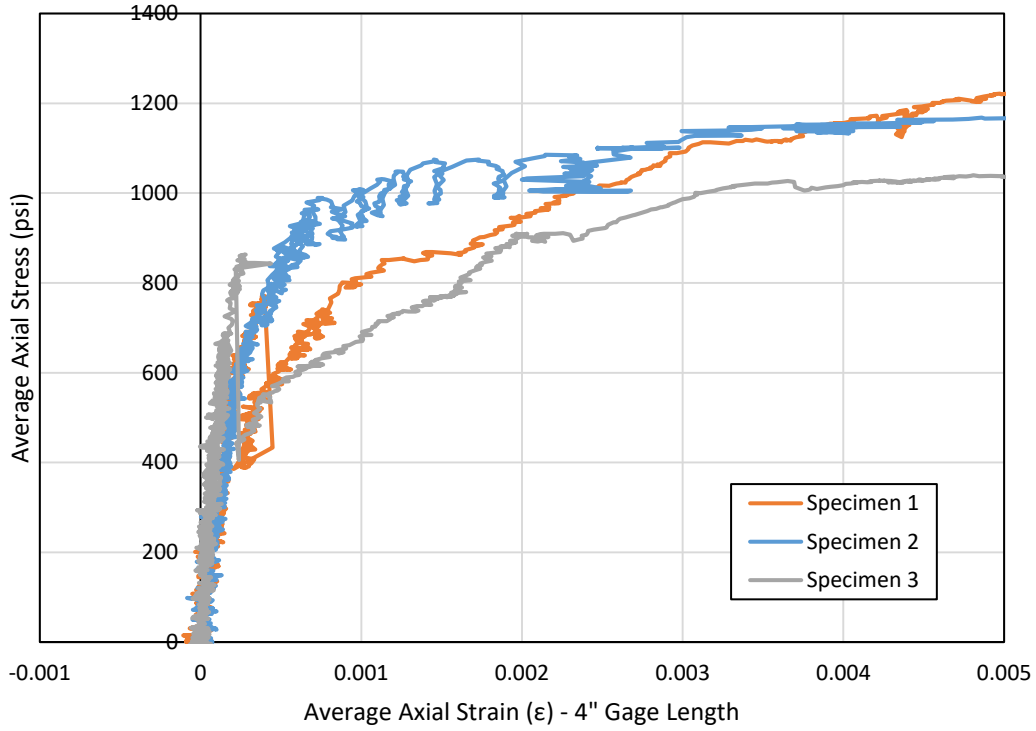


Figure 67: Stress vs. Average Axial Strain - Supplier 3 - 2% Combined of Type A and E Fiber - Zoomed In

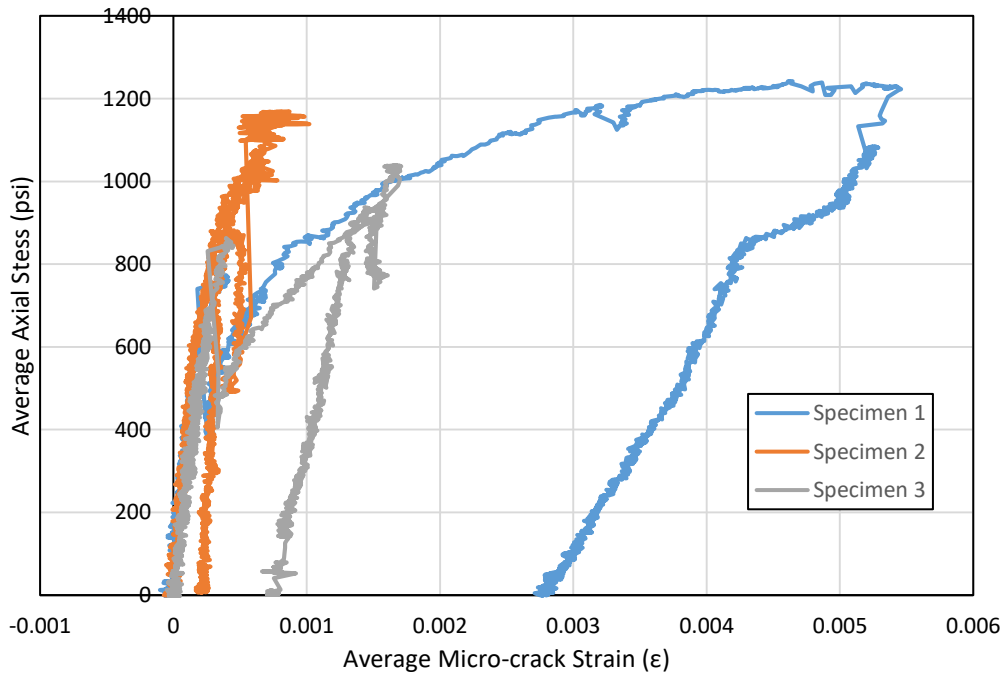


Figure 68: Stress vs. Average Micro-crack Strain - Supplier 3 - 2% Combined of Type A and E Fiber

3.3.10 Variation between Different Specimens

The amount of variation observed between specimens with the same fiber type and fiber content depended primarily upon the fiber content of the specimens. High variation in average micro-crack strain response was observed between specimens with 2% fiber while low variation in micro-crack strain response was observed in specimens with 1% fiber. The high variation in micro-cracking behavior for UHPC with 2% fiber makes it difficult to predict the tensile behavior this material will experience in the field. Variation in local crack behavior was observed in all specimens that experienced post-cracking strength, regardless of fiber type or content. As previously mentioned, this variation in local crack behavior is expected as fiber distribution and orientation will vary slightly at the cross-section of failure regardless of casting method.

The primary variation observed within specimens with 2% fiber were the values of micro-crack strains. As can be seen in Figure 69, supplier 1 specimen 1 experienced very small micro-crack strains with a maximum average micro-crack strain value of 0.23 me. The other two supplier 1 specimens experienced much higher maximum average micro-crack strains of 1.84 me and 2.79 me. Likewise, significant variation in micro-cracking behavior was observed for supplier 2 and supplier 3 specimens with 2% fiber that exhibited ductile responses. One of the two supplier 2 specimens exhibiting ductile responses also exhibited inelastic micro-cracking behavior. The maximum average micro-crack strain for the two specimens were 1.41 me and 5.64 me. Similarly, supplier 3 specimens experienced high variation in average micro-crack strain behavior. The range of maximum average micro-crack strains observed in these specimens was 1.02 me to 5.46 me. Additionally, all three supplier 3 specimens exhibited some inelastic micro-cracking behavior. However, the amount of residual micro-cracking strains observed varied by a factor of ten between

specimens with these values ranging from approximately 0.25 me to 2.8 me. Supplier 1 specimens with 1% fiber showed little variation in micro-crack strain values as shown in Figure 70.

Variation in local crack strain responses also occurred between specimens. This variation primarily affected the average axial strain responses observed. Photographs of specimen cross-sections after failure showed that although fiber distribution was similar, a notable difference in fiber orientation typically existed between specimens. This difference in orientation likely influenced the formation and propagation of the local crack within specimens which in turn may have influenced the maximum tensile strength of the specimen. Small variations in specimen thickness or cementitious make-up of the UHPC may also play a role but were not observed to be significant in these tests. Variation in average axial strain for supplier 1 specimens with 2% fiber can be found in Figure 71.

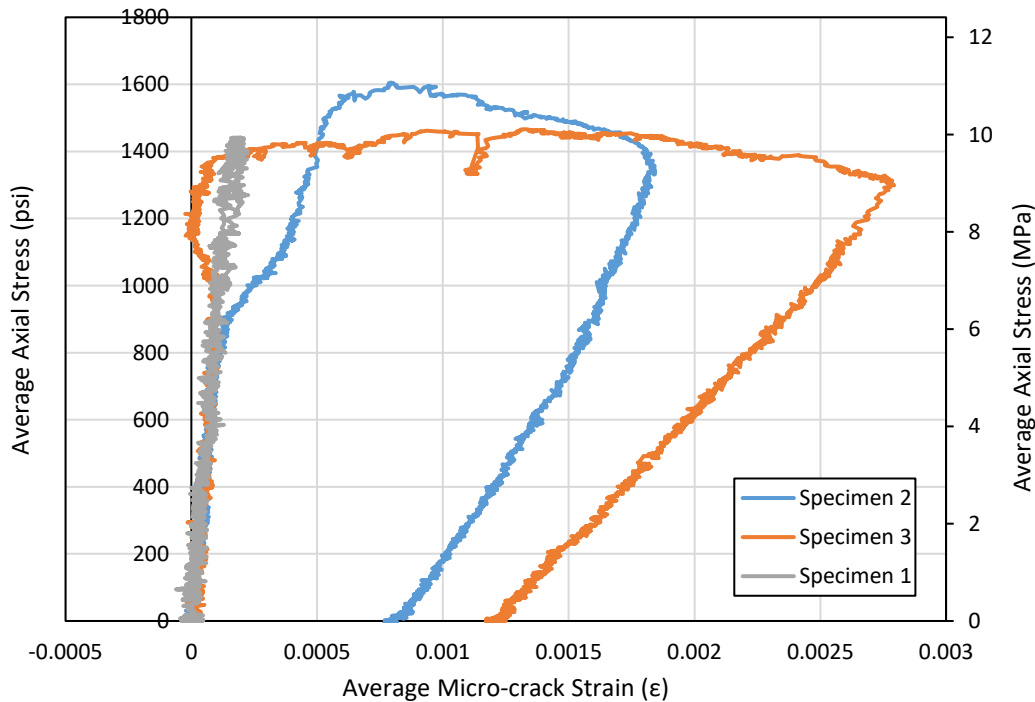


Figure 69: High Variation in Micro-cracking Behavior - Supplier 1 - 2% Type A Fiber

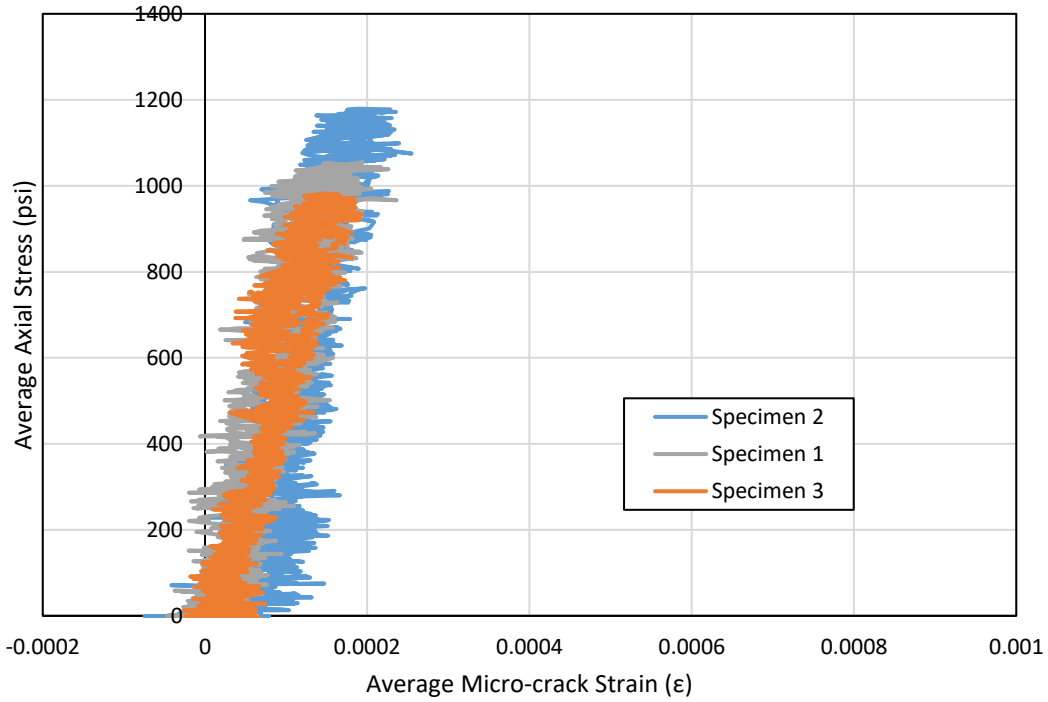


Figure 70: Low Variation in Micro-cracking Behavior - Supplier 1 - 1% Type A Fiber

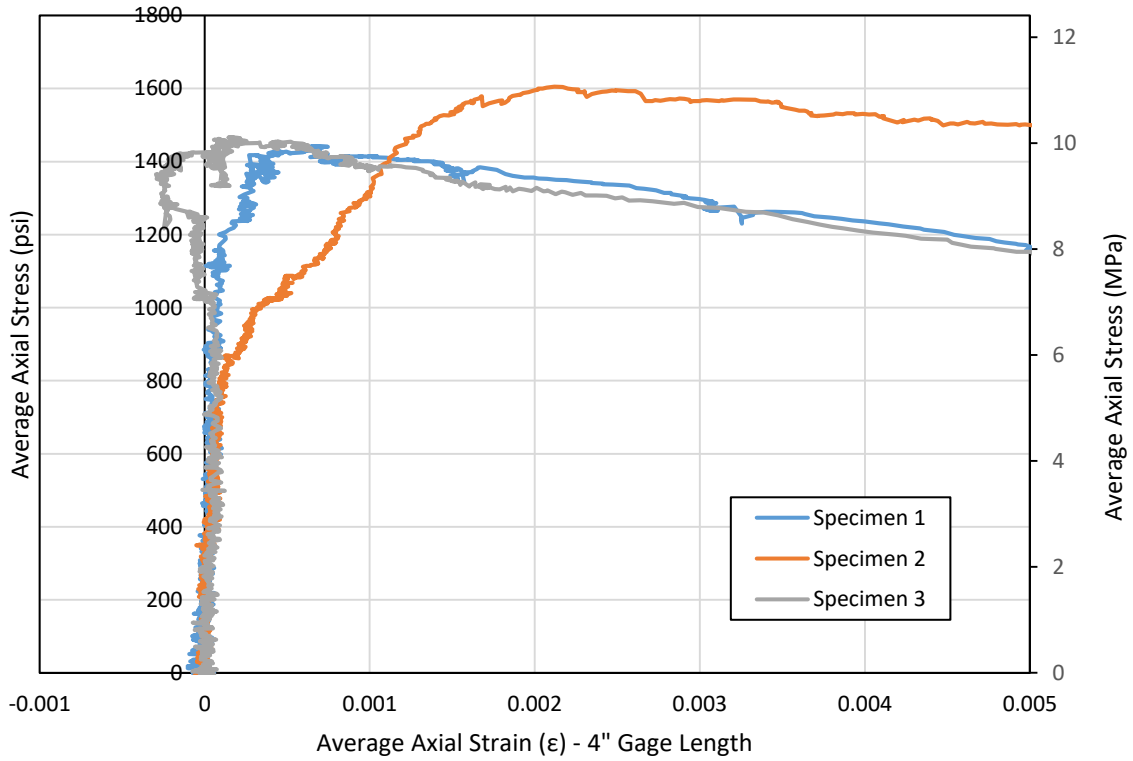


Figure 71: Variation in Average Axial Strain Responses – Supplier 1 – 2% Type A Fiber

3.3.11 Variation within a Specimen

The goal of investigating micro-crack variation within a specimen in this study was to determine if fiber distribution and orientation caused notable variation in strains in micro-cracking regions. From test results, variation observed between the right and left sides of specimens can be explained through the test setup used. Since some level of moment is unavoidable in direct tensile tests with fixed-end connections, it is inevitable that micro-crack strains will be higher on one side of the specimen than the other. Variation observed in strains between different regions of the specimen may be explained by stress concentrations induced by the dog-bone shape of the specimens or may be due to variations in fiber distribution and orientation. Since specimens typically failed near the same location at either end of the specimen, it can be inferred that stress concentrations were likely induced by the taper used in the dog-bone specimens. There will always be some stress concentrations present in direct tensile tests due to the transfer of forces from the testing machine to the specimen and will be present in dog-bone shaped specimens due to the tapered shape of such specimens. However, most specimens failed near the same location in this study suggesting notable stress concentrations occurred at these regions.

The tensile test setup used was chosen so that specimens with rebar could be tested using the same specimen shape. In this regard, this test method accomplishes its task very well. However, the presence of potential stress concentrations means that accurately measuring variation within the micro-cracking regions of the specimens is not possible. Therefore, a different tensile test setup or specimen shape must be used to determine if notable variation in micro-cracks occurs within specimens due to variation in fiber distribution and orientation. Redesign of specimen shape to reduce stress concentrations will be conducted in future research. Figure 72 through Figure 75

show individual micro-crack strains between each pair of LEDs, the average of micro-crack strains of the left and right side of the specimen at one-inch intervals, the average micro-crack strain \pm one standard deviation, and the minimum, maximum, and average micro-crack strain curves, respectively.

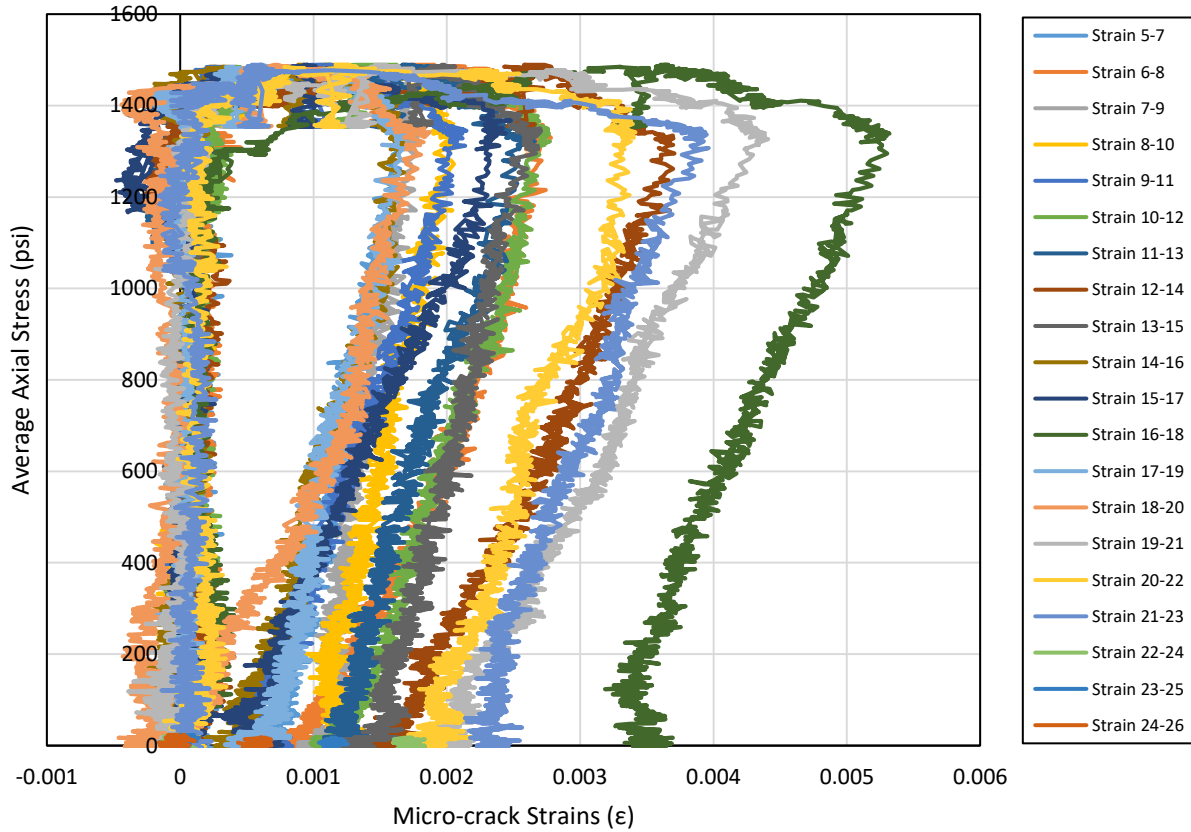


Figure 72: Variation within a Specimen - Micro-crack Strains at One-Inch Intervals – S13.A20

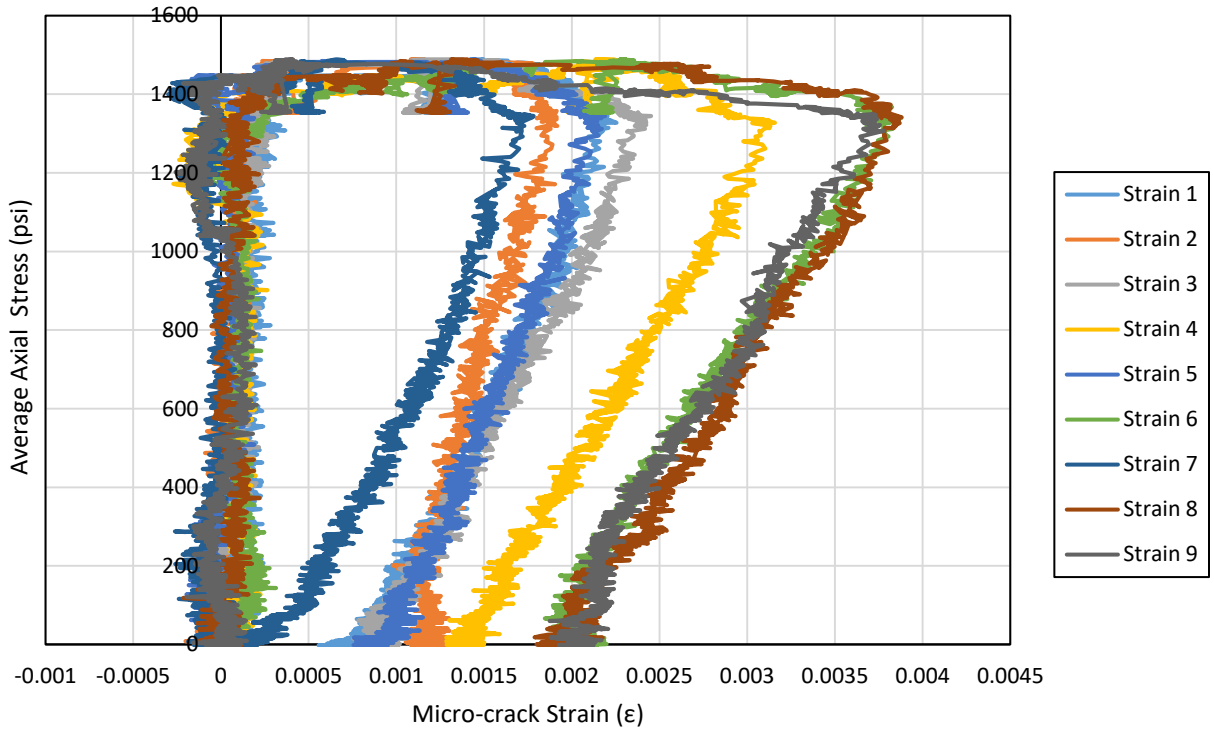


Figure 73: Variation within a Specimen - Average of Left and Right Micro-crack Strains at One-Inch Intervals – S13.A20

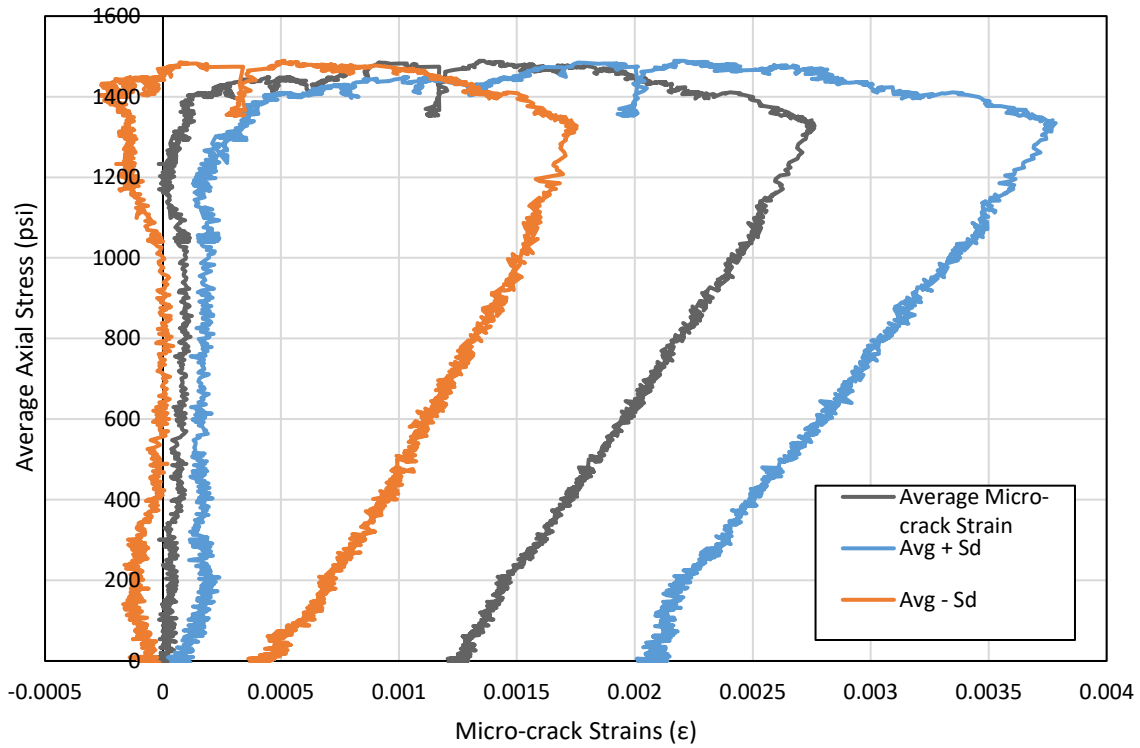


Figure 74: Variation within a Specimen – Average Micro-crack Strain +/- StdDev - S13.A20

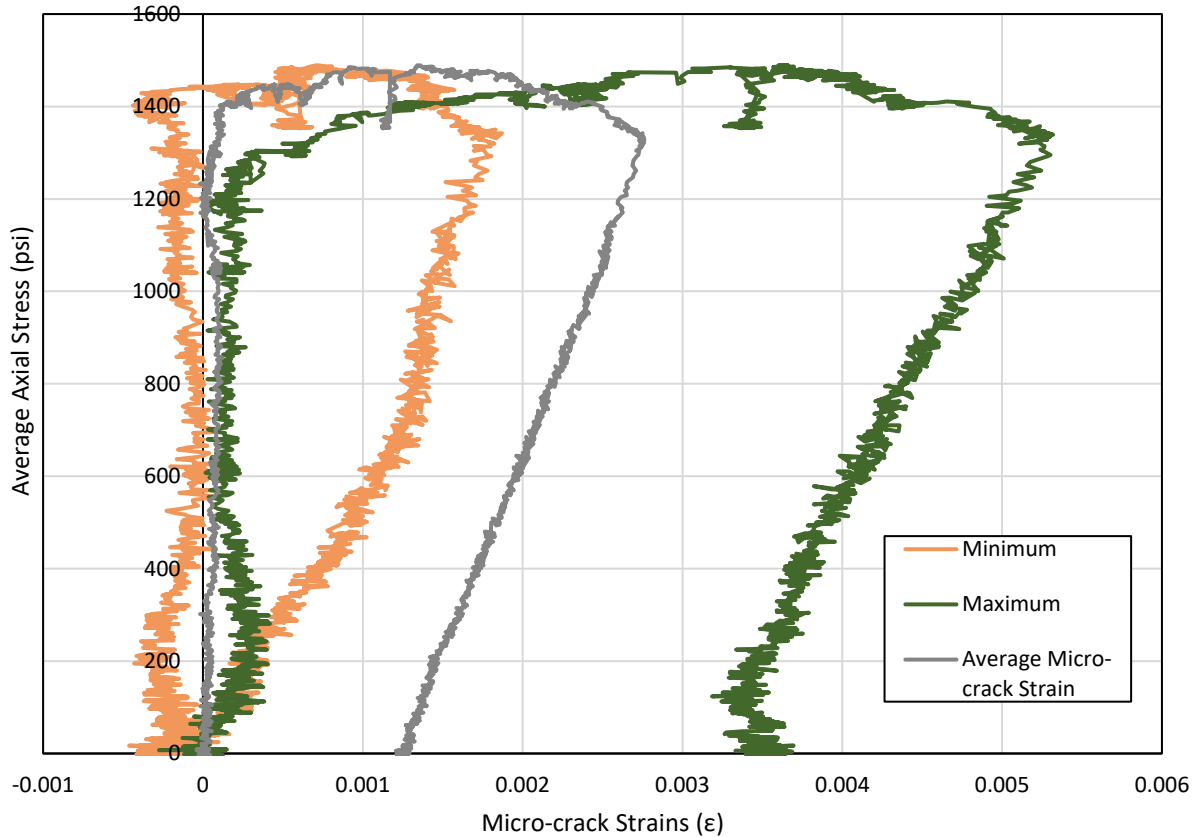


Figure 75: Variation within a Specimen - Micro-crack Strain Range - Min, Max, and Average Micro-crack Strains - S13.A20

3.3.12 Contribution of Micro-cracks to Global Specimen Displacement

The contribution of micro-cracks to axial displacement varied greatly for specimens with 2% fiber. This is due to the high variation in micro-cracking behavior between different specimens. Micro-crack contribution for specimens that experienced inelastic micro-crack deformation was observed to be high pre-peak strength. As can be seen in Figure 76 and Figure 77, the micro-cracking behavior for specimen S12.A20 contributed significantly to overall tensile displacement, even after the maximum tensile stress was reached. However, micro-crack contribution to overall deformation was relatively low during the all stages of testing for specimens with no inelastic

micro-crack deformation. Figure 78 through Figure 81 show that the contribution of micro-cracks to overall displacement for specimens S11.A20 and S11.A10, which contained 2% and 1% Type A fiber respectively, was minimal and demonstrate that micro-crack contribution to ductility can be minimal if the tensile stress necessary to engage fibers throughout the specimen is not reached. Contribution of micro-crack deformation to average micro-crack strain was small for all specimens with 1% fiber as no inelastic micro-crack deformation occurred. These results suggest that micro-cracks may not reliably provide significant ductility for UHPC in the field. Therefore, micro-cracks should not be relied on for substantial ductility when designing structures with UHPC. Instead, ductility solely from the localized crack should be included for design purposes until further research investigating the relationship between micro-crack and local crack formation and propagation is performed.

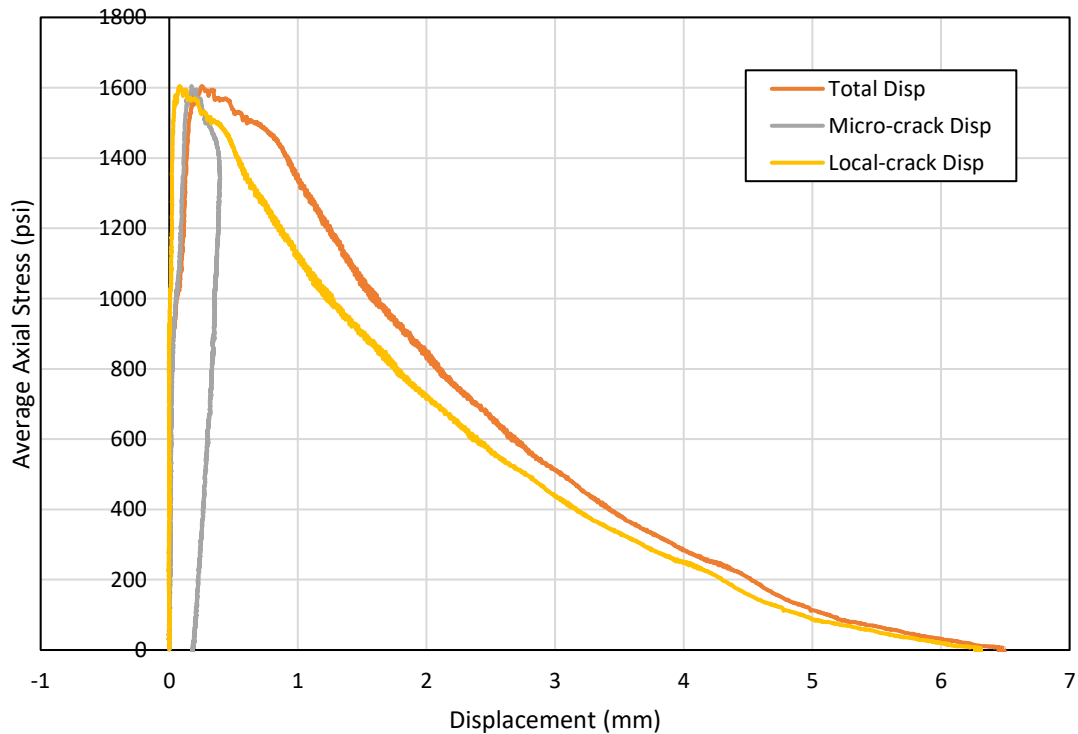


Figure 76: Contribution of Micro-cracks to Overall Displacement - S12.A20 Stress vs. Displacement

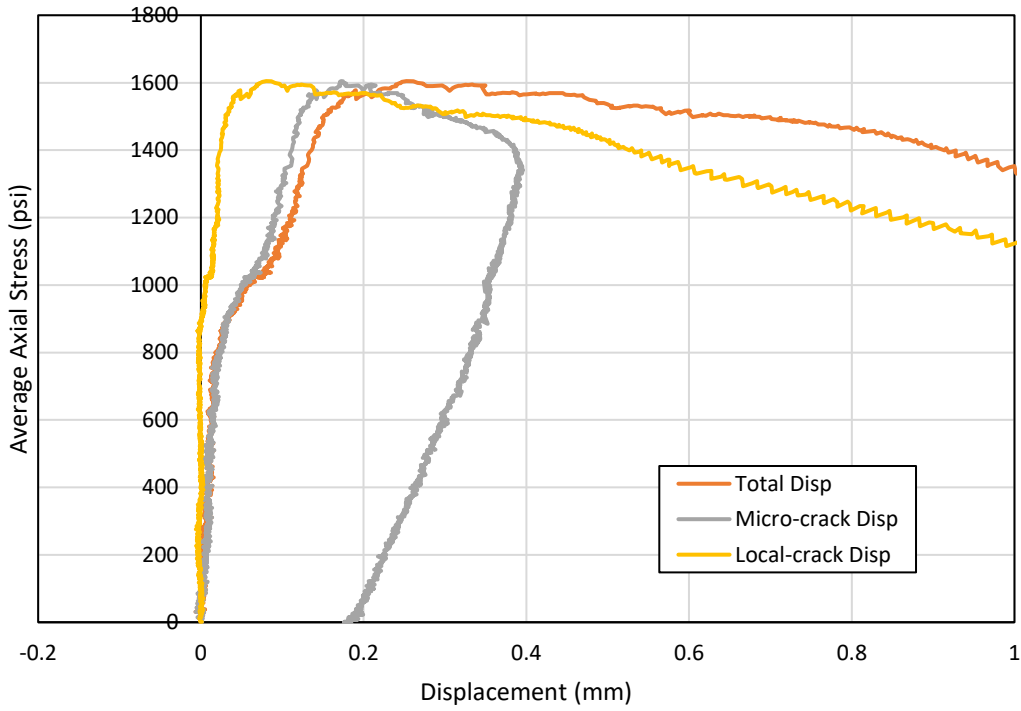


Figure 77: Contribution of Micro-cracks to Overall Displacement - S12.A20 Stress vs. Displacement - Zoomed In

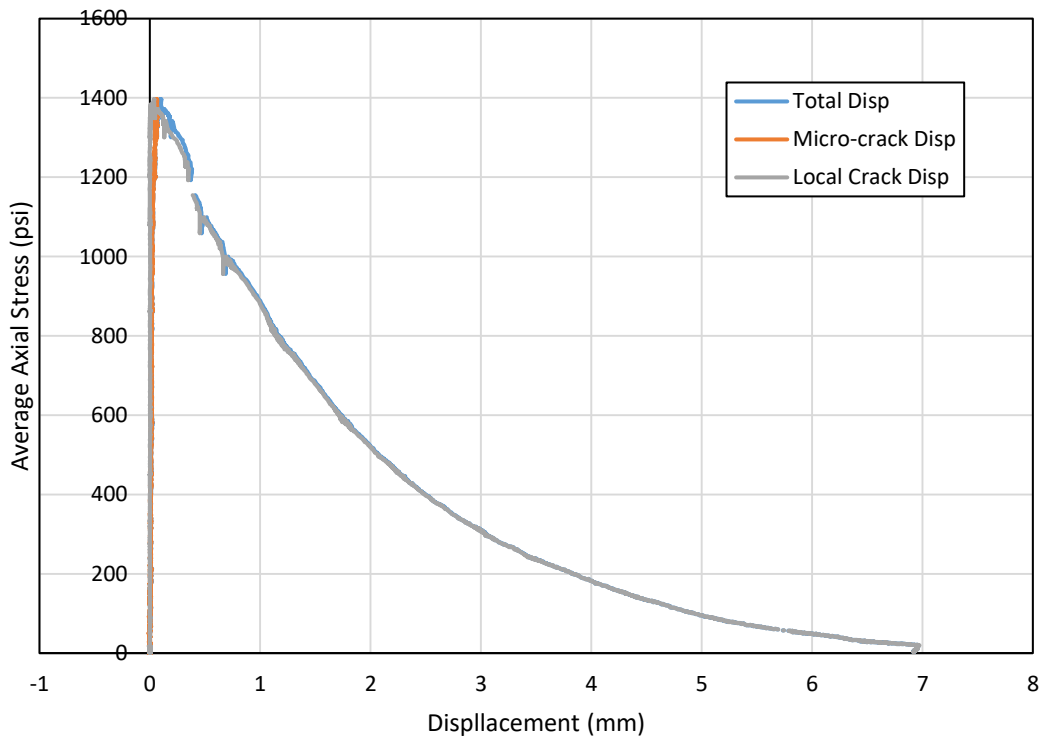


Figure 78: Contribution of Micro-cracks to Overall Displacement - S11.A20 Stress vs. Displacement

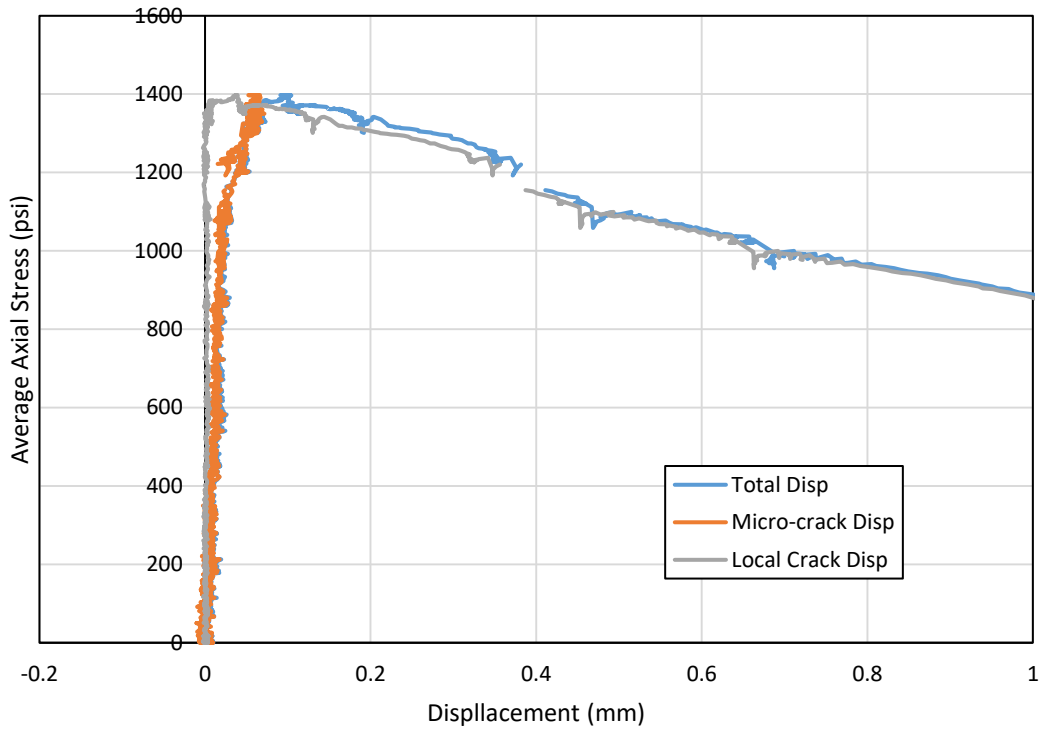


Figure 79: Contribution of Micro-cracks to Overall Displacement - S11.A20 Stress vs. Displacement – Zoomed In

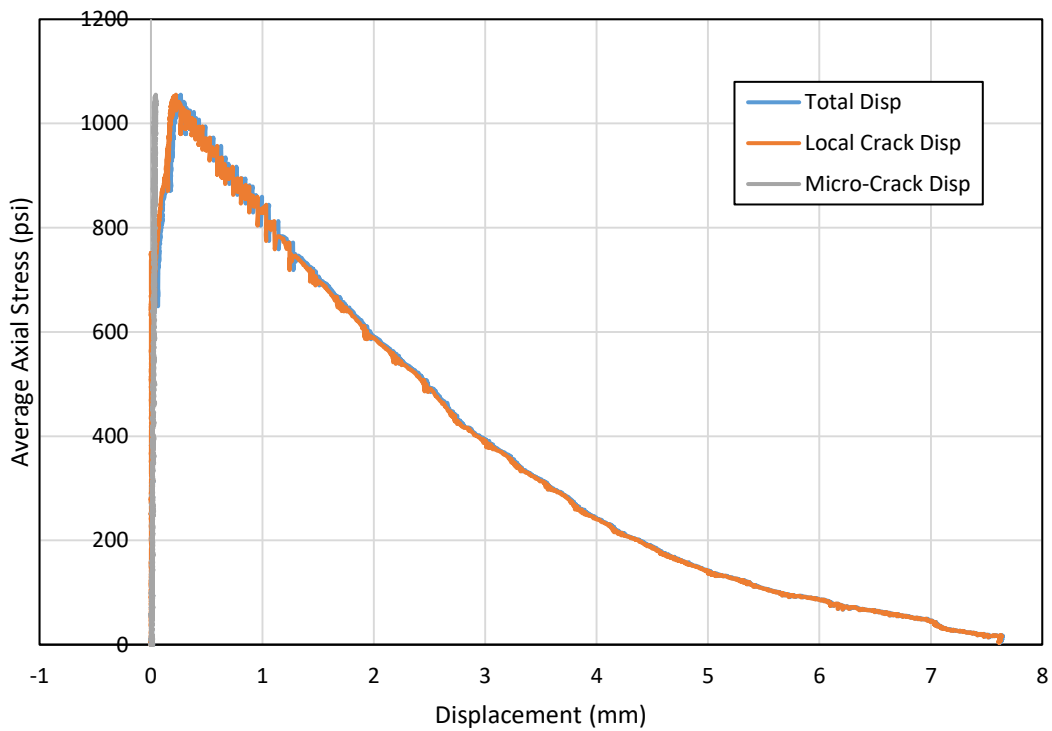


Figure 80: Contribution of Micro-cracks to Overall Displacement - S11.A10 Stress vs. Displacement

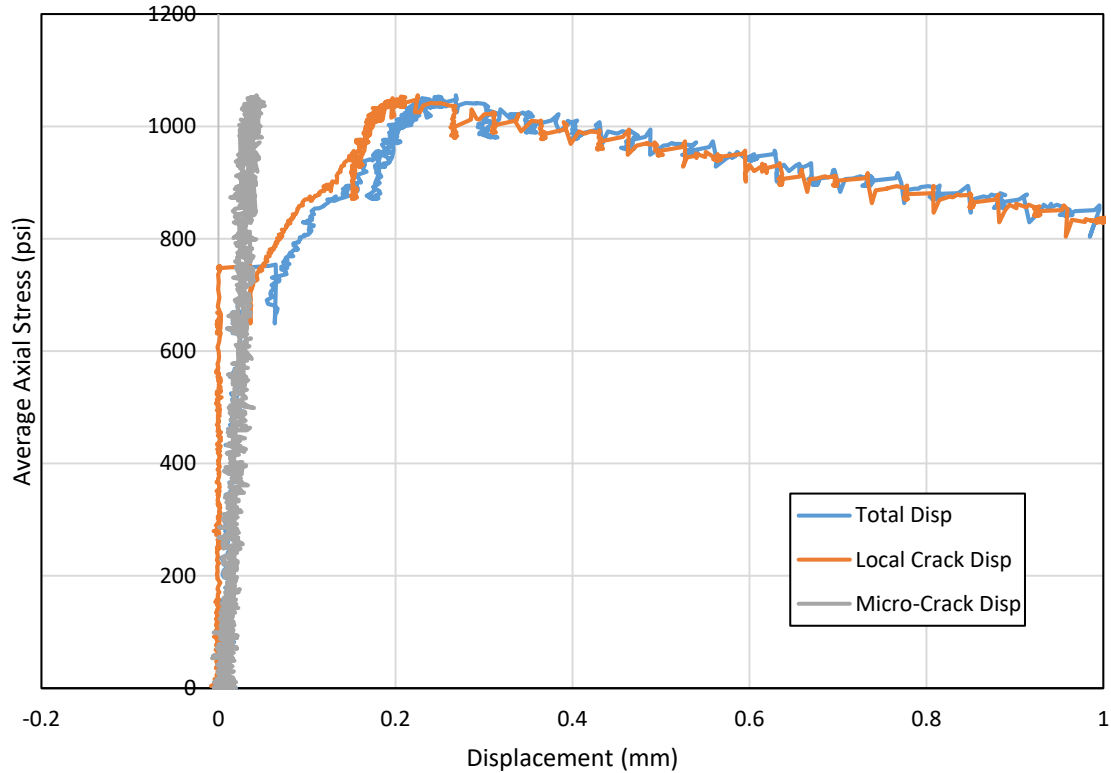


Figure 81: Contribution of Micro-cracks to Overall Displacement - S11.A20 Stress vs. Displacement - Zoomed In

3.3.13 Fracture Energy

Results show that fracture energy values were similar for supplier 1 UHPC with 1% and 2% Type A fiber by volume. Though the maximum tensile stress, f_t , was significantly higher for specimens with 2% fiber, the total local crack width/displacement, also known as COD, was significantly higher for specimens with 1% fiber. This resulted in average fracture energy values of 117.4 in-lb/in² and 114.1 in-lb/in² for UHPC with 1% and 2% fiber respectively. The results for fracture energy can be found in Table 8 and

Table 9. Figure 82 displays these values in a graphical format.

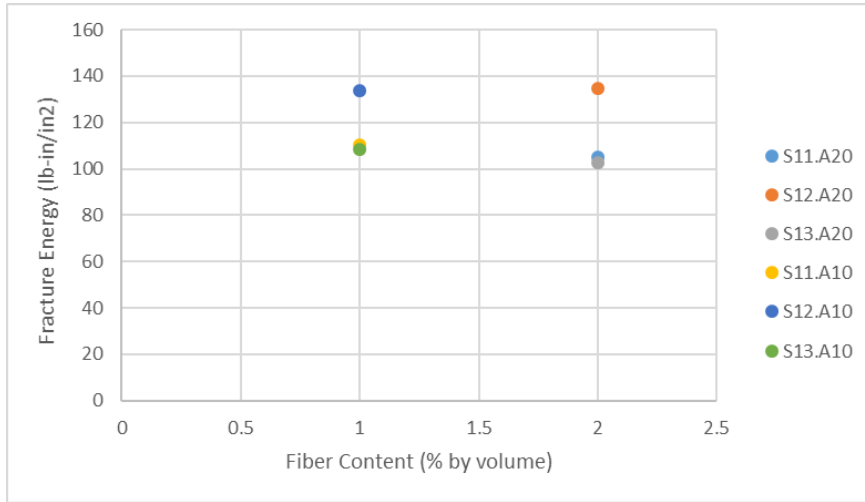


Figure 82: Fracture Energies for Supplier 1 Specimens

Table 8: Fracture Energy Values - Supplier 1 - 2% Type A Fiber

Specimen	Fracture Energy (lb-in/in ²)	Average (lb-in/in ²)	Standard Deviation (lb-in/in ²)
1	104.9	114.1	17.7
2	134.5		
3	102.8		

Table 9: Fracture Energy Values - Supplier 1 - 1% Type A Fiber

Specimen	Fracture Energy (lb-in/in ²)	Average (lb-in/in ²)	Standard Deviation (lb-in/in ²)
1	110.1	117.4	14.2
2	133.7		
3	108.3		

3.3.14 Characteristic Length

Characteristic length results show that UHPC with 1% fiber had significantly higher characteristic length values than UHPC with 2% fiber. Since materials with lower characteristic length values are more brittle, it can be concluded that supplier 1 UHPC with 1% fiber is more ductile than UHPC with 2% fiber according to the theory behind characteristic length. The average

characteristic length values were 709.6 inches and 401.2 inches for UHPC with 1% and 2% fiber respectively. These results generally align with tests performed by N. Tran, et. al for their experimental investigation published in 2015 as it was determined that characteristic length is higher for UHPC with 1% fiber than for UHPC with 1.5% fiber by volume in those tests. The results for characteristic length can be found in Table 10 and Table 11. Figure 83 displays these values in a graphical format.

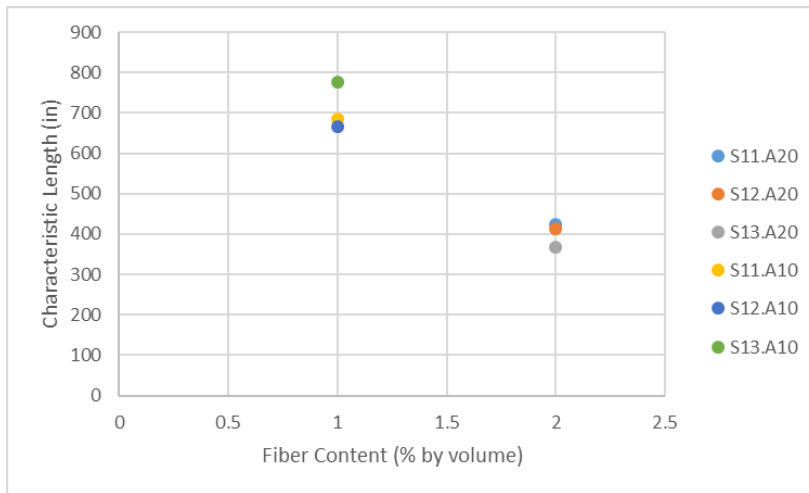


Figure 83: Characteristic Lengths for Supplier 1 Specimens

Table 10: Characteristic Length Values - Supplier 1 - 2% Type A Fiber

Specimen	Characteristic Length (in)	Average (in)	Standard Deviation (in)
1	424.5	401.2	30.7
2	412.7		
3	366.4		

Table 11: Characteristic Length Values - Supplier 1 - 1% Type A Fiber

Specimen	Characteristic Length (in)	Average (in)	Standard Deviation (in)
1	685.3	709.6	59.6
2	666.0		
3	777.4		

3.3.15 Stress and Strain Limits

Stress and strain limits for UHPC should be developed based on application as the mechanical requirements for the material change based on application. Based on the results in this study, a maximum tensile stress limit of 1000 psi and strain limit of 0.25 me are appropriate for UHPC with 2% Type A fiber to prevent local crack formation. UHPC containing 1% Type A fiber should be limited to tensile stresses of 500 psi and strains of 0.1 me to prevent local crack formation. To prevent local crack growth, the maximum allowable stress and strain values are 1300 psi and 0.5 me for 2% fiber and 900 psi and 0.8 me for 1% fiber based on results from this study.

All limits are based on the lowest values observed in relevant tensile tests, and all strain limits are based on a 4" gage length. From test results, using these values should ensure that significant local crack growth does not occur in similar tests, thereby limiting inelastic deformation at the localized crack location. It should be noted that fiber orientation depends greatly on the thickness of the member being poured and the casting procedure used. Therefore, tensile behavior of UHPC for field applications should be determined using specimens cast in the same way as the members cast in the field. Additionally, further testing must be completed to ensure the sample size of test specimens is large enough to accurately represent the possible range of stress and strain values for UHPC in tension. The strain values suggested in this section to prevent local crack growth were chosen as the strain value occurring at complete propagation of the local crack. If local crack growth is acceptable, higher strains may be appropriate.

The stress recommendations in this section do not include any fiber orientation coefficients. Recommendations proposed by various entities suggest a stress reduction factor due to fiber orientation ranging from 0.57 to 1.0. The French UHPFRC recommendations suggest a fiber orientation coefficient of $1/1.25 = 0.8$ for loading other than local effects and $1/1.75 = 0.57$ for local effects (FAGC, 2013). Similarly, the EPFL recommendations suggest a fiber orientation factor of 1.0 for loading other than local effects and 0.85 for local effects. Additionally, the Swiss recommendations include a fiber orientation factor due to element thickness that ranges from 0.8 to 1.0 (EPFL, 2016). Based on recommendation and design documents from applicable entities, an appropriate stress reduction factor due to fiber orientation, approximately in the range of 0.57-1.0, should be applied to these results for design purposes. Strain values currently being recommended by entities are higher than the value observed at the maximum tensile stress. Although strains higher than the value observed at maximum stress are acceptable for uses where local crack formation is not an issue, prevention of local crack formation and growth is often desirable to minimize crack widths. Therefore, to help prevent damage to UHPC over time, strains should be limited when local crack formation or local crack growth is a concern.

CHAPTER 4: CONCLUSIONS

Applications of UHPC to bridges and other structures have increased in the United States and throughout the world in recent years. This increase is primarily due to the many desirable properties of UHPC including its high compressive and tensile strength, chloride penetration resistance, freeze-thaw resistance, and increased bond strength with reinforcing bar and other forms of reinforcement. However, the tensile behavior of UHPC, particularly regarding the micro-cracks that form, is not well understood. Properly understanding UHPC's tensile behavior is critical for structures subject to flexure or shear action. As flexure or shear action occur in a vast majority of structural members, fully understanding the tensile behavior of UHPC is of the utmost importance to ensure the design of safe and efficient UHPC structures.

The micro-cracks that form in UHPC under tensile load are regarded by many researchers as essential to UHPC ductility allowing UHPC to reach significantly higher strains before reaching its maximum tensile stress. Additionally, it is assumed that they allow UHPC to remain durable, even past its maximum stress value, as micro-cracks widths are typically small enough to prevent damaging chloride penetration. However, traditional tensile test methods do not directly measure UHPC micro-cracking behavior under tensile loads, instead grouping the micro-cracking behavior in with the global tensile behavior over the chosen gage length. Therefore, results regarding micro-cracking behavior in UHPC are derived from these tests based on assumptions.

The primary goal of this research was to directly measure micro-cracking behavior in UHPC specimens under tensile loading to fully understand UHPC tensile behavior. In particular, this study focused on understanding the role of UHPC mix type, fiber type, and fiber content on micro-

cracking behavior through the direct tensile testing of dog-bone specimens. In separating the micro-cracking behavior from the global tensile behavior of UHPC, the relationship between the formation and propagation of micro-cracks and local cracks could be investigated. Furthermore, the effect of UHPC mix, fiber type, and fiber content on overall tensile behavior was explored. The contribution of micro-crack displacement to total displacement, variations in tensile behavior, and relative brittleness of UHPC exhibiting ductile behavior were also investigated.

4.1 Summary

This thesis is comprised of four chapters including an introduction, literature review, experimental results and analysis, and a summary of results and conclusions, the last of which this section is a part. Chapter 1 of this thesis introduces the subject, provides the scope and objectives of the study, and lays out a guideline for the rest of the document. The second chapter consists of a literature review focused on the properties of UHPC as well as UHPC's current applications to bridges and other structures. Additionally, the tensile behavior of UHPC is discussed in detail in this chapter, including various tensile behavior models, tensile testing methods, and previous experimental investigations relevant to UHPC tensile behavior. Chapter 3 details the experimental procedure for the direct tensile tests conducted in this study and a comparison of test results to tensile tests conducted in similar experimental investigations. Additionally, the relationship between micro-crack and local crack strains is investigated with an emphasis on directly quantifying micro-cracking behavior. The results of direct tensile tests performed in this study are presented in terms of micro-crack and average axial strains. Various other test results, such as fracture energy and characteristic length, are also discussed. This chapter, Chapter 4, presents a summary of the thesis and conclusions from the study regarding UHPC tensile behavior.

4.2 Conclusions

Based on the experimental investigation and analysis of relevant data conducted in this study, the following conclusions were derived:

4.2.1 Influence of Fiber Type

- Two different types of tensile responses were observed during testing of UHPC specimens. The observed response in specimens during testing was either a brittle response or a ductile response. It was determined that fiber type was the primary factor determining if a brittle or ductile response was observed due to the tensile strength of the fiber used. Brittle responses occurred when the tensile strength of the fiber at the cross-section of failure was lower than the tensile capacity of the cementitious matrix.
- A brittle response was observed in specimens with various combinations of Type B, C, and D fiber. No post-cracking strength was observed in these specimens as a maximum tensile load was reached and then the specimen failed suddenly.
- A ductile response was observed in specimens containing Type A or a combination of Type A and Type E fiber. These specimens experienced post-cracking strength and a strain softening region.
- Ductile behavior was observed in specimens with fiber contents as low as 1% by volume. Specimens with 1% Type A, 2% Type A, and a combination of Type A and Type E fiber at a combined dosage of 2% by volume exhibited ductile responses.

4.2.2 Proposed UHPC Tensile Behavior Model

- For specimens exhibiting ductile behavior, a four-stage tension model was proposed based on experimental results. These four stages are as follows:
 - The first stage is an elastic stage during which the specimen experiences small increases in tensile strain as the applied load increases. No cracking occurs during this stage.
 - The second stage is the micro-crack formation stage. This stage begins at first cracking, and micro-cracks form throughout this stage. Stress continues to increase throughout this stage.
 - The third stage is the local crack formation and propagation stage. This stage begins with the formation of the local crack and continues until the local crack has propagated across the entire cross-section. Micro-cracks continue to grow throughout this stage. Complete propagation typically occurred shortly after the maximum tensile stress was reached and approximately coincided with the maximum average micro-crack strain.
 - The fourth stage is the softening stage. This stage consists of local crack growth which results in increasing average axial strain and decreasing average axial stress. As average axial stress decreases, micro-crack strains decrease. If inelastic deformation occurred in micro-cracks during testing, residual micro-crack strains were observed. If no inelastic deformation occurred in micro-cracks during testing, micro-crack strains returned to approximately zero. This stage continues until specimen failure.

- This model is applicable for all direct tensile tests with fixed-end boundary conditions. For tests with pinned-end boundary conditions, the model may be adjusted by removing the propagation portion of the third stage. Since pinned-end connections induce no bending moment in the specimen, the local crack is not forced to propagate across the cross-section like it is in tests with fixed-end connections. A detailed explanation of this phenomenon can be found in Chapter 2.

4.2.3 Influence of Fiber Content

- Fiber content played a significant role in the tensile response observed in specimens and had a direct effect on the maximum stress observed. As fiber content increased, the observed maximum tensile stress increased. For supplier 1 UHPC with Type A fiber, the cementitious matrix tensile strength was approximately 500 psi, and each percent of fiber by volume added increased the maximum tensile strength by approximately 500 psi. Therefore, the maximum tensile strength for 1% fiber by volume was approximately 1000 psi and the maximum tensile strength for 2% fiber by volume was approximately 1500 psi.
- For specimens with no fiber, micro-cracking did not occur as was expected. This was due to the brittle failure of the cementitious matrix at the maximum observed tensile stress.
- Specimens with 1% fiber experienced micro-cracking. However, no inelastic micro-cracking was observed in specimens with 1% fiber.
- Specimens with 2% fiber experienced micro-cracking, and some specimens experienced inelastic micro-crack deformation. In total, six of the eight specimens exhibiting ductile responses and containing 2% fiber experienced inelastic micro-crack deformation. This includes two of the three supplier 1 Type A specimens, one of the two supplier 2 Type A

specimens, and all three of the supplier 3 Type A and E specimens. However, the amount of residual micro-cracking strain observed varied significantly between specimens. The residual micro-crack strain in the three supplier 3 specimens varied by a factor of approximately ten with a residual micro-crack strain range of 0.25 me to 2.8 me.

4.2.4 Contribution of Micro-crack to Overall Displacement

- The contribution of micro-crack displacement to overall tensile displacement within specimens depended highly on the micro-cracking behavior observed.
- Supplier 1 specimen 2 containing 2% Type A fiber by volume experienced inelastic micro-crack deformation during testing. Therefore, the observed micro-crack displacement in the specimen was relatively high. This resulted in micro-crack displacement contributing significantly to total tensile displacement, particularly pre-peak stress.
- Supplier 1 specimen 1 containing 2% Type A fiber by volume did not experience inelastic micro-crack deformation during testing. Therefore, micro-crack displacement in the specimen was low, and micro-crack contributed very little to total tensile displacement during testing.
- Supplier 1 specimen 1 containing 1% Type A fiber by volume did not experience inelastic micro-crack deformation during testing. Therefore, micro-crack displacement in the specimen was low, and micro-crack contributed very little to total tensile displacement during testing.
- The results of these specimens show that micro-cracking contribution can be minimal if the tensile stress necessary to engage fibers throughout the specimen is not reached. This suggests that micro-cracks may not reliably provide ductility in the field, and that they

should not be relied on for significant ductility for design purposes. Instead, ductility from the localized crack should be the only ductility included for design purposes unless future testing proves otherwise.

4.2.5 Fracture Energy and Characteristic Length

- Results show that fracture energy values were similar for supplier 1 UHPC with 1% and 2% Type A fiber by volume. Though the maximum tensile stress, f_t , was significantly higher in 2% fiber, the local crack width curve was significantly higher for UHPC with 1% fiber. This resulted in fracture energy values being roughly the same for UHPC with 1% and 2% fiber. The average fracture energy values of 117.4 in-lb/in² and 114.1 in-lb/in² for UHPC with 1% and 2% fiber respectively.
- Characteristic length results show that UHPC with 1% fiber had significantly higher characteristic length values than UHPC with 2%. Since materials with lower characteristic length values are more brittle, it can be concluded that supplier 1 UHPC with 1% fiber is more ductile than UHPC with 2% fiber. The average characteristic length values of 709.6 inches and 401.2 inches for UHPC with 1% and 2% fiber respectively.

4.2.6 Stress and Strain Limits

- Stress and strain limits can be suggested for various UHPC conditions based on results from these tests. These limits apply to UHPC with Type A fiber dosed at 1% and 2% by volume. Appropriate factors due to fiber orientation should be applied to recommended stress values in this section.

- Suggested stress and strain limits for UHPC with 2% Type A fiber by volume are 1000 psi and 0.25 me to prevent local crack formation and 1300 psi and 0.5 me to prevent local crack growth.
- Suggested stress and strain limits for UHPC with 1% Type A fiber by volume are 500 psi and 0.1 me to prevent local crack formation and 900 psi and 0.8 me to prevent local crack growth.
- All strain limits are based on a 4” gage length.
- Suggested strain limits to prevent local crack growth were chosen as the strain values at which the localized crack completed propagation across the cross-section. In this way, local crack nonlinear deformation would be limited to that which occurs before local crack growth. If local crack growth is acceptable, higher strain limits may be appropriate.
- The stress values provided in this section do not contain a stress reduction factor due to fiber orientation. Therefore, an appropriate stress reduction factor due to potential variation in fiber orientation, in the range of 0.57 to 1.0, should be applied to these results based on recommendation documents from applicable entities.

REFERENCES

AFGC, “Scientific and Technical Document on Recommendations for Ultra High Performance Fibre-Reinforced Concrete”, Association Francaise de Genie Civil (AFGC), Revised Edition, June 2013, Paris, France.

Alkaysi, M.; El-Tawil, A., “Factors Affecting Bond Development between Ultra-High Performance Concrete (UHPC) and Steel Bar Reinforcement,” Construction and Building Materials, 2017, pp. 412-422.

Alkaysi, M.; El-Tawil, S., “Effects of Variations in the Mix Constituents of Ultra High Performance Concrete (UHPC) on Cost and Performance,” Materials and Structures, 2016, pp. 4185-4200.

ASTM International, “ASTM C1856/C1856M-17 Standard Practice for Fabricating and Testing Specimens of Ultra-High Performance Concrete,” ASTM International, 2017.

Blais, P.Y.; Couture, M., “Precast, Prestressed Pedestrian Bridge – World’s First Reactive Concrete Powder Structure,” PCI Journal, 1999, Vol. 44, No. 5, pp. 60-71.

Caverzan, A.; Cadoni, E.; Prisco, M., “Tensile behavior of high performance fiber-reinforced cementitious composites at high strain rates,” International Journal of Impact Engineering, 2012, pp. 28-38.

Dobrusky, S.; Bernardi, S., “Uni-axial Tensile Tests for UHPFRC,” UHPFRC 2017, RILEM International Conference on Ultra-High Performance Fiber-Reinforced Concrete, Volume 1, 2017, pp. 165-174.

Federal Highway Administration Research and Technology, “Design and Construction of Field-Cast UHPC Connections,” Office of Research, Development, and Technology, U.S. Department of Transportation, Federal Highway Administration, 2014.

Federal Highway Administration, “Ultra-High Performance Concrete: A State-Of-The-Art Report for the Bridge Community,” Office of Research, Development, and Technology, U.S. Department of Transportation, Federal Highway Administration, 2013.

Graybeal, B., “Practical Means for Determination of the Tensile Behavior of Ultra-High Performance Concrete,” Journal of ASTM International, Vol. 3, No. 8, 2006.

Graybeal, B., “Compressive Behavior of Ultra-High-Performance Fiber-Reinforced Concrete. ACI Materials Journal,” Mar.-Apr., 2007, pp. 146-152.

Graybeal, B.; Baby, F., “Development of Direct Tension Test Method for Ultra-High-Performance Fiber-Reinforced Concrete,” ACI Materials Journal, March-April 2013, pp. 177-186.

Graybeal, B., "Compression Testing of Ultra-High-Performance Concrete," *Advances in Civil Engineering Materials*, Vol. 4, No. 2, 2015, pp. 102-112.

Gu, C.; Ye, G.; Sun, W., "Ultra-high performance concrete-properties, applications and perspectives," *Science China Technological Sciences*, Vol. 58, No. 4, 2015, pp. 587-599.

Heimenn, J., "The Implementation of Full Depth UHPC Waffle Bridge Deck Panels: Final Report," Federal Highway Administration, Publication No. FHWA-HIF-13-031, 2013.

Hillerborg, A., "Application of Fracture Mechanics to Concrete: Summary of a Series of Lectures 1988," Division of Building Materials, LTH, Lund University, 1988.

Lafarge Holcim, "Lafarge: Concrete Reborn," Lafarge, 2009.

Lewin, T.; Sritharan, S., "Design of 328-ft (100-m) Tall Wind Turbine Towers Using UHPC," Iowa State University, 2010.

Ma, J.; Schneider, H., "Properties of Ultra-High-Performance Concrete," Leipzig Annual Civil Engineering Report (LACER), No. 7, 2002, pp. 25-32.

Ma, J.; Orgass, M.; Dehn, F.; Schmidt, D.; and N.V. Tue, "Comparative Investigations on Ultra-High Performance Concrete with and without Coarse Aggregates," Proceedings of the International Symposium on Ultra-High Performance Concrete, Kassel, Germany, Sept. 13-15, 2004, pp. 205-212.

Mazzacane, P.; Ricciotti, R.; Teply, F.; Tollini, E.; Corvez, D., "MUCEM: The Builder's Perspective," International Symposium on Ultra-High Performance Fiber-Reinforced Concrete, 2013.

MCS-EPFL, "Recommendation: Ultra-High Performance Fibre Reinforced Cement-based composites (UHPFRC)," Maintenance Construction Sécurité – École Polytechnique Fédérale de Lausanne, 2016.

Meade, T.; Graybeal, B., "Flexural Response of Lightly Reinforced Ultra-High Performance Concrete Beams," 3rd fib International Conference, 2010.

Millon, O.; Riedel, W.; Thoma, K.; Fehling, E.; Nöldgen, M., "Fiber-Reinforced Ultra-High Performance Concrete Under Tensile Loads," DYMAT International Conference, 2009, pp. 671-677.

Perry, V.; White, P.; Ahlborn, T., "The First North American Broad Based Structural Design Guide on UHPC – ACI 239C," First International Interactive Symposium on UHPC, 2016.

Sritharan, S.; Bristow, B.; and Perry, “Characterizing an Ultra-High Performance Material for Bridge Applications under Extreme Loads,” Proceedings of the 3rd International Symposium on High Performance Concrete, Orlando, Florida, 2003.

Sritharan, S., “Design of UHPC Structural Members: Lessons Learned and ASTM Test Requirements,” Advances in Civil Engineering Materials, Vol. 4, No. 2, 2015, pp. 113-131.

Tran, N.; Tran, T.; Jeon, J.; Park, J.; Kim, D., “Fracture Energy of Ultra-High-Performance Fiber-Reinforced Concrete at High Strain Rates,” Cement and Concrete Research, 2015.

Vande Voort, T. L.; Suleiman, M.T., & Sritharan, S., “Design and Performance Verification of UHPC Piles for Deep Foundations,” Ames: Center for Transportation Research and Education, Iowa State University, 2008.

Vergoossen, R., “Tailor made bridge design with Ultra-High-Performance Concretes,” Tailor Made Structures, 2008, pp. 1067-1068.

Wille, K.; El-Tawil, S.; Naaman, A., “Properties of Strain Hardening Ultra-High Performance Fiber Reinforced Concrete (UHP-FRC) Under Direct Tensile Loading,” Cement & Concrete Composites, 2014, pp. 53-66.

Wille, K.; Kim, D.; Naaman, A., “Strain-Hardening UHP-FRC with Low Fiber Contents,” Materials and Structures, 2011, pp. 583-598.

Yu, R.; Spiesz, P.; Brouwers, H., “Mix design and properties assessment of Ultra-High Performance Fibre Reinforced Concrete (UHPRFC),” Cement and Concrete Research, 2014, pp. 29-39.